Surface layer O_3 and NO_x in the Arctic: the influence of boundary layer dynamics, snowpack chemistry, surface exchanges, and seasonality

by

Brie A. Van Dam

BSE, University of Michigan, 2007

A thesis submitted to the

Faculty of the Graduate School of the

University of Colorado in partial fulfillment

of the requirements for the degree of

Doctor of Philosophy

Department of Atmospheric and Oceanic Sciences

2013

This thesis entitled:
Surface layer O_3 and NO_x in the Arctic: the influence of boundary layer dynamics, snowpack chemistry, surface exchanges, and seasonality
written by Brie A. Van Dam
has been approved for the Department of Atmospheric and Oceanic Sciences

Dr. Detlev Helmig

Dr. Darin Toohey

Dr. David Noone

Dr. William Neff

Dr. Samuel Oltmans

Date

The final copy of this thesis has been examined by the signatories, and we find that both the content and the form meet acceptable presentation standards of scholarly work in the above mentioned discipline.

Van Dam, Brie A. (Ph.D., Atmospheric and Oceanic Sciences)

Surface layer O_3 and NO_x in the Arctic: the influence of boundary layer dynamics, snowpack chemistry, surface exchanges, and seasonality

Thesis directed by Dr. Detlev Helmig

The snowpack is a region of active chemistry. Aqueous chemistry in a quasi-liquid layer on snow grains and gas-phase chemical reactions in snow interstitial air can lead to the production or destruction of important trace gases. Physical transport parameters such as wind pumping and diffusion affect the vertical distribution of gases within the snowpack. The resulting emission or uptake of trace gases at the atmosphere-snowpack interface can have significant influence on the chemistry of the lower atmosphere. In this work the dynamic interactions between the snowpack and atmosphere are examined from multiple perspectives. The primary focus is on ozone (O_3) and nitrogen oxides (NO_x) in the Arctic, a region undergoing widespread environmental change. To investigate an ice-sheet location with year round snow cover, data from a two-year campaign at Summit, Greenland are implemented. At Summit this study examines (1) the processes contributing to vigorous chemistry in snow interstitial air, and (2) the role of the boundary layer over snow in determining surface layer NO_x. Physical and chemical processes are shown to contribute to distinct seasonal and diurnal cycles of O_3, NO, and NO_2 in the snowpack. Boundary layer depths estimated from sonic anemometer turbulence quantities are used alongside sodar-derived values to show that the depth of the stable to weakly stable boundary layer at Summit was not a primary factor in determining NO_x in early summer.

Motivated by observations of an increase in the length of the snow-free season in the Arctic in recent decades, data from a one-year experiment at the seasonally-snow covered location of Toolik Lake, AK are also incorporated. This study shows the first observations of springtime ozone depletion events at a location over 200 km from the coast in the Arctic. FLEXPART analysis is used to illustrate that these inland events are linked to transport conditions. Lastly at this

location, eddy-covariance O_3 fluxes were calculated to characterize deposition of O_3 to the Arctic tundra surface in the summertime. Surface deposition in combination with stability conditions is shown to contribute to the development of a diurnal cycle in surface O_3 with amplitude ranging 5-35 ppbv.

Dedication

This work is dedicated to the memory of my grandfather, John Hodge, who joyfully encouraged all of his grandchildren to experience and appreciate the natural world.

Acknowledgements

I am incredibly lucky to have a wonderful group of colleagues and friends who have helped me in this process. To begin, thanks to my advisor Detlev Helmig, who taught me that "you can't stop an excited scientist." This work would not have been possible without his academic, financial, and professional support. I would also like to thank my committee members Bill Neff, David Noone, Sam Oltmans, and Darin Toohey. Each have provided invaluable advice and assistance throughout my graduate career.

I have appreciated working alongside all of the graduate students in the Atmospheric Research Lab through the years, including Kathrin Lang, Brian Seok, Patrick Boylan, Ryan Daly, Molly Brodin, and others. Thanks for letting me be the worst social coordinator ever. Thank you to Jacques Hueber for his patience in explanations and infinite help with instrumentation. I have benefited from collaborations with several individuals at Michigan Technological University during field campaigns. Louisa Kramer and Claudia Toro: thank you for sharing data, scientific discussions, and laughter. Thank you also to Richard Honrath, Mike Dziobak, Paul Doskey, and Keenan Murray. Additional thanks to Laurens Ganzeveld for helpful discussions. Thank you to all of my co-authors including those listed above as well as John Burkhart and Daniel Obrist. My work has greatly benefited from their ideas, collaboration, and feedback.

A very sincere thank you goes to the Summit Station science techs and the staff of the Toolik Field Station for their willingness to go out in any and all extreme conditions to check on instrumentation. This data set would not be nearly so beautiful without their help. I wish I had space to name all the amazing scientists and staff I was privileged to work alongside at both Summit

and Toolik Lake. Thanks for being the most fun, helpful, encouraging, and positive group of people I've had the pleasure of interacting with. Thanks to the 109th Air National Guard and CH2MHill polar field services for logistical support, and the Danish Commission for Scientific Research for providing access to Summit. Funding was provided by the NSF under grant NSF-OPP-07-1399. The Atmospheric and Oceanic Sciences Department and the Graduate School both assisted with funding to travel to several conferences.

On a personal level, I want to thank all of my family and friends for their support and love during this endeavor. Particularly my parents for teaching me to look at the world with a positive attitude, never take myself too seriously, and for instilling in me their incredible work ethic. Ben and Erika: having your support, advice, and friendship means the world to me. To Anna and Robin, thank you for the hundreds of trail miles logged during this process. I'm so grateful to count two such fun, level-headed, and down-to-earth women as friends. Thanks to Thom for his patience, generosity, humor, and the constant encouragement to take adventures. Thank you to my fellow graduate students in ATOC and at INSTAAR for their friendship and conversation.

Lastly, I would like to acknowledge and honor the memory of my undergraduate advisor Dr. Jerry Keeler. Through his encouragement and support I took my first trip to the Arctic, a research experience that lit my initial spark of excitement for Arctic science. For that, I am eternally grateful.

Contents

Chapter

Figures

Figure

Chapter 1

Introduction

1.1 Background

Changes in the Earth climate system are being manifested rapidly in the Arctic. Complex feedback loops in this unique region lead to enhanced markers of change compared with the rest of the globe. The increase of surface temperature in the Arctic has been significantly greater than the global mean (Trenberth et al., 2007), the terrestrial snow cover in the Northern Hemisphere is declining with model predictions indicating a continuation of that trend (Serreze et al., 2000; Chapin et al., 2005; Post et al., 2009), and Arctic summer sea-ice extent has been trending downward for more than thirty years (Cavalieri and Parkinson, 2012). A new record low in sea-ice was observed in September 2012 that was two times lower than the overall average between 1979 and 2000 (Parmentier et al., 2013). Anthropogenic forcing to the chemical composition of the atmosphere is implicated in triggering observed changes to the climate system (Lemke et al., 2007). Through the study of global climate change in recent decades, it has become apparent that components of the Earth system are intimately linked, and one component cannot be considered without taking into account the others. The research presented here focuses on multiple aspects of the chemical connection between the cryosphere and the atmosphere.

Since the initial observations and findings that Arctic haze was comprised of anthropogenically sourced particulate matter originating from the mid-latitudes, it has been clear that the Arctic atmosphere is not as pristine and secluded as its remote geography would suggest (Barrie, 1986). Unlike the Antarctic atmosphere, which remains relatively undisturbed due to the surrounding

Southern Ocean and the polar vortex, the Arctic is subject to the transport of pollution due to its location near industrialized countries and a large portion of landmasses. The unique nature of the Arctic atmosphere − which is characterized by cold temperatures, drastic radiation cycles, and a stably stratified boundary layer − allows for the occurrence of distinctive chemical mechanisms in the surface layer.

One such occurrence was the detection of episodic, rapid reductions in ground-level ozone (O_3) mole fractions to levels below instrumental detection limits during the springtime in Arctic coastal environments. Tropospheric O_3 is of interest because of its contribution to greenhouse gas forcing, important role in the oxidation capacity of the atmosphere, and harmful impacts on plants and human health (Lippmann, 1991). Additionally, since the pre-industrial era tropospheric O_3 levels have at least doubled, primarily due to increased precursor emissions (Lelieveld and Dentener, 2000; Fusco and Logan, 2003; Vingarzan, 2004; Lamarque et al., 2005; Oltmans et al., 2006). The aforementioned low O_3 events have now been measured since the 1980s in polar coastal regions following sunrise (Oltmans, 1981; Bottenheim et al., 1986; Barrie et al., 1988; Kreher et al., 1996; Wessel et al., 1998). Halogens were quickly implicated as a primary contributor to these so-called O_3 depletion events (ODEs) after early studies showed a clear relationship between reductions in O_3 and enhanced levels of filterable bromide (Barrie et al., 1988; Oltmans et al., 1989). It is thought that a series of photochemical and heterogeneous reactions rapidly release bromide from sea salt (termed the bromine explosion), yet the precise nature of the release of bromine species to the gas phase is not defined (Wennberg, 1999; Platt and Honninger, 2003; Simpson et al., 2007; von Glasow, 2008). Recent research has suggested that one of the main sources of reactive bromine is the photochemical production of molecular bromine in surface snow (Pratt et al., 2013). The number of these depletion events that are recorded each spring is variable and closely linked to transport conditions (events typically occur over the Arctic Ocean and the depleted air masses are transported to coastal measurement sites). However, reductions in sea-ice thickness and extent in the Arctic have been linked to an increase in the number of ODEs in March over the last ∼40 years (Oltmans et al., 2012).

Following the first observations of ODEs, it was discovered approximately a decade later that reductions in gaseous elemental mercury (GEM, e.g. Hg^0) occurred near the Arctic coast and were correlated to ODEs (Schroeder et al., 1998). Existing research suggests that the primary oxidants converting GEM into oxidized inorganic reactive gaseous mercury (RGM) or fine particulate-bound mercury (FPM) are reactive bromine species (Lu et al., 2001; Lindberg et al., 2002; Berg et al., 2003; Sprovieri et al., 2005; Steffen et al., 2008; Stephens et al., 2012). GEM is a long-lived form of mercury that can be transported to the Arctic from lower latitudes. Atmospheric mercury depletion events (AMDEs) are a primary pathway by which GEM can be oxidized, efficiently scavenged, and deposited to the snowpack in the Arctic. Following deposition, mercury can be re-volatilized to the atmosphere or remain in the ecosystem with the potential to bioaccumulate into the environment and biota (Simpson et al., 2007).

Measurements of ODEs and AMDEs were some of the first indications that chemical processes in and on snow and ice surfaces can have significant impact on the chemistry of the planetary boundary layer. Another such process that has been the focus of many studies since first being observed in the 1990s is the production in snow of formaldehyde (HCHO) and oxidized reactive nitrogen gases (such as NO, NO_2, and HONO) at Summit, Greenland and Alert, Canada (Fuhrer et al., 1996; Sumner and Shepson, 1999; Honrath et al., 1999). Upward fluxes of nitrogen oxides (NO_x) have been shown to have a dependence on incoming solar radiation, and have been linked to the photolysis of nitrate in the snow (Dibb et al., 1998; Honrath et al., 2000). Since these initial measurements, the production and also destruction of a range of trace gases have been measured within snow at locations ranging from both poles to mid-latitude seasonal snowpack. The magnitude of the impact of emissions and uptake at the air-snow interface on the chemistry of the overlying atmosphere is dependent on a wide range of parameters including: the substrate beneath the snowpack; snow temperature and physical characteristics such as density and porosity; boundary layer characteristics; and whether the chemistry of the boundary layer is anthropogenically perturbed (Albert et al., 2002; Albert and Shultz, 2002; Domine and Shepson, 2002; Helmig et al., 2007a; Cohen et al., 2007; Bocquet et al., 2007; Grannas et al., 2007; Domine et al., 2008; Seok

et al., 2009). An interesting example of the impact snow chemical processes can have on the overlying atmosphere has been documented at South Pole. This location is unique due to a combination of low snow accumulation rates leading to intense focusing of nitrate in the near-surface snowpack, large NO_x fluxes out of the snow, a long fetch over the Antarctic Plateau allowing NO_x to accumulate in the surface layer, sustained periods of shallow boundary layers, and a chemical environment in which increasing NO_x levels can lead to a non-linear response in the NO_x lifetime (Davis et al., 2004). The combination of these conditions has been shown to lead to NO levels >500 pptv in the surface layer (Davis et al., 2004; Neff et al., 2008; Helmig et al., 2008b). Significant O_3 production in the near surface atmosphere was also observed to be initiated in this environment (Crawford et al., 2001; Helmig et al., 2008a).

O_3 destruction in snow interstitial air has also been observed in the Arctic snowpack, beginning with measurements at Summit, Greenland (Peterson and Honrath, 2001). Levels of O_3 within the snowpack are highly variable on a seasonal and diurnal scale (Helmig et al., 2007a). The mechanisms leading to this destruction are not currently understood. Recently, field measurements have shown that bromine oxide (BrO) is present at Summit even during periods not influenced by marine air (Stutz et al., 2011). The proposed BrO source is the photolytic formation of reactive bromine in snow interstitial air (Dibb et al., 2010; Stutz et al., 2011). Modeling studies have not yet been able to reproduce either the behavior of interstitial air levels of NO_x or the observed magnitude of O_3 depletion in the snow (Thomas et al., 2011, 2012). Accurately characterizing gas-phase chemistry in snow interstitial air is important not only due to the potential impact of emissions and uptake to the overlying atmosphere, but also for the accurate interpretation of ice core records.

Due to the complex dependencies of O_3 in interstitial air in the Arctic, it is expected that atmosphere-snowpack O_3 fluxes will also be variable depending on multiple parameters (Helmig et al., 2009a; Cohen et al., 2007; Bocquet et al., 2011). The sensitivity of surface layer O_3 in the Arctic to surface deposition to snow has been investigated by varying the ozone deposition velocity parameter in a chemistry and transport model while keeping all other conditions unchanged. Results

from this analysis indicated an O_3 sensitivity to surface deposition to snow of up to 20-30% in the Arctic surface layer during winter (Helmig et al., 2007b). This sensitivity study points to the necessity of accurately characterizing O_3 fluxes at the atmosphere-snow interface. With the length of the snow-free season increasing in the Arctic in recent decades (Chapin et al., 2005), quantifying O_3 fluxes to various Arctic vegetation regimes is also important in order to recognize the potentially changing role of O_3 deposition at the surface to the tropospheric O_3 budget in the Arctic.

1.2 Research objectives and thesis outline

The background provided above is intended to give an overview of current knowledge regarding the mechanisms through which snow can influence the chemistry of the overlying atmosphere in the Arctic. In this section I outline each of my research objectives driven by gaps in the current knowledge, and indicate where a discussion can be found in the thesis.

(1) While much progress has been made in describing snow chemistry, many of the mechanisms controlling production and destruction of gases within the snowpack are still not defined. Partially this is due to a lack in observations caused by the difficult nature of measuring trace gases in snow over time scales of weeks or months to years; a time scale that is essential to capturing seasonal variations. As a part of this work a unique snow sampling system was built to continuously measure gases in interstitial air with minimal disturbance to the snowpack. In **Chapter 2**, I address this observational need by presenting the first multi-year record of interstitial air O_3, NO, and NO_2 at multiple heights in the snowpack at Summit, Greenland. This measurement record highlights the significant variability of these trace gases within the interstitial air, with production of both NO and NO_2 and destruction of O_3 observed. The measured constituents were seen to vary along with seasonal and diurnal cycles in radiation and snow temperature, and wind speed variability. Using this extensive data set I examine previous theories for NO + NO_2 production in snow, the majority of which have centered on the photolysis of nitrate in snow leading to enhanced NO_2 in snow interstitial air. This mechanism does not entirely explain the observations presented here, so I close this chapter by investigating other possible processes by which O_3 destruction and

NO_2 production could occur.

(2) As described in Section 1.1 for South Pole, a combination of conditions including emissions of trace gases at the snow-air interface and atmospheric boundary layer dynamics have been shown to lead to significantly enhanced levels of NO in the near surface atmosphere (<50 m) (Davis et al., 2001; Neff et al., 2008; Helmig et al., 2008b). At South Pole, elevated levels of NO during periods of sustained stable conditions characterized by shallow boundary layers also led to significant O_3 production in the surface layer (Crawford et al., 2001; Helmig et al., 2008a). These results show that emissions and uptake at the snow-air interface have the potential to substantially impact surface layer chemistry. In **Chapter 3** I investigate the role of the boundary layer in determining near surface chemistry at Summit, Greenland. Using diagnostic models that incorporate measured surface turbulence parameters, I calculate estimates of the boundary layer depth at this location in the summer. These estimates are compared to boundary layer depths derived from a minisodar to assess the relative importance of surface stress and heat exchanges on the development of the stable boundary layer at Summit. Following this, boundary layer depths are evaluated alongside ambient O_3 and NO_x to quantify the importance of this feature in determining trace gas levels.

(3) Based on prior measurements (detailed in Section 1.1) snow chemistry is not expected to be the same at all locations. Rather, it is known that many factors contribute to air-snow interactions and the resulting influence reflected on tropospheric chemistry. Motivated by the rapid environmental changes observed in the Arctic in recent years, I was interested in looking at an Arctic location with seasonal snow cover to investigate surface layer chemistry during the transitional period in spring when solar radiation is reintroduced, and then snow melt rapidly occurs. Understanding this transitional period has implications for surface layer chemistry in the Arctic based on projections of reduced snow cover and sea ice at these latitudes. The springtime subset of a one-year record of measurements from Toolik Lake, AK was implemented for this purpose. Particularly, I was intrigued that springtime ozone and gaseous elemental mercury (GEM) depletion events were measured at this site, located several hundred kilometers from the coast where these events are typically observed. In **Chapter 4** I show detailed surface O_3 and GEM

measurements throughout the Arctic springtime at Toolik Lake and the available coastal location of Barrow, AK. These records are used to investigate the frequency and strength of inland occurring depletion events and FLEXPART simulations are applied to describe transport pathways prior to and during the occurrence of the observed events.

(4) As mentioned in (3), I was motivated to use the observational record from the seasonally snow covered site at Toolik Lake to investigate what differences in tropospheric O_3 chemistry evolve when snow cover is removed. This understanding is critical due to the interesting feedback loops present between reduced snow cover extent, enhanced regional warming, and vegetation changes in the Arctic (Chapin et al., 2005). Snow melt occurred on the order of days following warm spring temperatures at Toolik Lake, and surface layer O_3 behavior changed drastically at that time. Specifically, a significant diurnal cycle developed immediately, with amplitude greater than any observed north of the Arctic circle previously. In **Chapter 5** I investigate the factors contributing to this sudden change in atmospheric O_3 behavior over tundra during the summertime. O_3 deposition velocities to the tundra are also characterized at this location, adding to very limited prior observations of O_3 deposition to tundra in the high Arctic.

Lastly, a summary of the work accomplished and concluding remarks are presented in **Chapter 6**.

Chapter 2

Multi-year observations of O_3 and NO_x dynamics in Summit, Greenland snow

This chapter is adapted from: **Van Dam, B., Helmig, D., Toro, C., Doskey, P., Kramer, L., Murray, K., and Seok, B. (2013)** in preparation to be submitted to Atmospheric Environment.

2.1 Abstract

A multi-year record of ozone (O_3) and nitrogen oxides (NO_x) in snowpack interstitial air down to a depth of 2.8 m at Summit, Greenland, is presented. Snowpack O_3 values ranged from 30-40 ppbv during winter months, and dropped below 10 ppbv in summer. Wintertime NO_x levels were very low at all depths in the snowpack (below 10 pptv for NO and below 25 pptv for NO_2). In the summer, NO values up to 120 pptv and NO_2 values >500 pptv were observed. O_3 depletion within the snowpack was observed throughout all seasons, and the magnitude of depletion closely tracked the seasonal cycle of incoming short wave solar radiation. NO production within a shallow layer of the snowpack was recorded during the spring and summer months. NO_2 production also occurred, and heightened levels were measured down to 2.5 m in the snowpack. The average daily maximum in NO was observed at solar noon, and the minimum was seen during night. The daily peak in NO_2 was on average shifted 7-hr later than the incoming solar radiation and NO maximums. The investigation of a case study period showed that wind pumping has a distinct impact on snowpack interstitial air levels of O_3 and NO_x down to a depth of greater than 2 m. This extensive set of observations illustrates that the current understanding of snowpack physical

processes and chemical mechanisms is not adequate to describe the dynamic O_3 and NO_x chemistry occurring within snowpack interstitial air at Summit, Greenland. The understanding of how these constituents are cycled within the snowpack and the influence this chemistry has on the overlying atmosphere is critical for describing budgets within the boundary layer at this location and for the interpretation of ice cores.

2.2 Introduction

Since the discovery of the role of chemistry occurring on snow and ice surfaces in polar ozone (O_3) and mercury depletion events in spring (Oltmans, 1981; Barrie et al., 1988; Oltmans et al., 1989; Foster et al., 2001; Simpson et al., 2007), snow photochemistry has been the focus of field studies at numerous sites in the Arctic and Antarctic. Each snow-covered location investigated has shown a unique relationship between active snow photochemistry and the resulting influence on the overlying atmosphere. At Summit, nitrogen oxide (NO_x [NO + NO_2]) production in and subsequent release from the snowpack was first measured in the 1990s (Honrath et al., 1999). This NO_x production was hypothesized to be linked to the photolysis of deposited nitrate (NO_3^-) in snow and suggests a photochemical NO_x source in surface snow to the boundary layer (Honrath et al., 1999; Jacobi et al., 2004). At South Pole, the influence of sustained shallow boundary layers and photochemically mediated release of NO_x from the snow was shown to lead to significant increases of NO and photochemical production of O_3 in the surface layer (Crawford et al., 2001; Davis et al., 2001, 2004; Neff et al., 2008; Helmig et al., 2008b,a). Interestingly at Summit, surface energy exchanges and boundary layer depths exhibit diurnal cycles and dynamic behavior during the summertime as compared with South Pole, and a direct relationship between boundary layer depths and surface NO and O_3 has not been shown despite the observation of snowpack to atmosphere NO_x fluxes (Dibb et al., 2002; Honrath et al., 2002; Cohen et al., 2007; Helmig et al., 2009b; Van Dam et al., 2013).

At all Arctic, Antarctic and mid-latitude locations investigated, a reduction of O_3 concentrations with depth in the snowpack has been observed. This depletion with depth has been shown to

be influenced by various factors, including snow physical and chemical properties, incoming solar radiation levels, meteorological conditions, and the substrate underlying the snowpack (Seok et al., 2009; Helmig et al., 2007a; Bocquet et al., 2007). At Summit, O_3 depletion in the snowpack was first described in the early 2000s, and hypothesized to be due to either chemical or physical processes in the snowpack (Peterson and Honrath, 2001). The finding that O_3 is predominantly deposited or chemically destroyed in snow suggests that the Arctic snowpack acts as a sink for boundary layer O_3 (Helmig et al., 2007c). Modeling sensitivity studies have demonstrated the importance of O_3 deposition to snow in the accurate representation of Arctic tropospheric O_3 budgets, particularly during the wintertime (Helmig et al., 2007b).

The mechanism and dependencies of O_3 depletion in the snowpack (and as a result, chemical fluxes at the air-snow interface) are not well understood. Reactive bromine has been observed in the near-surface atmosphere recently at Summit (Dibb et al., 2010; Liao et al., 2011; Stutz et al., 2011), and it is hypothesized that bromine and NO_x chemistry in snow play an important role in observed O_3 depletion. Recent results from a one dimensional snow chemistry and atmospheric boundary layer model have not been able to accurately reproduce the magnitude of summertime O_3 depletion within snow incorporating only the hypothesized NO_x and bromine chemistry (Seok et al., 2010; Thomas et al., 2012). In the Thomas et al. (2012) study interstitial air NO_x measurements were cited as necessary to determine if the model was accurately representing snowpack NO_x chemistry.

Here, I present multi-year, continuous measurements of O_3 and NO_x in interstitial air in the Summit snowpack. With this extensive set of observations it is possible to quantitatively describe seasonal and diurnal cycles in O_3 and NO_x, the distribution of these constituents with depth in the snowpack, and the influence of wind pumping on various levels in the snowpack. Understanding the driving factors influencing O_3 and NO_x concentrations in snow is necessary in determining to what extent snowpack photochemistry is influencing trace gas levels in the lower atmosphere at this location. Observations presented here will be critical for use in assessing the ability of current models to reproduce NO_x chemistry in the snow, and determining the mechanisms responsible for the observed snowpack depletion of O_3.

2.3 Methods

2.3.1 Atmospheric measurements

Summit Station, Greenland is a research facility operating year-round near the summit of the Greenland Ice Sheet (72.6°N, 38.5°W; 3200 m above sea level). The study site for research described here included a buried laboratory facility, snow-sampling manifold, and a meteorological tower installed in the clean air sector ∼650 m south-west of the main camp structures. Year round measurements were conducted from June 26, 2008 to July 22, 2010, totaling 756 days (just over 2 years) in operation. Meteorological conditions were measured on a ∼9 m tower. Instrumentation included a cup anemometer for wind speed (Model 010C, MetOne Instruments), combined cup anemometer and wind vane for wind speed and direction (Model 030B, MetOne Instruments), and a type-E thermocouple housed in an aspirated radiation shield for ambient temperature (R.M. Young Co., Model 43408). Two pyranometers for incoming and reflected solar radiation (LI-COR Biosciences Model LI-200) were mounted at ∼1.25 m height on a separate tower several meters south of the meteorological tower. The wind speed and temperature measurements were originally installed at a height of 9 m and by the end of the sampling period were 6.2 m above the snow surface due to drifting and accumulation around the tower base.

2.3.2 Snow interstitial air

2.3.2.1 Sampling system

A multi-inlet snow sampling tower for measuring trace gases in interstitial air was constructed for use in this study. A schematic of this system and several pictures from throughout the measurement campaign are shown in Figure 2.1 (a)−(d). This tower has a similar design to that described by (Seok et al., 2009). The tower system originally consisted of a vertical post of square aluminum alloy (3.8 cm x 3.8 cm) with eight 60 cm long cross arms vertically spaced every 30 cm. To install the sampling tower, a 1 m deep hole with opening ∼1 m x 1 m was carefully excavated from the snowpack at the end of May 2008. The sampling tower was placed within the hole and snow was

allowed to accumulate naturally, a process which occurred on the order of days following increased wind speeds. Figure 2.1 (a) depicts the condition of the snow tower in July 2008, approximately one month after the system was installed.

Each cross arm on the tower hosted a pair of sampling inlets, and was rotated orthogonally to the arm above and below. This paired and rotated system was designed to minimize flow through each inlet and reduce disturbance to the snowpack. A flow rate of $1.5-2.5$ L min^{-1} was used depending on the number of chemical measurements conducted. Split between the inlet pairs, this gives an effective flow rate of $0.75-1.25$ L min^{-1} through each inlet. Additionally, as described later, due to the measurement method the snow at each inlet pair was only sampled for 10 min during each $80-140$ min sampling cycle. Each sample inlet was fitted with a 25 mm Acrodisc®hydrophobic polytetrafluoroethylene (PTFE) syringe filter (Pall Life Sciences, Ann Arbor, Michigan, USA). Inlet pairs were connected via a Teflon union tee to a 30 m Teflon sampling line (perfluoroalkoxy copolymer [PFA]) with 0.64 cm outer and 0.40 cm inner diameter. In addition to the gas sampling inlets, each cross arm was fitted with a type-E thermocouple to acquire the temperature at each level within and above the snow. The trace gas sampling lines and thermocouples were each $\sim$35 m and were carried under the snow surface inside an insulated, temperature controlled conduit to the buried laboratory where all instrumentation was housed. Within the laboratory, each of the original eight sampling lines was connected to a solenoid valve manifold which allowed for control of the measurement height (sample inlet pair). An automatic sampling pattern was implemented whereby each pair of inlets was measured sequentially from the uppermost to deepest level. During the snow tower sampling sequence, each inlet level was sampled for 10 min.

Due to snow accumulation and drifting, the uppermost level on the snow sampling tower was less than 10 cm above the snow surface by June 9, 2009. In order to ensure continued measurements through the near-surface snowpack levels an extension to the snow tower was installed on August 21, 2009. This extension added 6 additional vertical levels spaced 30 cm apart to the top of the original tower. Installing the added snow tower gas sampling lines required digging near the tower, yet it was possible to leave the snow in the immediate vicinity of the inlets undisturbed through

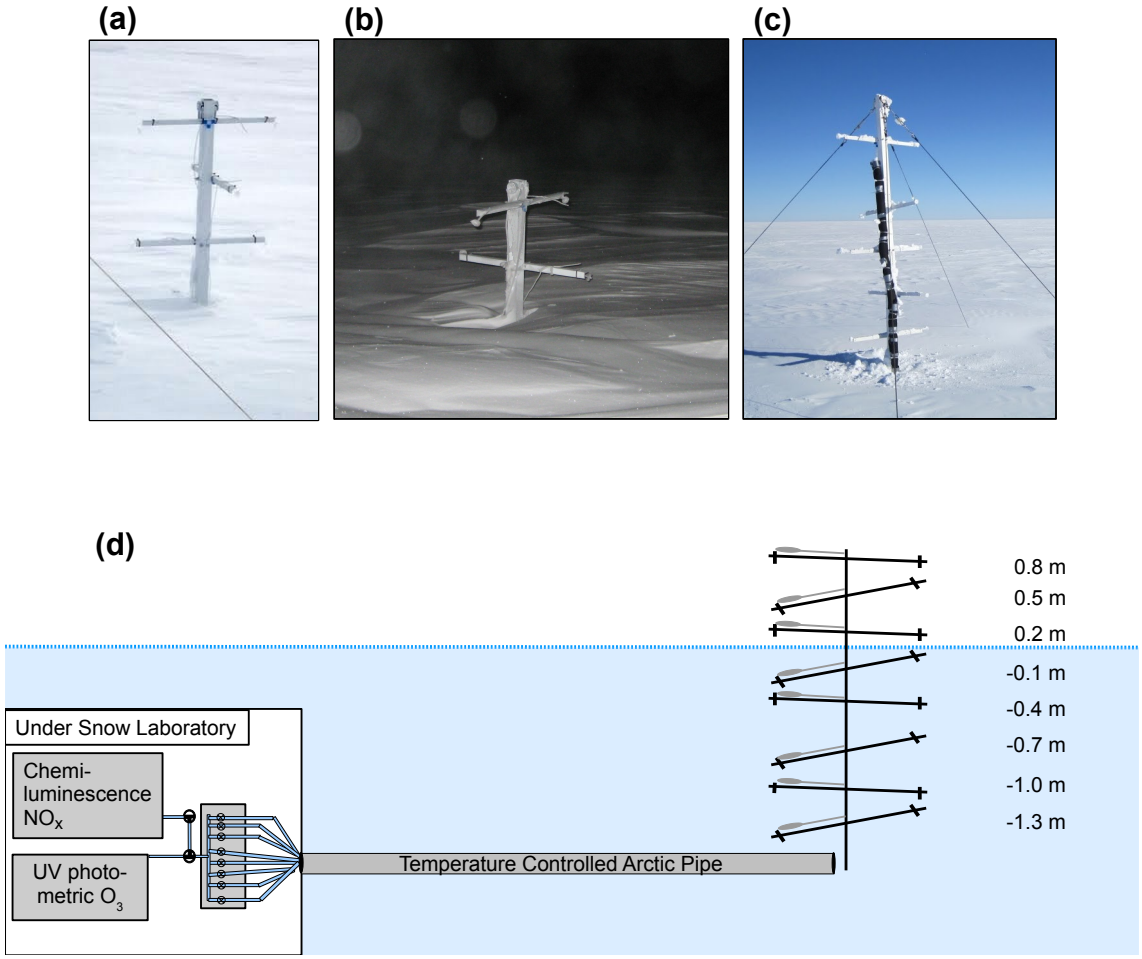

Figure 2.1: Images of the snow-sampling tower implemented in this study from (a) July 2008, (b) November 2008, and (c) April 2010. Part (d) shows a simplified schematic of the snow tower system. Grey lines on the tower indicate thermocouples used to measure snowpack temperatures, and black crosses indicate gas sampling inlets.

this process. Originally, the snow sampling tower acquired gas measurements at 8 levels spaced 30 cm apart with a minimum of 1 m depth in the snowpack, maximum of 1.1 m height above the snow surface, and a sampling sequence of 80 min. When the extension was installed in August 2009, the system began measuring a total of 14 levels at 30 cm spacing with a range of 2.1 m depth in the snowpack up to 2.2 m above the snow surface, and sampling sequence of 140 min. At the end of the measurement period in July 2010, gas measurements were acquired at 30 cm intervals from a snowpack depth of 2.9 m through 1.4 m above snow surface. Figure 2.1 (a), (b), and (c) show the status of the snow sampling tower in July 2008, November 2008, and April 2010, respectively.

2.3.2.2 O_3 measurement

O_3 was measured from the snowpack tower system using a Model 49 UV photometric O_3 analyzer (Thermo Environmental Instruments (TEI), Franklin, MA) with calibration traceable to the U.S. National Institute of Standards and Technology (NIST). The standard instrumental detection limit and precision are 1 ppbv, and the response time is 20 s. O_3 was sampled at 10 s, averaged to 1 min. Prior to operation the entire snow sampling system including inlet filters, sampling lines, and valve manifold were conditioned by purging with air containing ∼300 ppbv O_3 at a flow rate of 3 L min^{-1} for 24 hrs. In the course of switching between sampling levels gas concentration levels required ∼1-2 min to stabilize at the lower inlet level value. In the final data processing the first 3 minutes and last 2 minutes of each 10 minute sampling sequence were removed, and the mean of the 5 remaining values (5 minutes) was used as the final value for that inlet and sampling interval. An example of one snow tower cycle including the O_3 measurement, line pressure and flow rate is included in Figure 2.2.

2.3.2.3 NO_x measurement

The NO_x instrument implemented in this study was based on a previous version of the system deployed at Summit (Honrath et al., 2002) and Alert, Canada (Beine et al., 2002). The new system was updated to run autonomously and with an improved calibration system. NO and NO_2 mixing

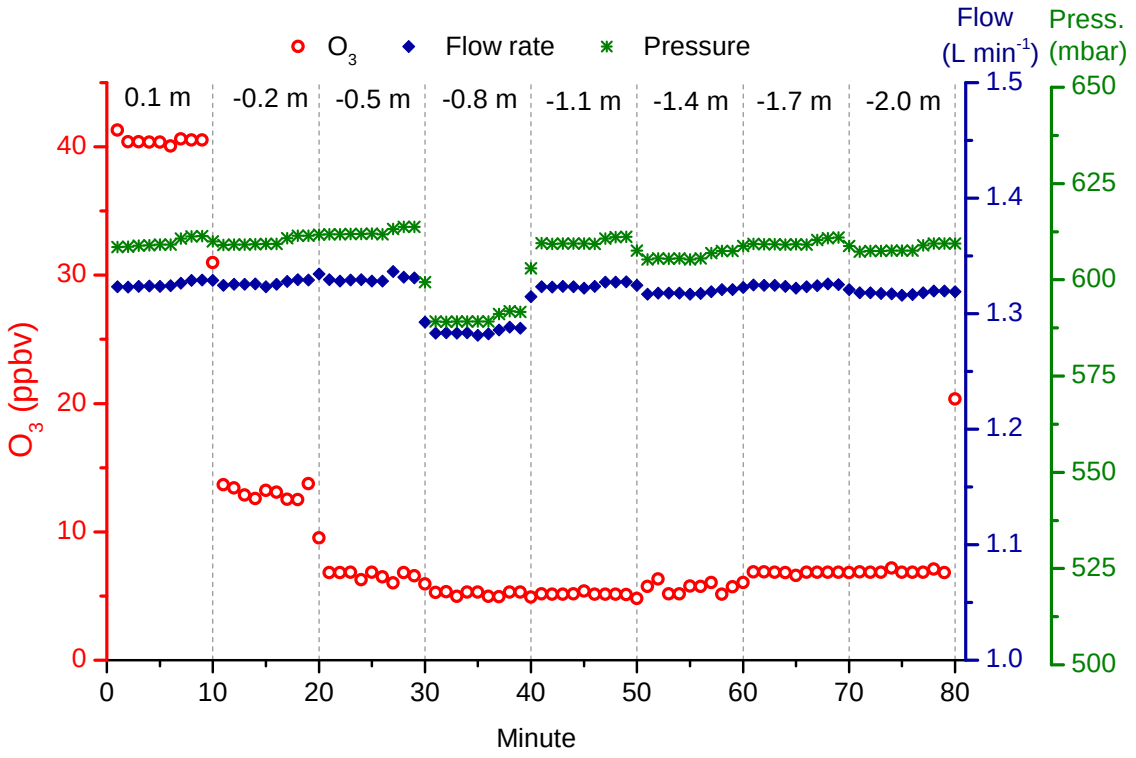

Figure 2.2: An example of one measurement cycle on the snow tower. One minute averages of ozone mole fractions (open circles), the flow rate in the sampling line (filled diamonds), and the pressure in the sampling line (stars) are shown as a function of time. Colors correspond to the sampling level in relation to the snow surface. Each level is sampled for 10 minutes.

ratios were measured by alternatively sampling between two inlets on the meteorological tower and the inlets on the snowtower. NO and NO_2 were determined using established techniques. NO was detected through the chemiluminescence reaction with O_3 (Ridley and Grahek, 1990) and NO_2 through the conversion to NO by UV photodissociation (Kley and McFarland, 1980). The updated instrument utilizes a photolytic NO_2 converter (Air Quality Design Inc., Wheat Ridge, CO, USA) to reduce any interference from the conversion of other gas species to NO.

Calibrations to determine the NO sensitivity and NO_2 conversion efficiency were incorporated twice daily by the standard addition of NO in N_2 ($\pm$2%; Scott Marrin, which was referenced to a NIST calibration) into an inlet on the meteorological tower. The NO_2 conversion efficiency was determined via the gas phase titration of NO and O_3 via a low pressure mercury lamp. Automated measurements for the NO and NO_2 artifacts are conducted using zero air (Breathing air grade, Airgas, Radnor, PA, USA) every 3 days. A cycle of measurements was performed every 10 minutes which included a 30 second average for NO and NO_2 from two inlets on the meteorological tower and one inlet on the snow tower.

Losses occur from the reaction of NO and O_3 within the sampling lines which results in an underestimation of NO mixing ratios and an overestimate of NO_2 mixing ratios. Corrections were applied for this loss based on the O_3 and NO mixing ratios and the residence time within the sampling line as given by:

$$[NO]_t = [NO]_0 e^{-kt[\mathrm{O_3}]} \tag{2.1}$$

Where $[NO]_t$ is the mixing ratio of NO detected at the instrument after a residence time, t, k is the rate constant for the reaction between O_3 and NO ($k = 1.2\text{x}10^{19}$ cm^3 molecule^{-1} s^{-1} at $T = 0°$C, (Atkinson et al., 2004)) and $[O_3]$ and $[NO]_0$ are the mixing ratios of O_3 and NO at the inlet.

The first step in the correction is to determine the decrease in the sensitivity of the instrument due to the loss of NO calibration gas from the reaction with ambient O_3 within the sampling line, using reaction 2.1. A further correction is then applied by applying reaction 2.1 to the measurements at each inlet. Through these calculations the overestimation of the NO mixing ratio can be defined

as:

$$\Delta[NO] = [NO]_t = [NO]_0 \tag{2.2}$$

All the sampling lines were covered and protected from any light source to ensure that the photolysis of NO_2 to NO does not occur and therefore it is possible to state that the magnitude of the overestimation in [NO] is equal to the underestimation in [NO_2].

2.3.2.4 Gas measurement uncertainties and data filtering

All trace gas data reported here is filtered first for north wind conditions, as during these conditions polluted air from the main camp facilities has the potential to be transported into the clean air sector. For the purposes here, these north wind conditions are defined to be between 315°-45°. During the entire snowpack measurement period, this filter removed 12% of the data. Additionally, a filter was applied to remove data when insufficient sample flow reached the instruments. This flow rate threshold was different for the O_3 and the NO_x instrument. The flow rate was monitored at the valve manifold. Due to drastic temperature changes near the snow surface, ice accumulation occurred in several of the near-surface sample lines during the springtime which resulted in restricted flow through the sampling tubing. Low flow conditions led to removal of 6% of the snowpack NO_x data. The commercial O_3 sensor implemented here is robust and can handle a wider flow range; thus the low flow rate filter removed only 1% of snowpack O_3 data.

2.4 Results

In order to comprehensively discuss O_3, NO, and NO_2 chemistry in the interstitial air of the snowpack at Summit during a multi-year period it is intuitive to begin with a broad view, and then incrementally investigate smaller time scale influences and variations. In this vein, section 3.1 begins with an investigation of seasonal changes in O_3 and NO_x. Smaller scale effects such as diurnal cycles, detailed depth distributions, and meteorological influences are discussed in sections 3.2−3.3. Section 4 contains hypotheses and potential mechanisms leading to the observations detailed within this section. In all measurement descriptions, various layers measured with respect to the snow

surface are referenced. For example, the 30−60 cm snowpack layer indicates a level that ranges from 30 cm depth in the snowpack (as measured downward from the snow surface) to 60 cm depth in the snowpack.

2.4.1 Seasonal cycles

2.4.1.1 Solar radiation and snow temperature

A box plot showing monthly variations of incoming solar radiation at Summit is displayed in Figure 2.3 to illustrate the drastic seasonal cycle. At Summit, wintertime solar radiation remains less than 30 W m^{-2} for the months of November, December, and January. In summer, incoming solar radiation varies on the order of 95% between night and day, with maximum levels approximately 700 W m^{-2} during clear sky conditions. During the transitional seasons of spring and summer, incoming shortwave radiation levels change rapidly between the winter and summer extremes.

Snowpack temperatures, as shown in Figure 2.4, show very different behavior at the near surface compared to deeper levels. Daily average atmospheric temperatures measured within 20 cm above the snow surface agreed with the snowpack temperature in the 0-30 depth layer to within ∼10%, indicating daily fluctuations in atmospheric temperature are reflected in the near-surface snowpack. Fluctuations in atmospheric temperature on a time scale of 10 days or less were not reflected at all within the snowpack below 150 cm depth. In general, the snowpack temperature measured deeper than 150 cm lagged approximately one month (30-32 days) behind the temperature measured within 30 cm of the surface (determined by comparing daily means). All daily mean temperatures measured at levels deeper than 150 cm in the snowpack agreed to within 1-2 °C during the cooling period in fall and winter. After reaching a minimum temperature in the spring (in 2009, for example, the minimum daily average recorded below 150 cm was -37°C, measured on March 28), each level generally lagged ∼5 days behind the level 30 cm above it during an initial warming period. The maximum daily average temperature recorded below 150 cm in snow was

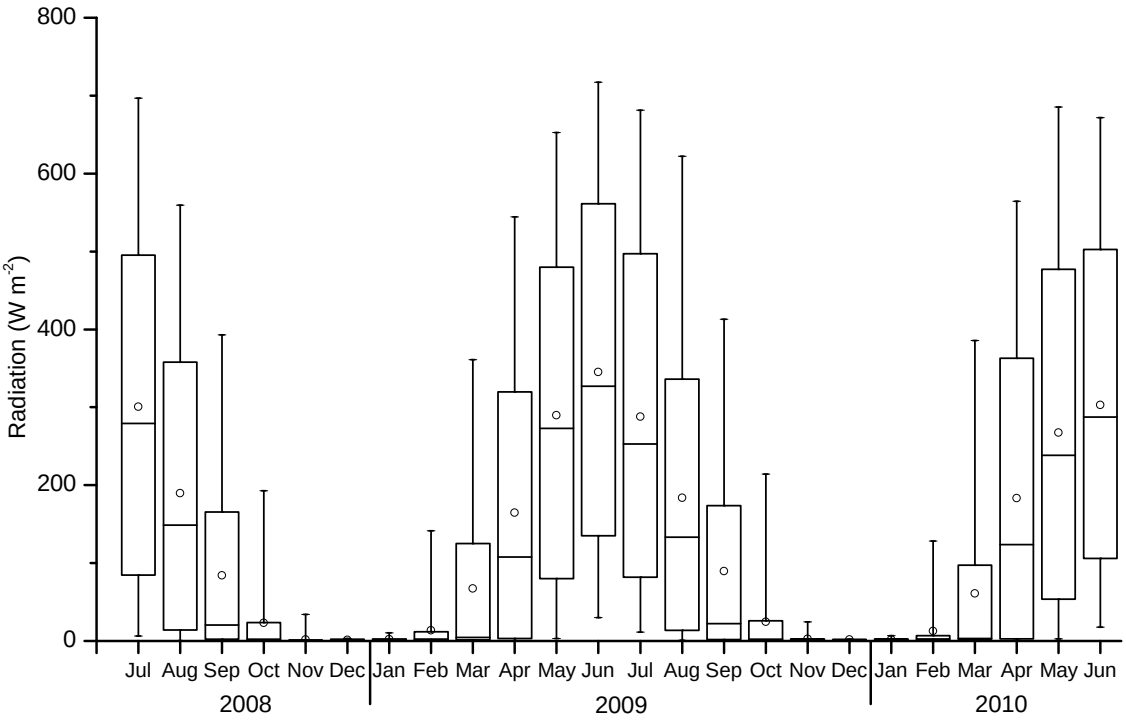

Figure 2.3: Monthly box plots of the incoming solar radiation through the entire measurement period. Upper and lower lines of the box correspond to the 5th and 95th percentile levels, whiskers indicate the minimum and maximum monthly value, the line within each box corresponds to the monthly median value, and the open circles indicate the monthly mean.

-20°C on August 27. Thus, the 2009 seasonal amplitude of daily average snowpack temperature below 150 cm was 17°C. The spring season varied significantly between 2009 and 2010. In 2009 there was an extreme cold period, where the daily average atmospheric temperature at 10 cm and the snowpack temperatures between 0 and 60 cm depth all dropped below -40°C for 26 days straight. The lowest daily average in snow during that period was -56°C. In contrast, no such extreme and persistent cold period was recorded in 2010, although a shorter intense cold period was measured at the surface to 60 cm depth for ∼10 days in December.

Figures 2.5 (a), (b), and (c) show color contour plots of O_3, NO, and NO_2 respectively, as a function of time and depth within the snowpack. These data were obtained from the snow sampling system described above, and show for the first time a continuous, multi-year record of these trace gases in the interstitial air of the snowpack at Summit. Daily averages are plotted as a function of the inlet height (or depth) relative to the snowpack surface. Changes in snowpack depth relative to the tower inlets were measured daily during summer and 2-3 times per week during late fall, winter, and early spring. Color contours describe mole fractions in ppbv (O_3) or pptv (NO_x). This extensive data set highlights a pronounced seasonal cycle present in O_3, NO, and NO_2 in snow interstitial air at this high latitude site. Within the snowpack O_3 varies from less than 10 ppbv to ∼45 ppbv; NO varies from less than 10 pptv to greater than 100 pptv; and NO_2 varies from less than 50 pptv to greater than 600 pptv. The seasonal cycle in each of these constituents is described in the following sections.

2.4.1.2 O_3

Figure 2.5 (a) shows depletion of snowpack O_3 as compared with ambient levels during the year; no instances of a negative gradient (ambient−snowpack levels) are recorded. While snowpack levels are always either on the order of or lower than ambient levels, the magnitude of the reduction of O_3 in the snowpack changes considerably between summer and winter. During the wintertime, O_3 levels within the 60-90 cm snowpack depth layer were similar to atmospheric levels. In May, June, and July, minimum daily O_3 values in the 60-90 cm snowpack depth layer are up to 91%

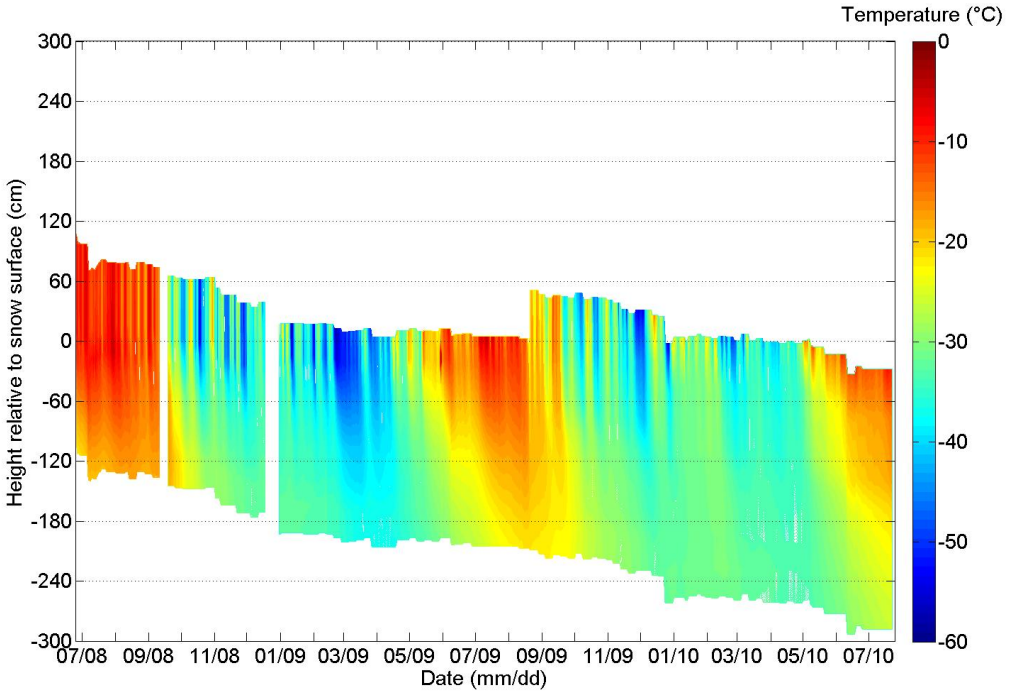

Figure 2.4: Snowpack temperature through the entire measurement period. The vertical axis is the height or depth of the measurement relative to the snowpack surface. The horizontal axis shows the month and year. Color contours show daily mean temperature in degrees Celsius.

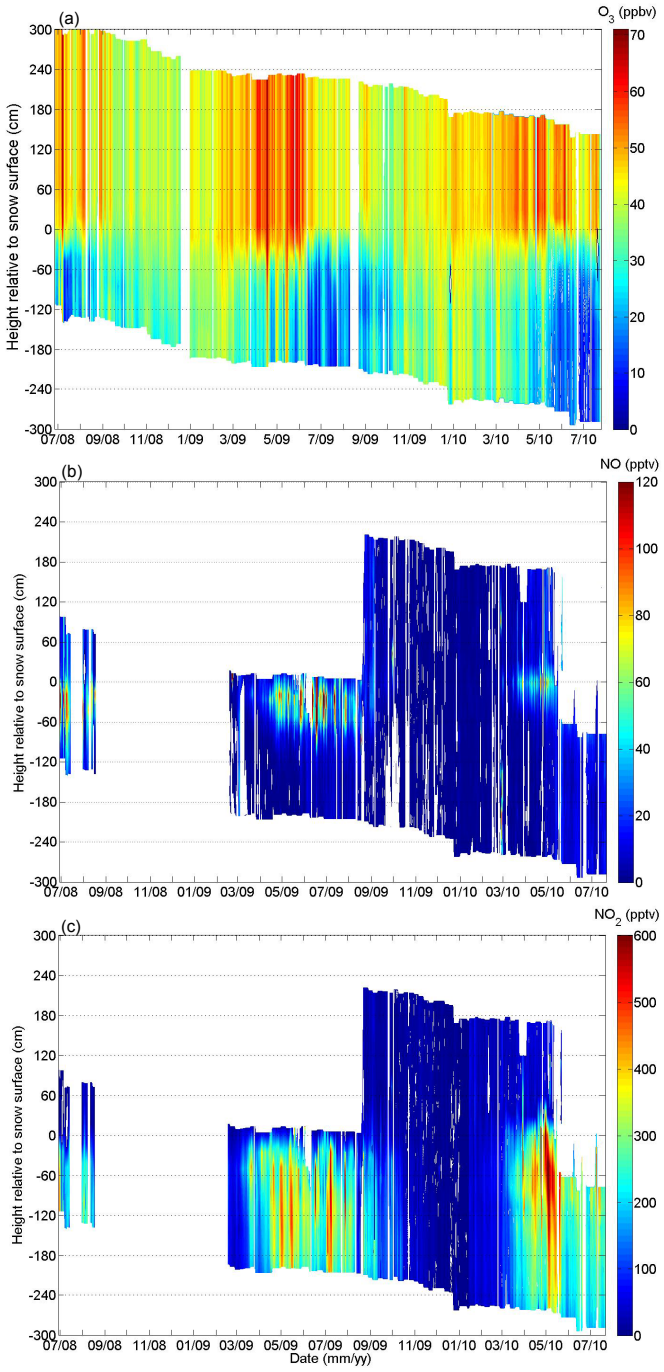

Figure 2.5: Daily mean levels of (a) O_3, (b) NO, and (c) NO_2 through the entire measurement period. The vertical axis is the height or depth of the measurement relative to the snowpack surface. The horizontal axis shows the month and year. Color contours show trace gas mole fractions.

lower than ambient levels. In contrast, during the months with the lowest solar radiation levels (November, December, and January) minimum daily O_3 values in the same snowpack depth layer show on average 12%, and up to 28%, loss compared to ambient values.

To investigate in more detail seasonal changes in snowpack chemistry with depth, Figure 2.6 (a)−(f) provides seasonally averaged depth profiles of O_3, NO, and NO_2. For the purposes of this analysis, summer is defined as May 1 − July 31, and winter is defined as November 1 − January 31, based on the months with the seasonal maximum and minimum solar radiation levels shown in Figure 2.3. These figures combine the entire measurement period, therefore two winter seasons and portions of three summer seasons are shown. Trace gas mole fractions were binned by 30 cm depth layers in the snowpack, and statistics for each depth and season were calculated.

In general, a larger standard deviation is observed in O_3 during the summer, indicating dynamic behavior (reductions and recovery) within the snowpack compared to winter. Summertime atmospheric O_3 levels are higher in summer than winter. In snow, median O_3 values in winter and summer are within 1 ppbv of ambient in the 0-30 cm depth layer (38.9 ppb and 38.2 ppbv respectively). Summertime median O_3 values decrease rapidly in the shallow snowpack layers, and then remain less than 23 ppbv at depths below 90 cm.

2.4.1.3 NO + NO_2

Figures 2.5 (b) and (c) detail snowpack interstitial air levels of NO and NO_2 through the entire measurement period. There was little temporal or spatial variation in ambient or snowpack NO and NO_2 during winter. Mean and median NO levels were below 10 pptv, with maxima not exceeding 50 pptv in the snowpack. Mean and median NO_2 levels were below 25 pptv during winter, with maxima not exceeding 100 pptv in the snowpack. Beginning in March, enhancements of NO and NO_2 were observed in snow. Enhancements of NO were constrained primarily to a near surface layer ranging from 0 to 60 cm depth within the snowpack. Meanwhile, enhanced NO_2 mole fractions were observed much deeper in the snowpack, down to the lowest measurement inlet available (as deep as 2.5 m in the spring of 2010). The amplitude and diurnal cycle of these enhancements is

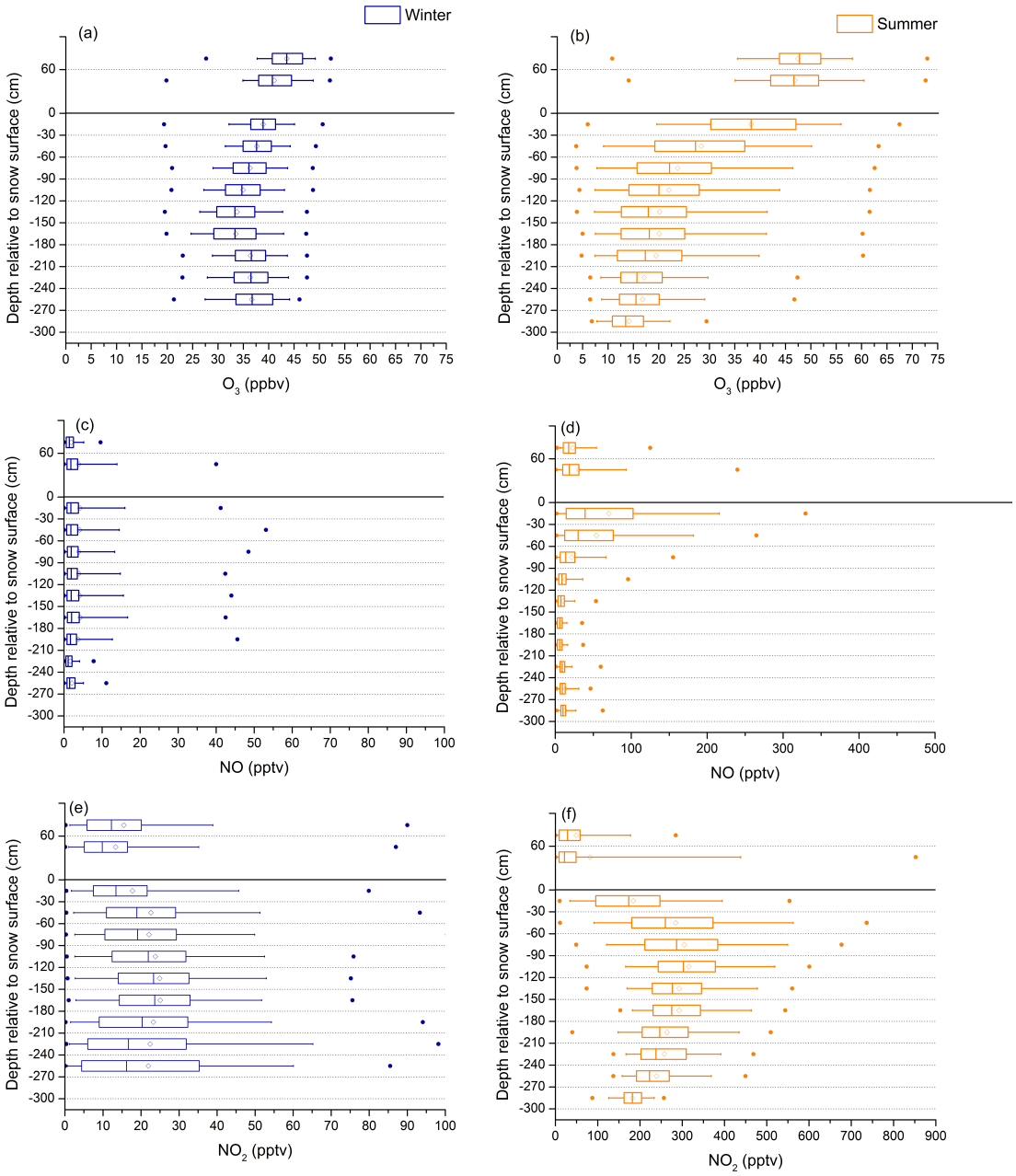

Figure 2.6: Seasonally averaged (a) O_3, (b) NO, and (c) NO_2 as a function of depth. All data from 2008 – 2010 were filtered by season, and then binned by 30 cm depth layer within the snowpack. Open circles indicate the median value, upper and lower box limits are the 25th and 75th percentile with the line indicating the mean, whiskers indicating 5th and 95th percentile, and the filled circles showing maximum and minimum values. Two layers were used above the snow surface: a 0-30 cm layer, and then all data over 30 cm were combined into the ambient measurement. Note the different scales on the x-axis for each constituent.

discussed below.

Figure 2.6 panels (c) − (f) show the seasonally averaged depth profiles of NO and NO_2 observations. In the winter (panels (c) and (e)), NO remained below 10 pptv and NO_2 below 50 pptv at all snowpack levels, as well as in the atmosphere. During summer (panels (d) and (f)), NO and NO_2 values showed dissimilar behavior with depth in the snowpack. NO enhancements occurred in a narrow depth range from 0 to 60 cm below the surface. Atmospheric levels of NO close to the surface were elevated slightly over winter time data, with a larger range in values. Below 60 cm in the snowpack, summertime median NO was similar to winter median values, on the order of 10-15 pptv. While NO_2 also shows enhanced concentrations in the shallow layer between 0 and 60 cm depth, the highest median mole fraction (300 pptv) is observed deeper within the snowpack, in the 90-120 cm depth range. The distribution of NO mole fractions below a depth of 60 cm was not significantly different between seasons. In contrast, summer NO_2 enhancements peaked at the $90 - 120$ cm depth and remained enhanced significantly over atmospheric values to the lowest measured depth range of $270 - 300$ cm below surface. Also interesting to note is that while the highest summer snowpack NO median was measured in the $0 - 30$ cm depth layer, this was the layer corresponding to the lowest median snowpack NO_2 level in summer (although still higher than ambient values).

2.4.2 Diurnal cycles

The higher standard deviations of snowpack interstitial air O_3 and NO_x in summertime beg an investigation into diurnal cycles in O_3 and NO_x during the different seasons. Figures 2.7-2.9 display the median hourly O_3, NO, and NO_2 value for each layer in the snowpack; panels (a)−(d) for each figure further divide the data by the winter, spring, summer, and autumn seasons (as described above based on radiation levels in Figure 2.3, the seasons are defined for the purposes of this study as: winter is Nov − Jan; spring is Feb − Apr; summer is May − Jul; and autumn is Aug − Oct). Local time at Summit is GMT − 2. These figures present an average diurnal cycle for each constituent within each snowpack layer during all seasons. All atmospheric values are binned

together in this analysis, as are measurements below 150 cm depth in the snowpack. The hourly averaged radiation cycle is included with each figure panel for reference.

2.4.2.1 O_3

Figure 2.7 focuses on O_3 in the snowpack in (a) winter, (b) spring, (c) summer, and (d) autumn. Panel (a) in this figure demonstrates that no diurnal cycle is present on average during the winter months. Hourly averaged O_3 mole fractions remain in a narrow range between 30−45 ppbv. Looking at panels (b)−(d), it is clear that when incoming solar radiation is present conditions are drastically different in the snowpack. O_3 values are reduced below ambient at all levels within the snowpack. The maximum depletion occurs deepest in the snowpack during summer. The highest magnitude of the hourly averaged diurnal cycle occurs in the 30−60 cm depth layer during the summer, where the daily amplitude is 13 ppbv.

Interestingly, the spring and autumn conditions are not identical even though the amount of incoming radiation present is very similar. Hourly-averaged daily atmospheric O_3 concentrations are at a maximum during the spring, as has been described previously by Helmig et al. (2007c), while autumn atmospheric concentrations are ∼10 ppbv lower and in the same range as winter. In the snowpack, springtime interstitial air O_3 values are generally higher than fall. In particular, significant O_3 depletion is not observed in the shallowest snowpack layer (0−30 cm depth), in contrast to summer and fall. However, the magnitude of the average diurnal cycle is greater in spring (on the order of 10−15 ppbv difference between daily median maximum and minimum in the layers between 30 and 120 cm depth in the snow) than in autumn (8−10 ppbv difference between daily median maximum and minimum in the same snowpack layers).

2.4.2.2 NO + NO_2

Figures 2.8 and 2.9 follow the same format as Figure 2.7 except showing NO and NO_2, respectively. Panel (a) in both figures demonstrates that, similar to O_3, no diurnal cycle is present on average during the winter months. As noted in section 3.1, wintertime NO mole fractions stayed

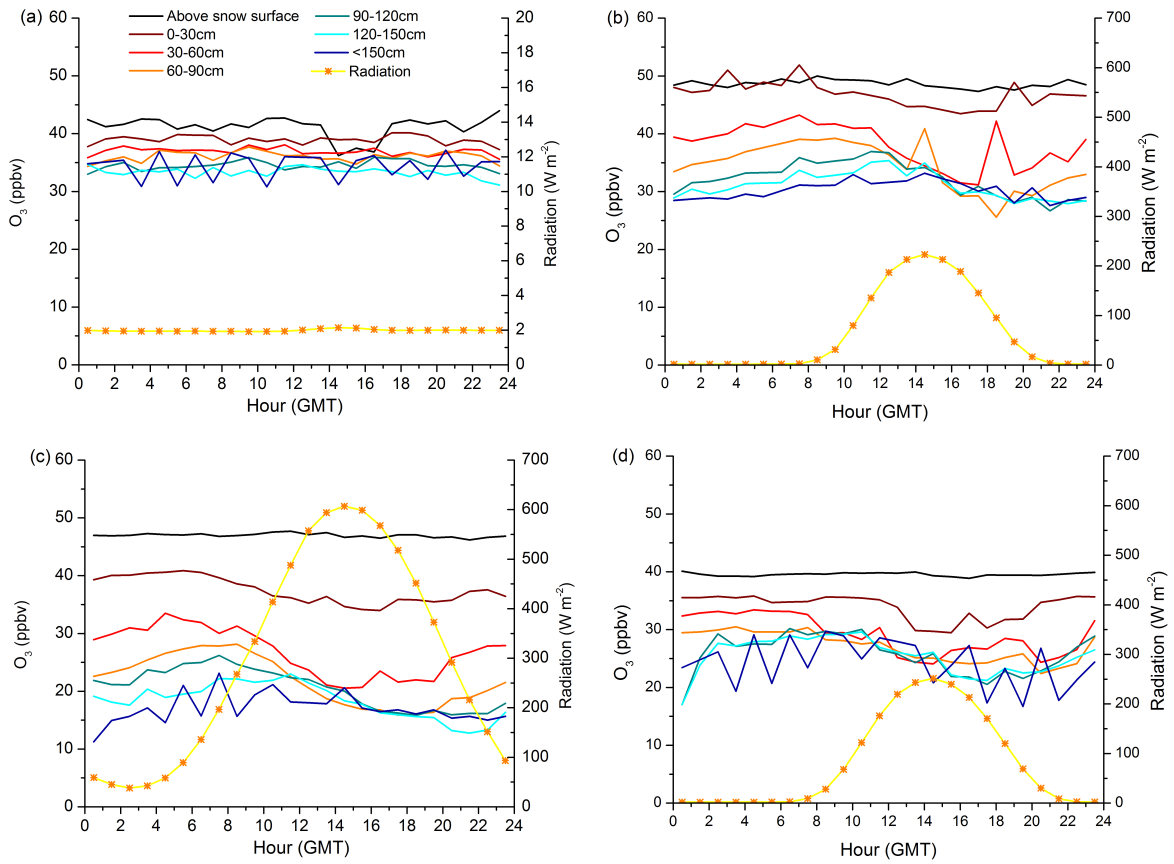

Figure 2.7: Hourly median values of O_3 in (a) winter (Nov, Dec, Jan), (b) spring (Feb, Mar, Apr), (c) summer (May, Jun, Jul) and (d) autumn (Aug, Sep, Oct). Observations from the entire record were separated by season, then binned by depth and median hourly values are shown here to give an average diurnal cycle at each level and each season.

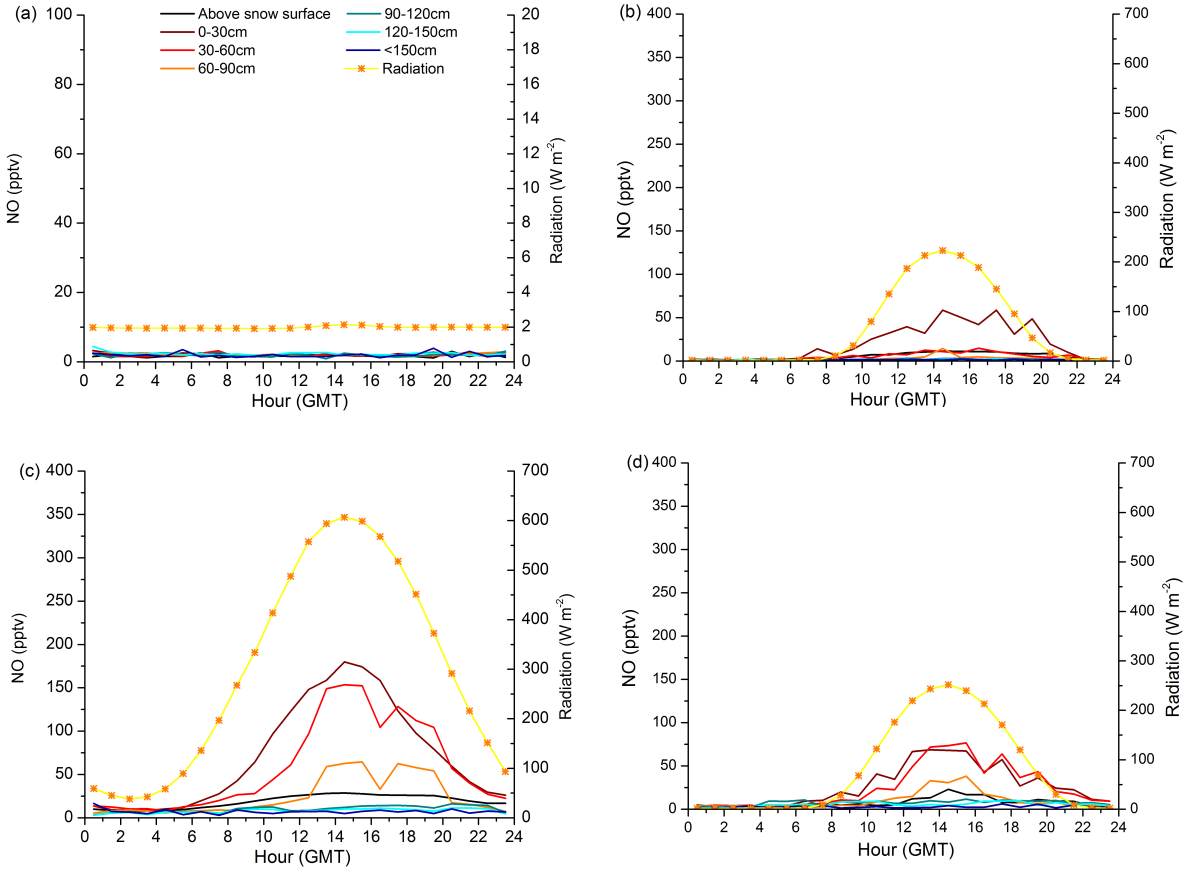

Figure 2.8: Hourly median values of NO in (a) winter, (b) spring, (c) summer, and (d) autumn. Observations from the entire record were separated by season, then binned by depth and median hourly values are shown here to give an average diurnal cycle at each level and each season. Note that the range of the vertical axis in panel (a) in winter is 100 pptv, whilst the panels for the other three seasons extend to 400 pptv.

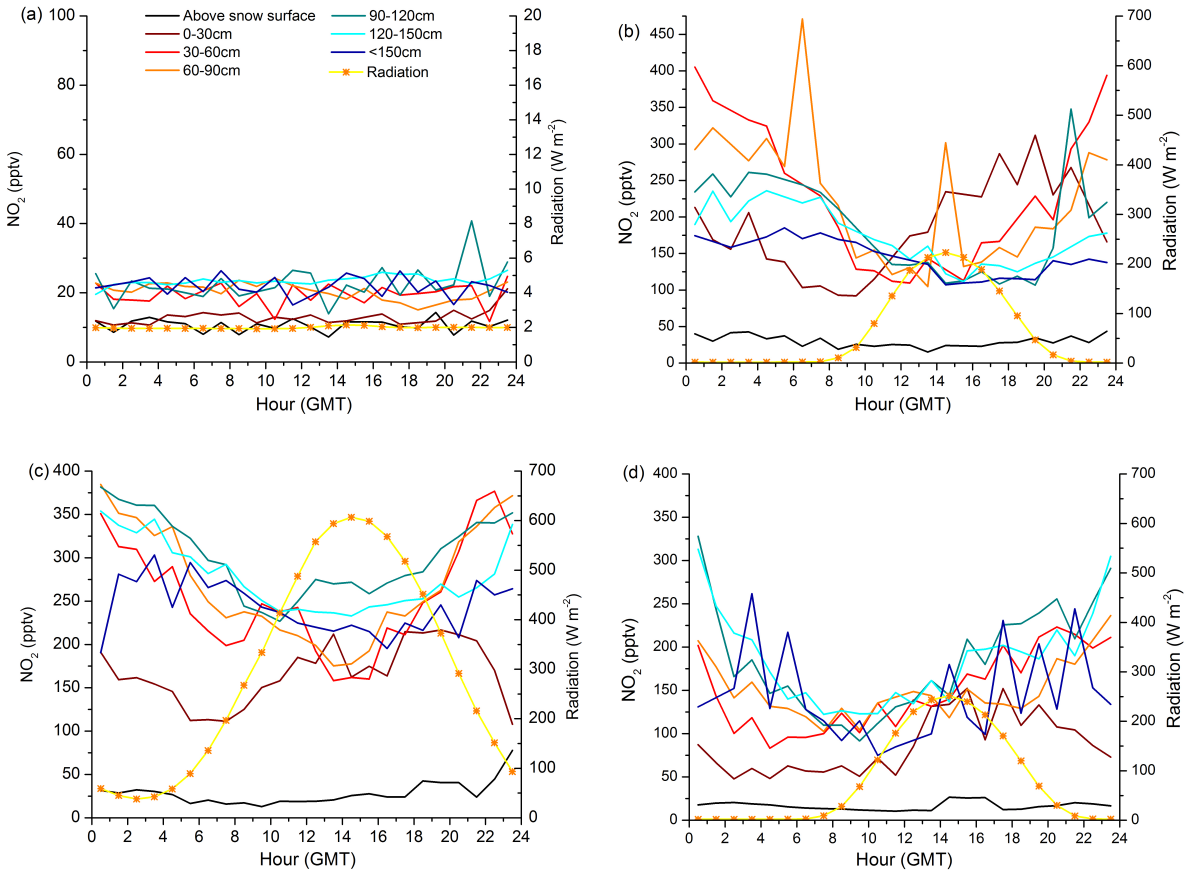

Figure 2.9: Hourly median values of NO_2 in (a) winter, (b) spring, (c) summer and (d) autumn. Observations from the entire record were separated by season, then binned by depth and median hourly values are shown here to give an average diurnal cycle at each level and each season. Note that the range of the vertical axis in panel (a) in winter is 100 pptv, in panel (b) for spring is 450 pptv, and the panels for the other two seasons extend to 400 pptv.

below 10 pptv and NO_2 mole fractions on average were less than 25 pptv. NO and NO_2 levels exhibit the development of a diurnal cycle during summertime as well. NO values at snowpack depths between 90 cm and the surface are enhanced over atmospheric values, with this increase closely tracking the daily solar radiation cycle. Peak NO mole fractions at these depths occur precisely during the peak in the incoming solar radiation cycle (Figure 2.8). Maximum median NO levels occurred in the 0−30 cm layer at 14:00 GMT (12:00 local, West Greenland Time, WGT), when the median value in that snowpack layer was 6 times greater than the median atmospheric value during the same hour. Interestingly NO_2 also shows enhancements in the snowpack but below 30 cm depth that enhancement is offset by an average of 7 hours after the peak in the radiation cycle and the observed peak in NO. This difference in timing of NO_2 enhancement has been observed in a previous controlled experiment (Honrath et al., 1999), and possible mechanisms are discussed in section 4. NO_2 is heightened above atmospheric concentrations at all levels within the snowpack during the summer.

As discussed in section 3.2.1 for O_3, spring and autumn NO and NO_2 conditions are not identical even though the amount of incoming radiation present is similar. Looking at the magnitude of NO within the snowpack interstitial air, the main difference between spring and fall is that during spring the only layer showing a significant enhancement is the shallowest layer between the surface and 30 cm depth. In autumn, the $30 - 60$ cm depth layer shows enhanced levels similar to the $0 - 30$ cm layer, and the $60 - 90$ cm layer is also enhanced above ambient. NO_2 levels during springtime exhibit drastic diurnal cycles in several depth levels approximately inversely related to radiation (minimum NO_2 measurement at maximum incoming solar radiation). The most extreme example is the $30 - 60$ cm depth layer, where a difference of almost 300 pptv between the average daily maximum and minimum is observed in spring. This across the board difference between spring and fall indicates that trace gas concentrations in snowpack interstitial air are not solely linked to the amount of incoming radiation.

2.4.2.3 Surface snowpack gradients

To investigate other parameters influencing trace gas levels in snow interstitial air, a time series plot showing chemical gradients between the atmosphere and the snowpack level that exhibits the most variability is shown in Figure 2.10 (a). All gradients were calculated as the atmospheric value (the mean of all inlets above the surface) minus the snowpack value. For simplicity in the text I define ΔO_3 to be the O_3 gradient between the atmosphere and a mid-depth layer (90−120 cm depth), ΔNO to be the NO gradient between the atmosphere and the near-surface snowpack level of 0−30 cm depth, $\Delta NO_{2\,15}$ to be the NO_2 gradient between atmosphere and the 0−30 cm snowpack depth layer, and $\Delta NO_{2\,45}$ to be the NO_2 gradient between atmosphere and the 30−60 cm depth layer. Two layers were chosen for NO_2 since they demonstrate strikingly different behavior as shown in Figure 2.8. ΔO_3 is a 4-hr average, while the NO and NO_2 gradients are daily averages. Panel (b) of this figure shows a time series of 4-hr averages of incoming solar radiation, atmospheric temperature (T_a), and median snowpack temperature in the 60−120 cm depth layer (T_{s90}). Linear regression analysis was performed between each of the chemical gradients mentioned above and atmospheric temperature, snowpack temperature (at a near surface layer between 0−60 cm not shown in Figure 2.10 (T_{s30}), as well as the 60−120 cm depth layer), and incoming solar radiation. Using the entire measurement period in the analysis, an R^2 value of less than 0.4 was observed between all gradients and solar radiation, atmospheric temperature, or snowpack temperature. The highest R^2 value overall when using the entire data set was that of 0.4 between ΔO_3 and incoming solar radiation.

Broken up by season, the spring and fall periods displayed the highest R^2 values between several of the variables. In summer and winter, R^2 values between all parameters were less than 0.2 indicating very little of the variation in the chemical gradients during summer and winter can be explained solely by incoming solar radiation, atmospheric temperature, or snowpack temperature changes alone on the same time scale. In springtime, the highest R^2 value was calculated of all the linear regression analysis. This was an R^2 of 0.5 between the springtime $\Delta NO_{2\,45}$ and T_{s30}. This

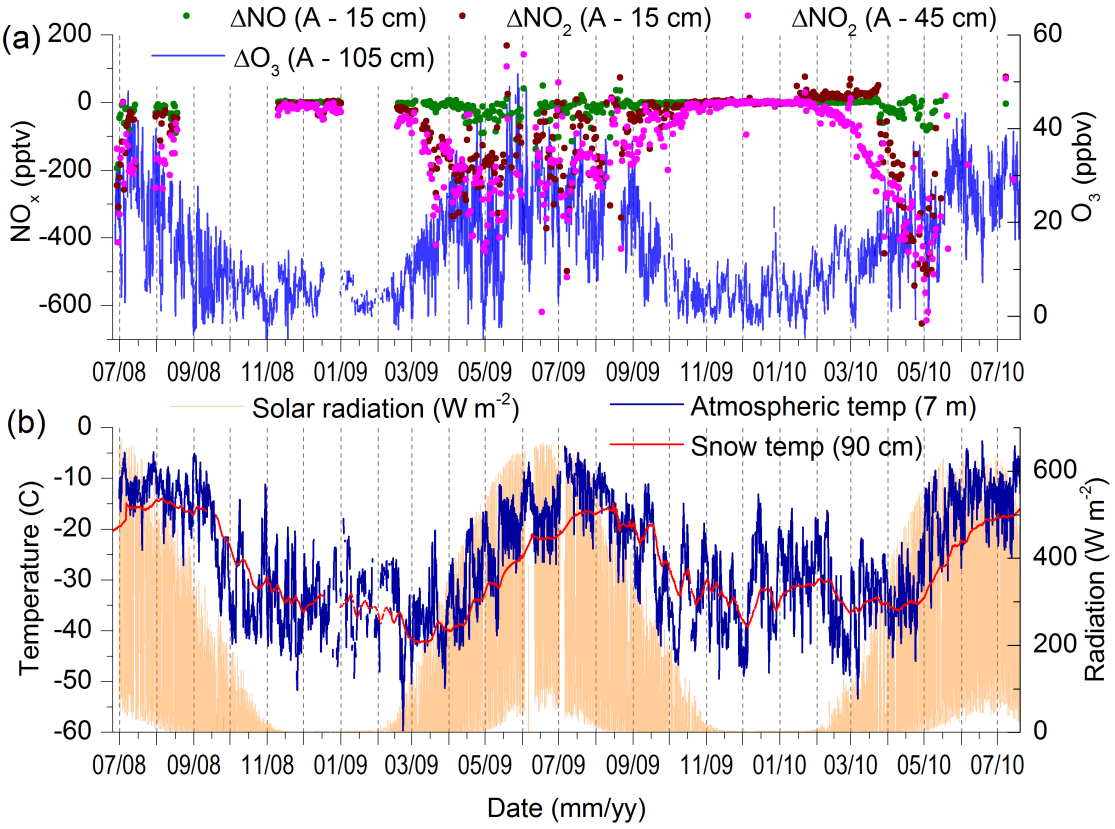

Figure 2.10: Time series plots showing chemical gradients between the atmosphere and snowpack along with relevant meteorological parameters for the entire measurement period. In all legend text, "A" designates "Atmospheric." Panel (a) shows the daily average NO gradient between the atmosphere and the 0−30 cm layer in the snowpack in green circles, the daily average NO_2 gradient between the atmosphere and the 0−30 cm snowpack layer in dark red circles, the daily average NO_2 gradient between the atmosphere and the 30−60 cm snowpack layer in pink circles, and the blue line designates the 4-hr average O_3 gradient between the atmosphere and the 90−120 cm layer in the snowpack. Panel (b) shows the incoming solar radiation in light orange, the atmospheric temperature measured at ∼7 m height from the meteorological tower, and the snow temperature averaged from the 60−120 cm depth layer in the snowpack from thermocouples on the snow sampling manifold. Solar radiation and temperatures are 4-hr average values.

R^2 value points toward a possible relationship between variations in snowpack temperature at 30 cm and observed variations in ΔNO_{245} during spring. ΔNO and ΔNO_{215} both correlated with this particular snowpack temperature with an R^2 of 0.3 during spring. ΔO_3 was found to have an R^2 of essentially zero ($R^2 < 0.1$) with all temperature variables (snowpack or ambient) during winter, spring, or summer. During the autumn season, the R^2 between ΔO_3 and T_{s30} was slightly higher at 0.3. This result is in contrast to ΔNO, ΔNO_{215}, and ΔNO_{245} which all had lower R^2 values with T_a, T_{s30}, and T_{s90} in autumn compared to spring.

To demonstrate competing influences on daily concentrations of the measured constituents in snowpack interstitial air 20-day time series plots of wind speed, incoming solar radiation, snowpack O_3, NO, and NO_2 are shown in Figure 2.11 (a)−(d). This time series spans the period May 5, 2009 through May 24, 2009. This particular period was chosen because it is during one of the months with highest median and maximum daily insolation (Figure 2.3), and a high wind event was observed with wind speeds remaining over 10 m s^{-1} for a period of several days. The effect of high winds on snowpack trace gas concentrations are discussed in the following section. In the present section, I would like the reader to take the following from Figure 2.11: (1) O_3, NO, and NO_2 all exhibit diurnal cycles within the snowpack as discussed previously; (2) the timing of the observed maximum and minimum O_3 mole fraction in the snowpack is offset by ∼1-hr between each level and the level above, with the minimum value occurring between the hours of 12:00−22:00 GMT (the ∼1hr lag at progressively deeper levels is discussed below); (3) the timing of the observed maximum NO mole fraction in the snowpack is between 12:00−14:00 GMT for the upper snowpack layers (down to 90 cm) where a diurnal cycle is observed; (4) NO_2 in the layer closest to the surface ($0 - 30$ cm) displays a diurnal cycle in opposition to the rest of the snowpack layers − values in the near-surface layer peak at 16:00 − 17:00 GMT whereas values in the layers below 30 cm peak at 23:00 − 03:00 GMT; (5) during the observed high wind period between day 133 and 136 snowpack O_3 mole fractions increased to within $5 - 10$ ppbv of atmospheric values; (6) during the same high wind event, snowpack NO concentrations were unaffected, while an overall increase in NO_2 mole fractions within snowpack interstitial air was observed. All of these features indicate that multiple

processes influence snowpack concentrations of these constituents.

An interesting feature in Figure 2.11 is the short lag observed in the peak daily maximum and minimum O_3 value at each level. Each 30 cm level within the snowpack exhibits maximum depletion ∼1-hr later than the layer above it throughout the afternoon. Recovery following depletion also occurs at ∼1-hr intervals between each binned 30 cm snowpack level. A simple calculation was performed to examine whether diffusion processes could account for this observed lag. To do this, I used the gas diffusion coefficient for O_3 in air of 0.1444 cm^2 s^{-1} reported in Massman (1998), and estimates of porosity and tortuosity in the Summit, Greenland snowpack reported in Albert and Shultz (2002) to calculate a gas diffusion coefficient of O_3 in snowpack of 0.0407 cm^2 s^{-1}. Implementing the equation for characteristic gas diffusion time from Seinfeld (2006) I estimate that it would take approximately 1.5 hours for O_3 to travel through a 30 cm layer of the snowpack purely by diffusion. Helmig et al. (2007a) used mean time shifts of the minima and maxima at progressively deeper snowpack levels to estimate a mean transport time of 55 min between 50 and 80 cm depth in snow, and 48 min between 80 and 100 cm depth. This is slightly faster than the time estimate based purely on diffusion. This is sensible due to other transport processes acting in the snowpack (such as the impact of wind pumping described in the next section).

2.4.3 Snowpack wind pumping effect

The distribution of gases vertically throughout the snowpack is determined by several gas exchange processes including diffusion and wind pumping. Besides the traditional time series in Figure 2.11 which clearly shows the influence that elevated surface wind speed can have on snowpack gas mixing ratios, Figure 2.12 gives another way to visualize wind pumping in the snowpack. Figure 2.12 shows conditions in the snowpack from April 14−20, 2009. Colors indicate mole fractions of O_3 (ppbv), NO (pptv), and NO_2 (pptv), and these values are plotted as a function of depth relative to the snow surface. Mole fractions are 4-hr averages, so the focus of this plot should not be precise timing; rather it provides a visually striking picture of the general impact of a high wind event on snowpack trace gas levels. During this period surface wind speed increased to greater than

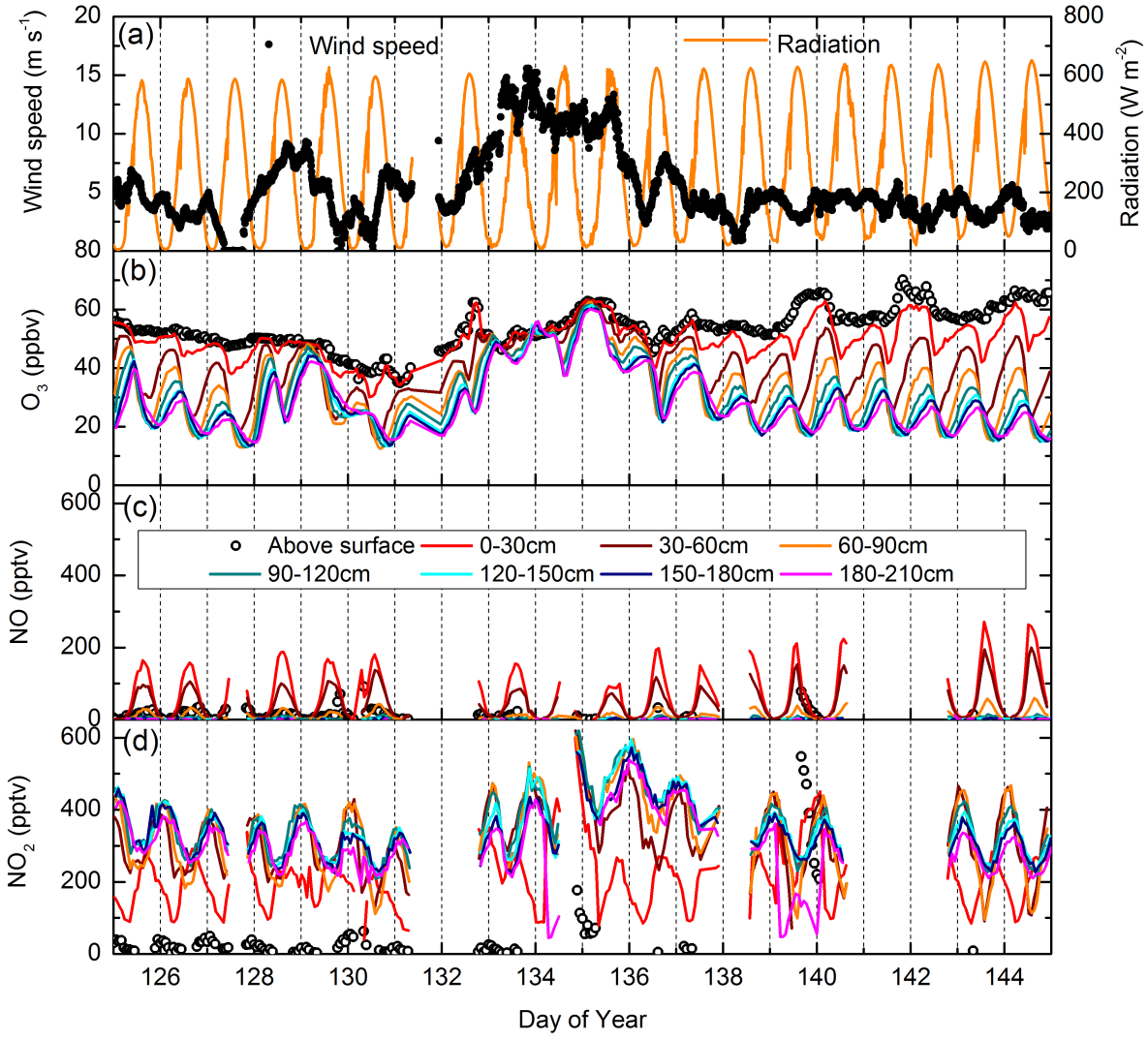

Figure 2.11: Time series plots of (a) wind speed and incoming solar radiation, (b) O_3 in ppbv above the surface and at all levels within the snowpack, (c) NO in pptv above the surface and at all levels within the snowpack, and (d) NO_2 in pptv above the surface and at all levels within the snowpack. Data span the period from May 5, 2009 to May 24, 2009.

10 m s^{-1} on April 16, stayed above this level until increasing again and peaking at nearly 25 m s^{-1} by the end of the day on the 17th. Along with this high wind event atmospheric O_3 mole fractions increased to levels above 70 ppbv, likely due to transport from the upper troposphere or stratosphere, or advection of a polluted airmass (Helmig et al., 2007d). In the snowpack, O_3 levels increase up to 70 ppbv correlated with the period of high wind. Similar to what is shown in Figure 2.11, despite this drastic influence of wind speeds on O_3, NO levels appear unaffected, while the magnitude of the NO_2 enhancement within snow increases.

The overall impact of wind pumping on gas transport in firn air is not adequately understood. Previously the relationship between the surface − snowpack O_3 gradient and wind speed was investigated by Helmig et al. (2007a), and a linear relationship with $R^2 = 0.3$ was determined for high radiation conditions down to 30 cm depth in the snowpack. In the current study, I attempted to parameterize the relationship between snowpack O_3 concentrations and surface winds, and to determine to what depth in the snowpack surface turbulence processes influence. To accomplish this, a regression analysis was performed using a 2nd order polynomial fit ($y = a + bx + cx^2$) between wind speed measured from the meteorological tower at ∼7 m and snowpack O_3 at every 30-cm depth layer down to 2.1 m in the snowpack. For this analysis (shown in Figure 2.13) one month of data was implemented (June 2009) and only data for conditions when radiation was greater than 300 W m^{-2} were used in an attempt to partially remove the effect of diurnal changes in snowpack O_3 due to the amount of incoming shortwave radiation. Following analysis by Seok et al. (2009) the regression terms in the polynomial equations can be interpreted in the following way: a is the expected O_3 value in the layer when the wind speed is zero; b is the strength of the effect of winds on the O_3 mole fraction at each level; and c determines the amount of curvature relative to a linear fit. This analysis indicates that the shallowest layer in the snowpack (0−30 cm, panel (a)) is influenced by wind speeds to the greatest extent. The influence of wind decreased continuously further down in the snowpack. In the lowest snowpack layers the c term became very small, with the data nearing a linear fit. R^2 values of 0.5 were observed between wind speed and all snowpack levels except for the 30−60 cm level, where the R^2 value was slightly lower at 0.4.

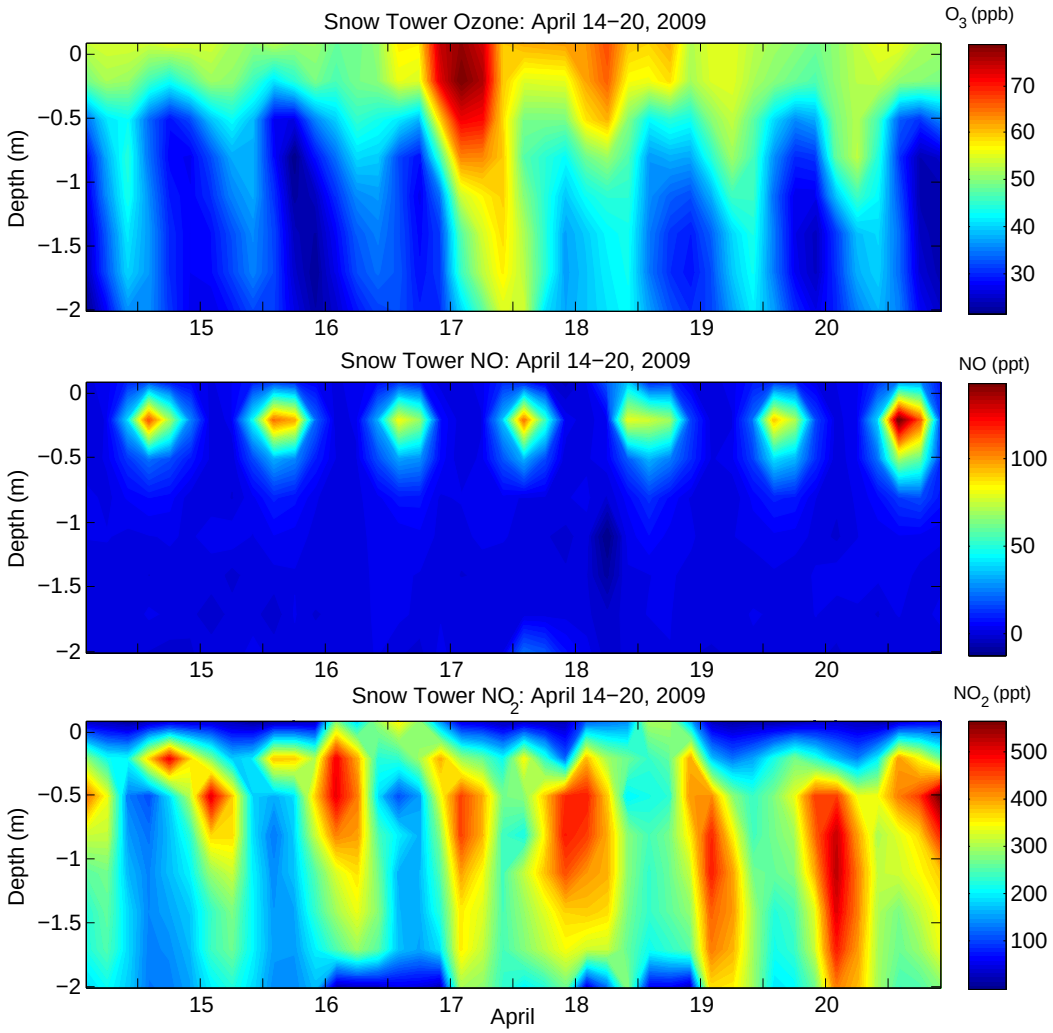

Figure 2.12: Color contour plot of (a) O_3, (b) NO, and (c) NO_2 for the time period of April 14-20, 2009. Snowpack mole fraction data are 4 hour averages plotted by depth relative to the snow surface. Colors indicate mole fractions of each constituent in ppbv or pptv. High winds up to 20 m s^{-1} were experiemced during the beginning and middle of this period as described in the text.

This is a significant result, as it indicates that changes in wind speed could explain up to ∼50% of the variation in O_3 concentrations consistently down to at least 2 m depth in the snowpack.

2.5 Discussion

2.5.1 Why do NO_2 enhancements within the snowpack occur at a different time than peak radiation?

The difference in timing of peak daily NO_2 within each layer of the snowpack is one of the fascinating findings from these measurements. Specifically, the observations that (a) NO_2 in the 0-30 cm layer has a daily peak occurring at a similar time as the maxima observed in incoming solar radiation, NO, and maximum depletion of O_3 and (b) all other layers deeper in the snowpack show a maximum in NO_2 shifted approximately 6-12 hours from that of the 0-30 cm layer. The observation outlined in (a) supports the hypothesis that enhanced NO_2 observed in the near-surface 0-30 cm layer is a result of the photolysis of nitrate. In the majority of previous studies, NO_2 in the snow interstitial air has been attributed to production in a liquid-like layer, via:

$$NO_3^- + hv \longrightarrow NO_2 + O^- \tag{2.3}$$

with resulting volatilization of NO_2 (Warneck and Wurzinger, 1988; Honrath et al., 2000; Jacobi and Hilker, 2007; Thomas et al., 2011). NO production observed in the near-surface snowpack can occur via the other, minor, nitrate photolysis channel:

$$NO_3^- + hv \longrightarrow NO_2^- + O(^3P) \tag{2.4}$$

$$NO_2^- + hv \longrightarrow NO + O^- \tag{2.5}$$

with subsequent volatilization to gas-phase NO. NO production is also expected through the photolysis of NO_2 (given below in Reaction 2.6). These reactions have been used in part in several modeling studies and provided good estimates of NO_x fluxes from the snow surface (Jacobi and Hilker, 2007; Bock and Jacobi, 2010; Thomas et al., 2011, 2012), although measurements within the snowpack were lacking to validate model estimates of NO and NO_2 in snow interstitial air.

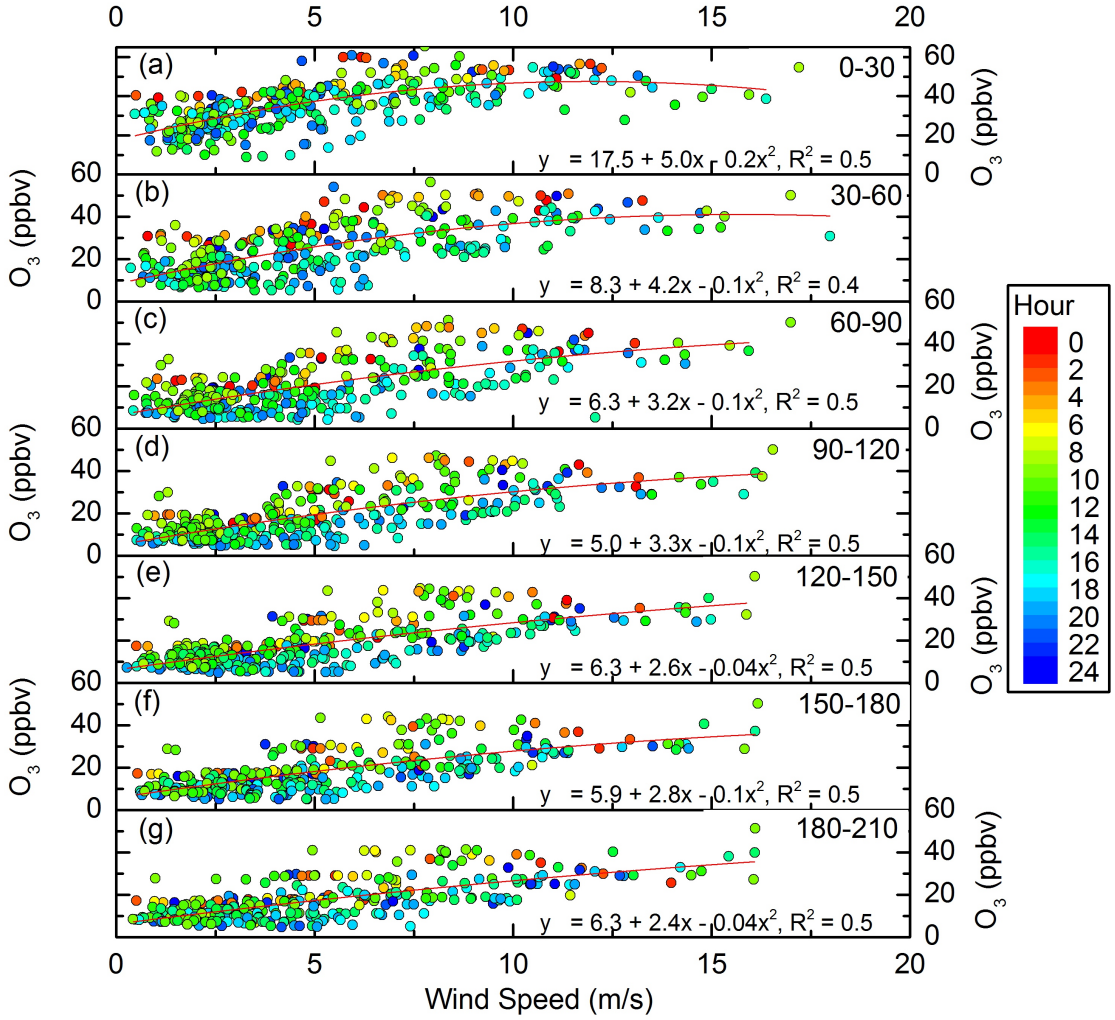

Figure 2.13: Panels (a) (g) show regression analyses using a 2nd order polynomial fit between wind speed at ∼7 m and O_3 values at binned 30 cm layers within the snowpack down to 2.1 m. Data are from June 1−30, 2009. Snowpack data were filtered to include only time periods when the incoming solar radiation was greater than 300 W m^{-2} in order to remove some of the variability attributed to changes in solar radiation. Data points are color contoured by the hour of the day simply to illustrate that remaining dependency.

This system of reactions could explain the observations of NO enhancements in the interstitial air of the upper snow layers, and the behavior of NO_2 in the $0 - 30$ cm snow layer. However, the above mechanisms are not adequate to explain the NO_2 measurements below 30 cm depth in the snowpack.

Several hypotheses are investigated for the behavior of NO_2 at levels below 30 cm in the snowpack. One mechanism was originally proposed by Honrath et al. (2000) to explain the difference in timing of maximum and minimum daily NO_2 observed during a shading experiment. The timing of maximum NO_2 in the snowpack could be due to the higher solubility of NO_2 relative to NO. NO_2 has a Henrys law constant that is ten times higher than that of NO (Finlayson-Pitts and Pitts, 2000). This higher solubility would indicate a greater capacity for NO_2 compared to NO in the liquid-like layer, which would result in a higher threshold for NO_2 in snow before volatilization, yielding a lag in the observed enhancements in interstitial air.

The second hypothesis is that of a summertime dark reaction mechanism (catalyzed by increased snowpack temperatures during the summer), occurring throughout the day below ~30 cm in the snowpack and leading to persistent high levels of NO_2. A temperature modulated mechanism could be supported by the moderate correlation between snowpack temperature at 30 cm depth and the NO_2 gradient between the atmosphere and snowpack in springtime (R^2 value of 0.5). During and following the time of maximum incoming radiation, when the minimum in NO_2 is observed, a photochemically driven destruction mechanism would be necessary to explain the daily decrease in NO_2 near the time of peak daily solar radiation.

Another possibility for the observance of high NO_2 at deep levels within the snowpack is production of NO_x occurring in the near-surface snowpack, and resultant transport down through the snow via diffusion and advection. High levels of NO_2 observed at all measured levels of the snowpack down to >2 m depth would be achieved via the interchange of NO_2 and NO in snow interstitial air via the following established reactions:

$$NO_2 + h\nu \xrightarrow{O_2} NO + O_3 \tag{2.6}$$

$$NO + O_3 \longrightarrow NO_2 + O_2 \tag{2.7}$$

Near the surface reaction 2.6 dominates with resulting NO production. Further down in the snowpack where there is lower actinic flux this pseudo steady state reaction scheme would shift towards reaction 2.7 leading to NO_2 production. This reaction scheme (evaluated at steady state this gives the photostationary state relation) essentially tells us that most of the NO_x transported deeper in the snowpack will be present as NO_2. Similarly to the calculations done to estimate the diffusion time for O_3 through snow interstitial air, using a diffusion constant in air for NO_2 of 0.1361 cm^2m^{-1} (Massman, 1998), it can be estimated that the time of diffusion for NO_2 through a 30 cm layer of snowpack is approximately 1.6 hours, with no other processes acting. While there is a small delay observed in NO_2 enhancements in each layer below 30 cm depth, looking at the time series plot the delay is not as apparent as with O_3 (which shows a clear ∼1-hr offset between levels), indicating diffusion is probably not the process responsible for heightened NO_2 levels at depth. Reactions 2.6 and 2.7 along with diffusion and simplified wind pumping processes were incorporated into the coupled MISTRA-SNOW model recently for Summit but the timing of peak NO_2 in snow interstitial air was not accurately represented (Thomas et al., 2011). A final hypothesis, involving nitrite, is investigated with respect to O_3 loss in the next section.

2.5.2 What leads to depletion of O_3 within the snowpack at Summit?

From previous studies there exists some insight into possible mechanisms leading to the drastic depletion of O_3 in the snowpack, but none of the currently proposed pathways fully explain the low levels observed, and thus far modeling studies have not been able to reproduce the observed depletion (Seok et al., 2010; Thomas et al., 2011, 2012). It is documented from past shading experiments and the current observations that the mechanism is very rapid. Peterson and Honrath (2001) established that observed O_3 losses were faster and more complete than could be explained by reaction with NO_x or HO_x. Those authors also showed that reactions with the observed levels of NO and NO_2 could only explain up to 6% of the observed O_3 loss rate. Using a single-column model, (Seok et al., 2010) demonstrated that in simulations using solely gas-phase NO_x-O_3 chemistry only

$\sim$10% of the observed snowpack O_3 gradient was represented.

Recent field measurements have shown that BrO is present at Summit even during periods with non-marine sourced air (Stutz et al., 2011). That study and Dibb et al. (2010) proposed that the BrO source was likely photolytic formation of reactive bromine at the surface and in snow interstitial air. Accompanying modeling work from Thomas et al. (2011) showed that the probable source of gas phase reactive bromine in the Summit boundary layer is formation in the snowpack. O_3 destruction from bromine proceeds rapidly via a catalytic cycle:

$$\mathrm{Br} + \mathrm{O_3} \longrightarrow \mathrm{BrO} + \mathrm{O_2} \tag{2.8}$$

$$\mathrm{BrO} + \mathrm{BrO} \longrightarrow \mathrm{Br_2} + \mathrm{O_2} \tag{2.9}$$

$$\mathrm{Br_2} + h\nu \longrightarrow 2\,\mathrm{Br} \tag{2.10}$$

Using median sodium levels measured in Summit snow Peterson and Honrath (2001) estimated that there could possibly be enough bromine in interstitial air as BrO to account for measured O_3 depletion if there was a fast recycling mechanism such as that proposed in springtime Arctic coastal O_3 depletion events.

Even with the incorporation of halogen chemistry, models have been unable to reproduce the observed O_3 depletion in snow. This was cited to be in part due to low BrO levels predicted in interstitial air as well as replenishment of O_3 in interstitial air due to physical mixing processes between the atmosphere and snowpack (Thomas et al., 2011). An alternative hypothesis that I would like to present here is associated with nitrite (NO_2^-) oxidation by O_3.

There are several sources of nitrite in the snowpack. Direct formation can occur from the minor channel for nitrate photolysis (reaction 2.4). The main photolysis pathway (reaction 2.3) exceeds reaction 2.4 by a factor of 8 to 9 (Dubowski et al., 2001). Additional sources of nitrite include the main nitrate photolysis channel (reaction 2.3). Reaction 2.3 also produces an oxygen atom, which could then react with nitrate to produce nitrite and oxygen via (Jacobi and Hilker, 2007; Boxe and Saiz-Lopez, 2008):

$$\mathrm{NO_3^-} + O(^3P) \longrightarrow \mathrm{NO_2^-} + \mathrm{O_2} \tag{2.11}$$

Or, reaction 2.3 could lead to:

$$NO_2 + H_2O \longrightarrow HONO + HNO_3 \tag{2.12}$$

Where nitrous acid (HONO) quickly dissociates to nitrite on snow grains, however the kinetics of reaction 2.12 are not well understood on ice (Finlayson-Pitts et al., 2003; Chu and Anastasio, 2007). The main sinks for nitrite are photolysis (reaction 2.5) and oxidation by O_3 or OH (Chu and Anastasio, 2007):

$$NO_2^- + O_3 \longrightarrow NO_2 + {}^{\cdot}O_3^- \tag{2.13}$$

$$NO_2^- + OH \longrightarrow NO_2 + OH^- \tag{2.14}$$

While reaction 2.13 could contribute to observed O_3 loss in the snowpack, it indicates a dark reaction loss for O_3, which begs an investigation of why this would not occur during winter. Possibly this is because nitrite is known to be slowly oxidized in the liquid phase to nitrate by dissolved oxygen in the dark, and the rate of this oxidation increases drastically during freezing (Takenaka et al., 1992; Finlayson-Pitts and Pitts, 2000). This could lead to very little nitrite being present in snow during winter. Additionally, several of the sources of nitrite (including nitrate photolysis) are light-dependent, which could explain the dependence of O_3 depletion on solar radiation.

Using reactions 2.4, 2.12, 2.5, and 2.13 as the primary sources and sinks, Chu and Anastasio (2007) calculated a summertime steady state concentration of NO_2^- on near-surface snow grains of 13 nM, with a lifetime of ∼5 hr. This concentration is on the order of 100 times less than typical nitrate levels. Using these estimates, the calculated O_3 loss rate with respect to nitrite is fast enough to account for observations of rapid O_3 loss. A missing source of nitrite has been hypothesized at this location (Chu and Anastasio, 2007), so further investigation in to the nitrite budget in the Summit snowpack is needed. Additionally, even though estimated $[NO_2^-]$ is small, the photolysis rate of NO_2^- is similar to that of NO_3^-, indicating even at small concentrations it could have an important role in NO_x cycling (Galbavy et al., 2007a,b). While nitrite has the potential to play a significant role in snowpack chemistry, little is known about its budget or potential contribution to O_3 loss (Chu and Anastasio, 2007). As a result of the observations described herein, it is recommended

that a mechanism involving nitrite should continue to be investigated, with relevance for both NO_2 observations and destruction of O_3 in snow interstitial air.

2.6 Conclusions

Multi-year measurements of O_3, NO, NO_2, and temperature in snow interstitial air were presented and analyzed in detail on a seasonal and diurnal basis in a dry polar snowpack. Near-complete removal of O_3 in snowpack interstitial air is observed during spring through autumn, and this removal also exhibits a diurnal cycle with peak depletion in snow occurring several hours following the peak in solar radiation. NO and NO_2 also show seasonal and diurnal cycles in snowpack interstitial air. Both constituents are enhanced in the snowpack during the spring, summer, and fall seasons. Enhancements in NO are constrained to a layer between the surface and 60 cm depth, while NO_2 levels are heightened throughout the depth of the measurements. Daily NO_2 maxima in the 0-30 cm snowpack depth layer tracked the diurnal solar radiation cycle, while daily NO_2 maxima in all layers below 30 cm were offset from the solar radiation cycle by an average of 7 hours. Enhancements in NO and NO_2 in the 0-30 cm layer are attributed to be a result of direct production via nitrate photolysis. Several possible mechanisms are proposed for the difference in timing of NO_2 maxima below 30 cm in the snowpack. To account for the observed O_3 loss in the snowpack, nitrite oxidation by O_3 as a potential mechanism to be included in future analysis is suggested, as the combination of NO_x and halogen chemistry have not been an adequate explanation. The reaction between NO_2^- and O_3 could be a potential mechanism influencing both the timing of peak NO_2 and depletion of O_3. Modeling studies implementing this set of observations as constraints to snowpack mole fractions of the described trace gases will be critical in determining the acting mechanisms.

Chapter 3

Evaluation of boundary layer depth estimates at Summit Station, Greenland

This chapter is adapted from: **Van Dam, B., Helmig, D., Neff, W., Kramer, L. (2013)** which is currently in review in the Journal of Applied Meteorology and Climatology as part of the ISARS 2012 Special Issue.

3.1 Abstract

Boundary layer conditions in polar regions have been shown to have a significant impact on the levels of trace gases in the lower atmosphere. The ability to properly describe boundary layer characteristics (e.g. stability, depth and variations on a diurnal and seasonal scale) is essential in understanding the processes controlling chemical budgets and surface fluxes in these regions. Surface turbulence data measured from 3-D sonic anemometers on an 8-m tower at Summit Station, Greenland (GEOSummit) were used for estimating boundary layer depths (BLD) in stable to weakly stable conditions. Direct BLD measurements from an acoustic sounder (sodar) located ∼50 meters away from the tower were used to evaluate the turbulence-derived boundary layer depth estimates during June 2010. BLDs during this period varied diurnally; minimum values were less than 10 m and maximum values were greater than 150 m. BLD estimates provided a better comparison with sodar observations during more stable conditions. Measurements of ozone (O_3) and nitrogen oxides (NO_x) in the surface layer were also measured at the meteorological tower and investigated for their dependence on boundary layer structure. These analyses, in contrast to observations from South Pole, Antarctica, did not show a clear relation between surface layer atmospheric trace gas

levels and diurnal variability in the BLD.

3.2 Introduction

Recent studies on photochemistry occurring within polar snowpacks and the influence reflected in the overlying atmosphere have revealed that reactions occurring in the snowpack can be both sources and sinks of reactive trace gases to the atmosphere (Grannas et al., 2007). Understanding this dynamic chemistry, as well as physical processes in the snowpack, is critical in evaluating how chemical constituents are preserved in ice cores, and in assessing the influence of snow cover on polar tropospheric chemistry. One important factor influencing surface trace gas levels is the atmospheric boundary layer. Studies at South Pole (SP) have shown that a combination of conditions including low snow accumulation rates allowing for efficient recycling of nitrogen from the snowpack, emissions of NO_x from the snowpack, a long fetch allowing NO_x accumulation in the surface layer, and sustained shallow stable boundary layers romote elevated levels of nitric oxide (NO) and ozone (O_3) production near the surface (Davis et al., 2001, 2008; Neff et al., 2008; Helmig et al., 2008a). Understanding the cycling and budgets of tropospheric O_3 and nitrogen oxides (NO_x, NO + NO_2) is essential for characterizing the oxidation capacity of the lower atmosphere.

Cohen et al. (2007) investigated the behavior of the boundary layer and its influence on atmospheric trace gas chemistry at Summit Station, Greenland. Their study estimated BLDs using a diagnostic model previously applied in Neff et al. (2008). However, without access to frequent BLD observations, an evaluation of the efficacy of implementing the model at Summit was not viable. In this study, two main objectives were addressed: (1) assess the accuracy of BLD estimates derived from two diagnostic models which rely on sonic anemometer turbulence quantities using BLD measurements from a minisodar at Summit; and (2) evaluate ambient NO_x levels alongside minisodar-derived BLDs to test for a linear relationship such as that seen in two different Antarctic locations (one subjected to diurnal cycles in heat exchanges and one where persistent shallow BLDs occur).

3.3 Methods

3.3.1 Site and instrumentation

Measurements were conducted at Summit Station, Greenland (72°34'N, 38°29' W, 3210 a.s.l.). Instrumentation was installed during May 2008 and measurements conducted continuously through July 2010. This study focuses on data from June 2010. Turbulence measurements were taken on a meteorological tower located ∼660 m southwest of the main camp structures within the Summit clean air sector. Surface turbulence quantities were derived from a Metek USA-1 3-D sonic anemometer (Metek Gmbh, Germany) located at 5.6 m above the snow surface. Turbulence data were processed and filtered as described in Cohen et al. (2007), with several modifications. Sonic anemometer data were collected at a sampling rate of 10 Hz and turbulent covariance values were then calculated in $\frac{1}{2}$-hr blocks. Data for periods of north wind were removed due to tower contamination. The sonic anemometer used in this study was equipped with a self-heating feature which was programmed to turn on automatically when riming of the sensor head was detected.

A high resolution acoustic sounder (minisodar) was deployed approximately 50 m to the north-east of the meteorological tower. A thorough description of the minisodar implemented in this study as well as an explanation of the BLD extraction method are described in Neff et al. (2008). The minisodar measured up to a height of ∼165 m with a lower detection limit of 4 m in order to focus on high-resolution detection of the near-surface layer at Summit. BLD estimates from the minisodar were time-averaged to $\frac{1}{2}$-hr, allowing for equivalent comparisons between the turbulence and minisodar data. Figure 3.1 shows a photograph of the sodar and meteorological tower.

Air was sampled from an inlet at 6.3 m for determination of NO. NO was detected by chemiluminescence after reaction with O_3 (Ridley and Grahek 1990); NO_2 was determined as NO via UV photodissociation (Kley and McFarland, 1980) with a photolytic NO_2 converter. Ambient levels of O_3 in the surface layer were measured at 1.6 m using a Model 49C UV photometric O_3 analyzer (Thermo Environmental Instruments, Franklin, MA).

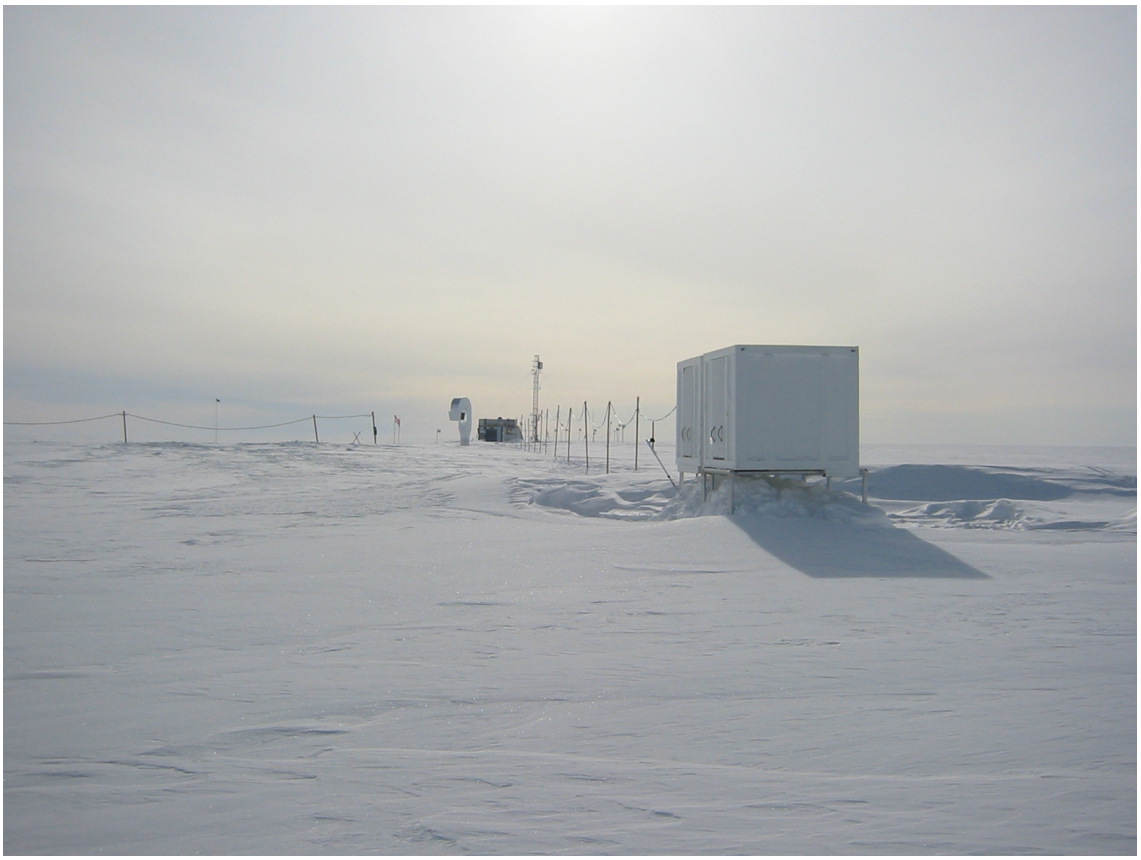

Figure 3.1: The bistatic minisodar at Summit Station, Greenland, in the foreground; shown are the two boxes that house the transmitting and receiving antenna systems. The meteorological tower, which held the 3-d sonic anemometer implemented in this study, can be seen in the rear of the photo.

3.3.2 Theoretical background

A variety of diagnostic equations have been proposed to estimate BLD based on simple scaling approaches (Zilitinkevich and Baklanov, 2002; Zilitinkevich et al., 2002; Vickers and Mahrt, 2004). A primary motivation for developing these diagnostic equations is the desire to use surface turbulence measurements to estimate BLD. Two such diagnostic equations were investigated previously using surface turbulence data from SP (Neff, 1980; Neff et al., 2008). Conditions at SP are unique due to the lack of a diurnal solar cycle, which allows the boundary layer to approach an equilibrium depth. The first of these equations for the BLD (H), is an expression originally devised by Pollard (1973) for an oceanic mixing layer driven primarily by surface stress and assuming equilibrium at inertial time scales:

$$H = 1.2u_*(fN_b)^{-\frac{1}{2}} \tag{3.1}$$

In this equation, u_* is the friction velocity, f is the Coriolis parameter, and N_b is the Brunt-Väisälä frequency given by

$$N_b = \sqrt{\frac{g}{T}\frac{\partial\theta}{\partial z}} \tag{3.2}$$

g is the gravitational acceleration, T is the absolute temperature recorded by the sonic anemometer, and $\frac{\partial\theta}{\partial z}$ is the potential temperature gradient. Neff (1980) found that this diagnostic model gave a good estimation of BLD during weak to moderate stability conditions at SP when compared to sodar measurements. This model was tested against sodar measurements more recently at SP using vertical temperature gradients from a 22-m tower as well as rawinsonde temperature profiles. It was found that model results were representative of the BLD during very stable conditions, but overestimated in other cases. It should be noted that in this expression, H is only weakly dependent on vertical static stability. The Pollard (1973) model assumes a sensible heat flux (H_s) of zero (a reasonable approximation at SP) and is dominated by the value of the surface stress (u_*) as a measurement of turbulence-induced mixing. Another diagnostic model is included

which is sensitive to the value of H_s. This scaling expression derived by Zilitinkevich and Baklanov (2002) is described by:

$$H = C_s^2 (\frac{u_* L}{|f|})^{\frac{1}{2}} \tag{3.3}$$

where C_s is 0.7, u_* and f are the same as above, and L is the Monin-Obukhov length defined as:

$$L = \frac{-u_*^3 T_0}{kgH_s} \tag{3.4}$$

where T_0 is the temperature, and k is the von Karman constant. In the SP experiments, Equation 3.3 proved to be problematic when compared with sodar data. This was a result of transient changes in H_s, for example, due to passage of clouds, which changed the surface radiative balance but did not affect the more slowly evolving BLD. It was determined that the friction velocity was the surface parameter with the most influence on boundary layer mixing at SP (Neff et al., 2008).

Aside from SP, these diagnostic equations were also tested at Summit and Barrow, AK. As mentioned in the introduction, the Cohen et al. (2007) study used Equation 3.1 to estimate BLDs at Summit. In lieu of frequent direct observations, BLDs inferred from four radiosonde profiles were used for a limited assessment. Comparing the four available observations indicated that Equation 3.1 estimated the BLD to within 55 m. At Barrow, in comparison with a minimum of twice-daily radiosonde data, Equation 3.1 estimated BLD within 50 m 76% of the time, while Equation 3.3 estimated BLD within 50 m 61% of the time (Boylan et al., 2013). Both models primarily underestimated the inferred BLDs.

3.4 Results

3.4.1 Boundary layer characteristics

A frequency distribution of June 2010 stability conditions (estimated by the Monin-Obukhov length ratio, $\frac{z}{L}$) is shown in Figure 3.2. Unstable conditions ($\frac{z}{L} \leq 0$) were common during the month of June 2010, occurring 47% of the period available. Similarly, Cullen and Steffen (2001) reported unstable conditions occurring $11 - 43\%$ of the time for the years $1998 - 2000$ during the June $-$ October period at Summit; Cohen et al. (2007) reported unstable conditions 51% of the time during July and August 2004. The average diurnal cycle (median measurement for each hour of the day over the entire month) of H_s and atmospheric stability is shown in Figure 3.3. Positive H_s and negative $\frac{z}{L}$ values (indicating unstable conditions) existed between the hours of $9 - 19$ GMT. This diurnal variation in stability is a noteworthy contrast to conditions observed at SP, and early spring observations at Barrow, where extended multi-day periods of very stable conditions have been observed (Neff et al., 2008; Boylan et al., 2013). Detailed discussion of the surface energy balance at Summit can be found in, for example, Albert and Hawley (2000) and Cullen and Steffen (2001).

Parameters contributing to changes in the depth of the stable to weakly stable boundary layer at Summit are investigated in Figure 3.4. Sodar observations of BLD are binned by 15 m depth intervals, and the median BLD within each bin are compared to the median and H_s values. These data only incorporate the late evening to early morning hours, when atmospheric conditions are transitioning towards stronger stability and the BL could be moving towards an equilibrium depth. The correlation coefficient of R^2=0.83 reveals the relationship between u_* and the BLD during the nighttime and early morning hours (Figure 3.4 part (a)). This demonstrates that u_* plays a role in the development of the stable boundary layer at this location. In contrast, Figure 3.4 part (b) shows binned BLD versus H_s. There is no significant relationship between the two, and the large variance in H_s experienced for each BLD bin indicates that observed rapid changes in H_s are not reflected in the development of the BLD. These results point to u_* as the more important scaling

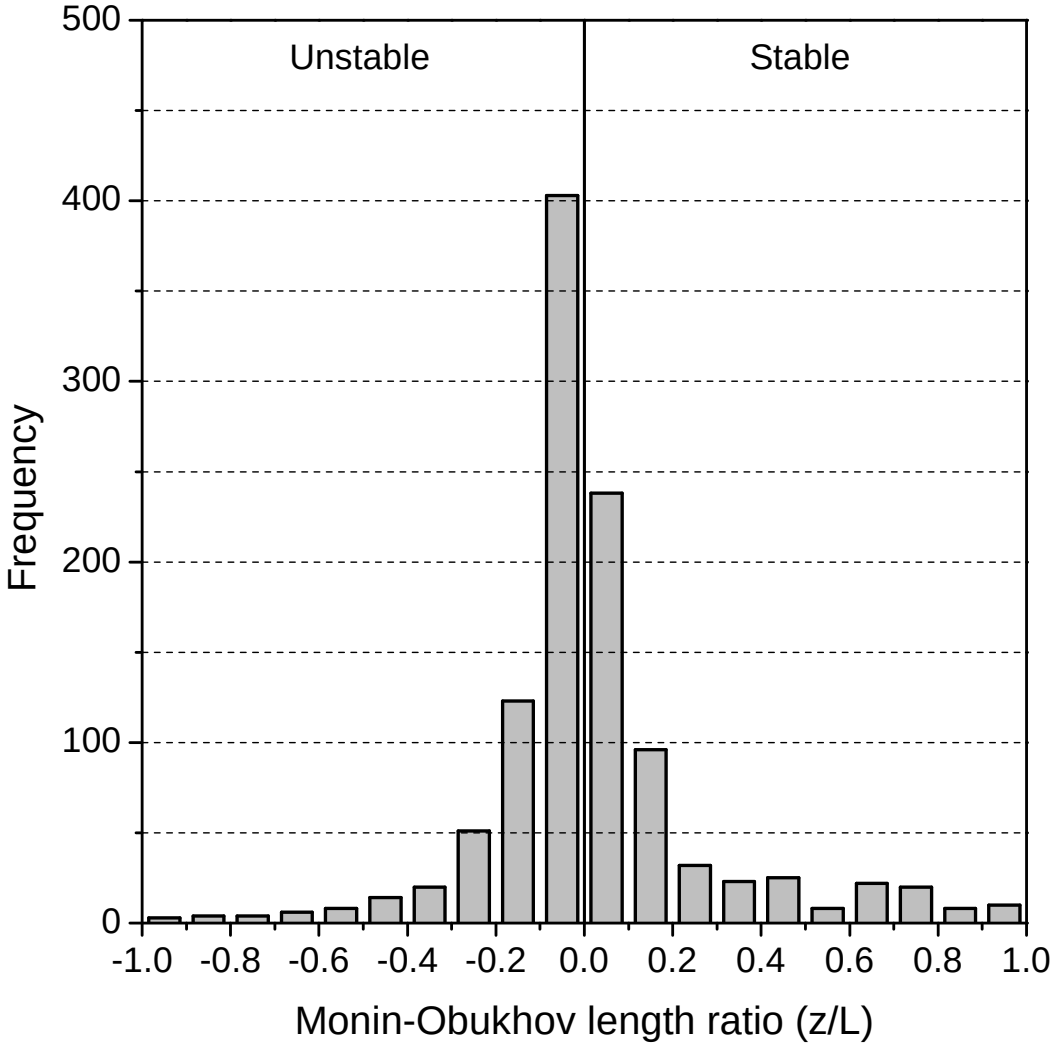

Figure 3.2: Histogram showing the frequency distribution of 30 minute average results of surface stability during June 2010 using the Monin-Obukhov length ratio ($\frac{z}{L}$).

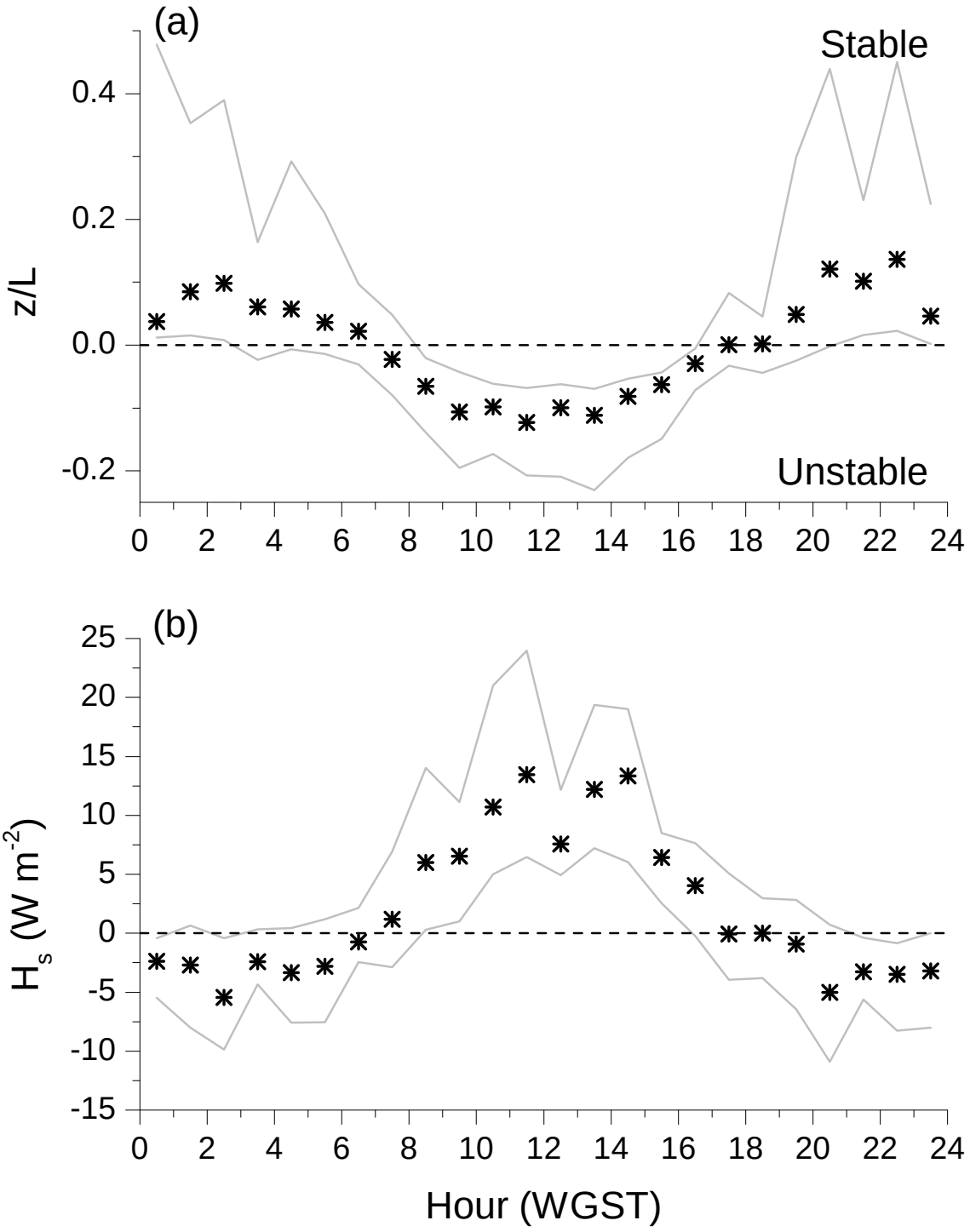

Figure 3.3: Median hourly values (black stars) of (a) $\frac{z}{L}$ and (b) sensible heat flux, H_s for the month of June 2010. The grey lines indicate the 25th and 75th percentile ranges of the hourly data.

parameter in estimating BLD at Summit; this is investigated further in the following section.

3.4.2 BLD estimation

Equations 3.1 and 3.3 were used to estimate the BLD from the sonic anemometer surface turbulence data. Figure 3.5 part (a) shows a linear regression analysis of Equation 3.1 calculations versus the sodar measurements; the linear regression line slope of 1.16 with an R^2 value of 0.71 indicates that this model slightly overestimates BLD. Figure 3.5 part (b) shows a similar plot using estimates from Equation 3.3. Here, the linear regression line has a slope of 1.6, demonstrating that this model also overestimates the BLD, and to a larger degree than the model derived from Pollard (1973). Color-contouring the data in these figures according to $\frac{z}{L}$ shows that there is less variability in the model estimates when conditions are highly stable, as compared to weakly stable or neutral. In order to improve estimations of BLD at Summit, diagnostic models such as the two described here could be implemented for stable conditions, and a separate method used when conditions become neutral to unstable. One example is the method of calculating BLD based on the integral length scales of turbulence data (Oncley et al., 2004). In that study an empirical result from Liu and Ohtaki (1997) was applied by using similarity relationships to calculate estimates of BLD during unstable conditions. It is shown here that despite the fact that a prominent diurnal cycle in heat exchange and atmospheric stability is present during the summer months at Summit, an estimation which uses u_* as the primary scaling parameter still provides a better estimate of BLD than one which utilizes H_s. Very different boundary layer conditions have been observed at Barrow (Boylan et al., 2013) and SP (Neff et al., 2008), where sustained periods of strong stability and low BLD were observed. Yet both of these studies also determined that u_* was the primary scaling parameter and that Equation 3.1 provided the closest estimate of BLD especially during stable conditions.

Figure 3.6 part (a) illustrates a time series of the sodar measurements and the estimated BLD using the two diagnostic equations implemented in this study. Both equations capture the general day-to-day variations observed in the BLD, however it is apparent that both models overestimate

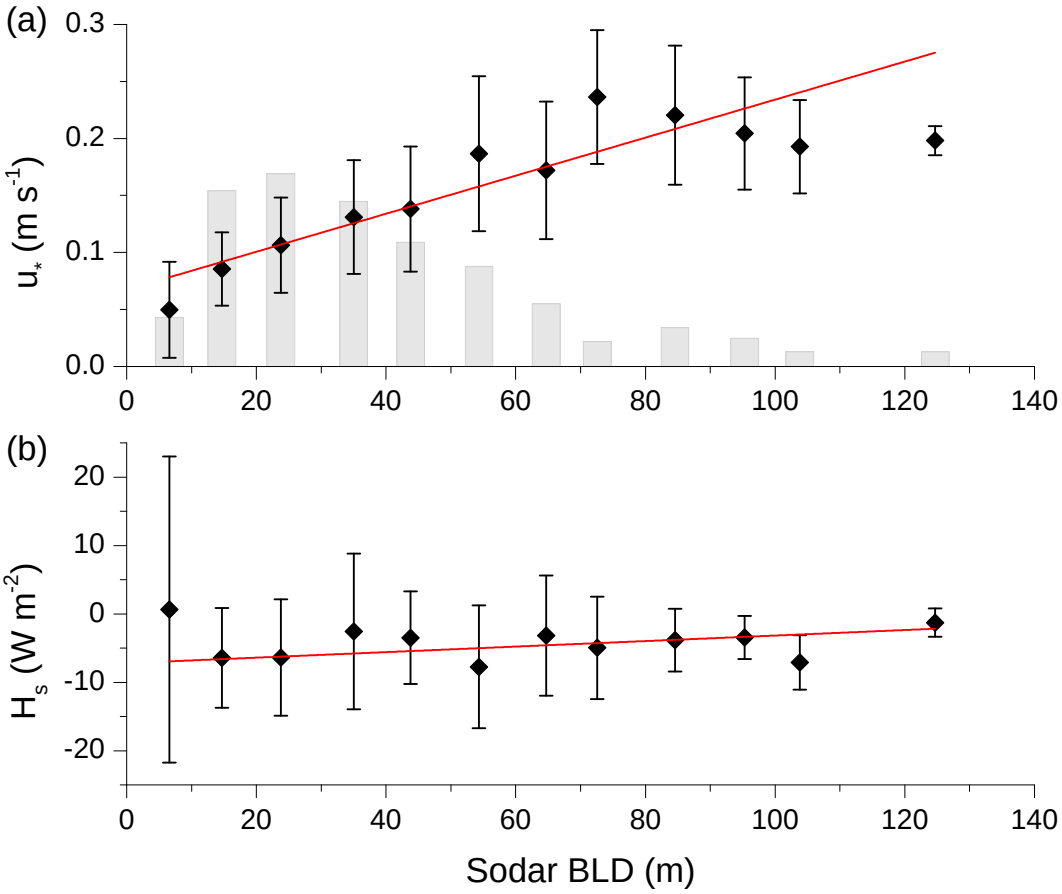

Figure 3.4: Late evening through early morning (19:00 − 03:00 WGST) data were binned by sodar observations of the BLD. Median values of the (a) friction velocity and (b) sensible heat flux are shown as a function of binned BLD. A linear regression analysis was conducted for each data set, with the data weighted by the fraction of the total number of observations available in each bin (indicated by the grey bars in panel (a), the same weighting was used in panel (b)). The linear regression R^2 value in (a) is 0.83, and for (b) is 0.29.

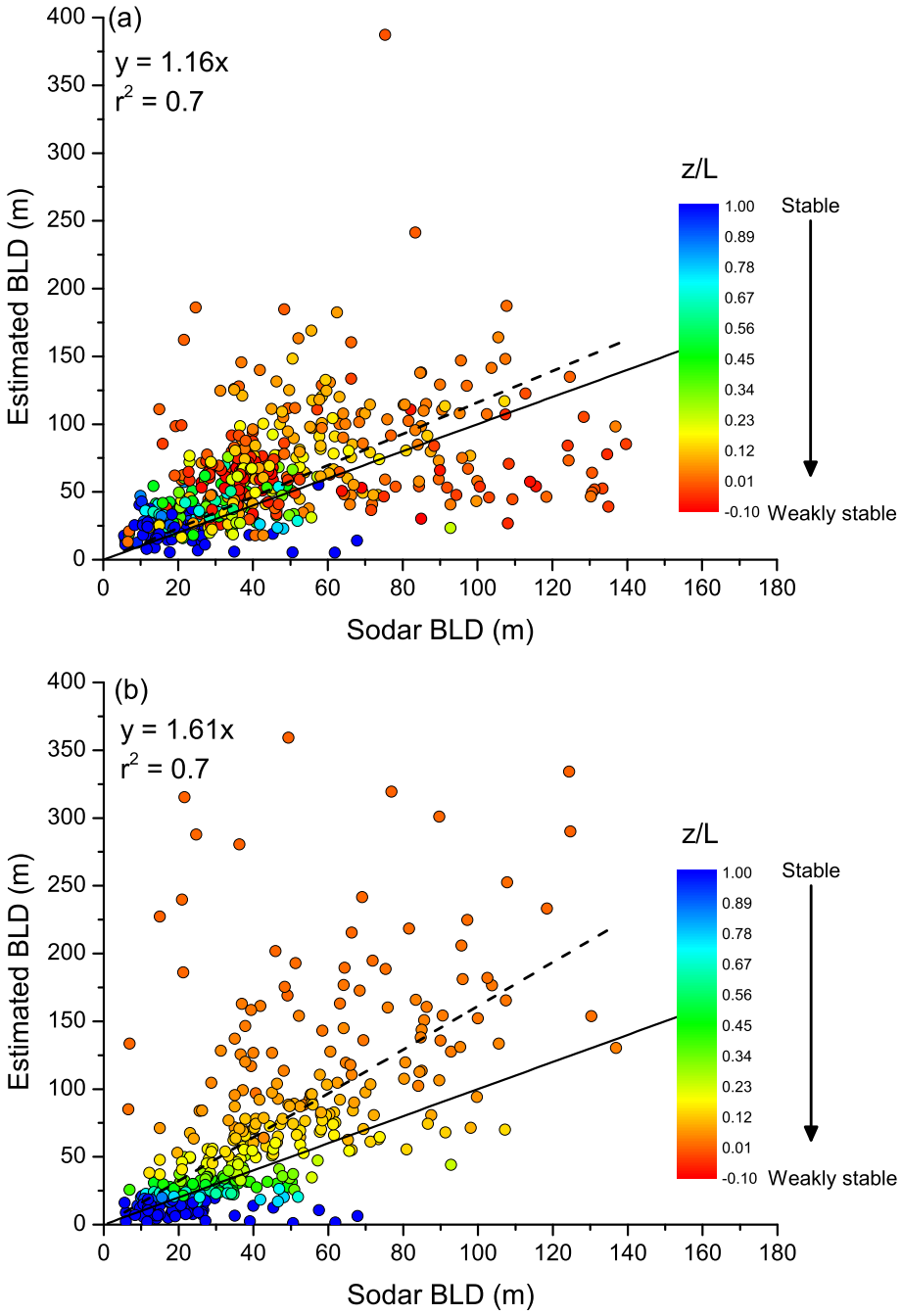

Figure 3.5: Regression analysis of boundary layer depth estimates using (a) equation 3.1 derived from Pollard (1973) and (b) equation 3.3 derived from (Zilitinkevich and Baklanov 2002) for June 2010. Only stable to weakly stable were considered. The solid black line is a 1-to-1 line, the dashed line is the linear regression fit to the data. Colors correspond to the value of the stability parameter.

the boundary layer, with Equation 3.3 more substantially so. H_s and u_*, the primary scaling parameters for Equations 3.1 and 3.3, are shown in Figure 3.6 part (b). This figure demonstrates the faster fluctuations in H_s which are not reflected in the growth or variation in the BL. Figure 3.6 (c) shows a time series of surface layer atmospheric trace gas levels during the same time period. [NO_x] was examined to test whether a linear relationship existed between BLD and NO levels. This relationship was documented at SP, where high [NO] was observed during sustained highly stable conditions characterized by low BLD (Davis et al., 2001; Helmig et al., 2008b; Neff et al., 2008). BLD was also shown to exhibit strong control on diurnal cycles of NO_x mixing ratios at Dome C, Antarctica (Frey et al., 2013). To determine if a relationship between [NO] and BLD was evident at Summit, binned [NO] and binned [NO_x] were both compared with BLD (similar to Davis et al. (2004)). Linear regression analysis gave R^2 values of less than 0.3 for both comparisons. This implies BLD did not play a critical role in determining [NO_x] at Summit during the period investigated, likely because of diurnal changes in turbulence, the lack of sustained shallow BLDs, the absence of the long fetch present on the Antarctic Plateau allowing high levels of NO_x to accumulate in the surface layer, and differences in chemical fluxes between the snowpack and the atmosphere. During June mean ($\pm 1\sigma$) [NO] was 10 $\pm$5 pptv. A one-way analysis of variance (ANOVA) demonstrated a statistically significant difference between the nighttime (defined here as 22:00−02:00 WGST) and daytime (defined as 12:00−16:00 WGST) [NO] at the $\alpha = 0.05$ level, illustrating a diurnal cycle in [NO] with a median nighttime value of 5 pptv and daytime value of 11 pptv. These levels are approximately $\frac{1}{10}$ or less of observed summertime [NO] at SP and at Dome C (Helmig et al., 2008b; Frey et al., 2013). Sustained shallow boundary layers are not the only contributor to the high levels of [NO] on the Antarctic plateau, additional factors causing differences between Summit and the Antarctic sites include the longer fetch and lower snow accumulation rates (Davis et al., 2001, 2004, 2008).

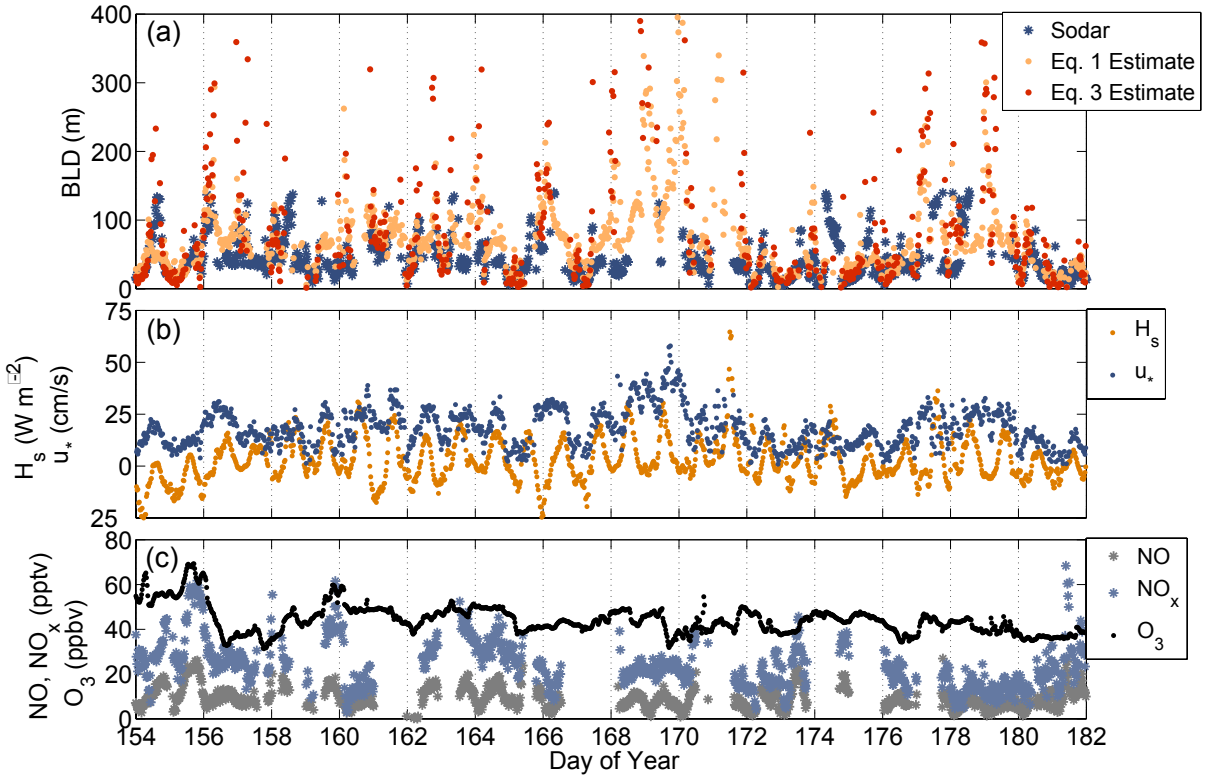

Figure 3.6: Time series of (a) BLD observations from the sodar and estimates using Equations 3.1 and 3.3, (b) friction velocity (u^*) and sensible heat flux (H_s), and (c) NO, NO_x and O_3 measured at 2.5 m on the meteorological tower.

3.5 Conclusions

Two diagnostic equations developed for estimating the BLD from surface layer turbulence data were applied for conditions encountered at Summit, and results were evaluated using data from an acoustic sounder. These models scaled well with sodar BLD for stable to weakly stable conditions. Both overestimated the BLD, with the model that was sensitive to H_s overestimating to a larger degree. The error in both estimates increased when stability conditions shifted towards neutral. A possibility for expanding BLD estimates to include neutral and unstable conditions at Summit would be to employ a tactic similar to Oncley et al. (2004) used at SP. In this study the primary focus was the boundary layer during stable to weakly stable conditions. This focus follows prior results at SP that have shown the important influence of shallow BLDs and stable conditions on near-surface trace gas levels over snow (Davis et al., 2004; Helmig et al., 2008b; Neff et al., 2008).

Using concurrent measurements of BLD and ambient trace gases, it was shown that BLD in June 2010 at Summit was not as important a factor in determining summertime trace gas levels when compared to SP, where a linear relationship between [NO] and BLD was evident. Future directions of this work should include investigating how the diagnostic models for the stable BL examined here perform seasonally at Summit (since variations in BLD are expected to change drastically during the dark winters and transitional seasons), and examining if the BLD and NO_x relationship varies during other time periods.

Chapter 4

Springtime boundary layer O_3 and GEM depletion at Toolik Lake, Alaska

This chapter is adapted from: **Van Dam, B., Helmig, D., Burkhart, J.F., Obrist, D., and Oltmans, S.J. (2013) Journal of Geophysical Research, doi:10.1002/jgrd.50213.**

4.1 Abstract

Atmospheric surface ozone (O_3) was measured at Toolik Lake, Alaska, from September 2010 to August 2011, along with winter and springtime (January − May) measurements of gaseous elemental mercury (GEM). Concurrent episodic springtime depletion of both O_3 and GEM was observed between April and May 2011. To investigate these depletion events, surface O_3 measurements from Toolik Lake were compared with similar measurements from Barrow, the only Alaskan site available to use as an indicator of conditions at the Arctic Ocean coastline. Barrow is located approximately 400 km to the northwest of Toolik Lake. In all cases where O_3 and GEM depletion was observed at Toolik Lake, similar O_3 depletion events (ODEs) were observed at Barrow. Conversely, in over half of the instances where ODEs were observed at Barrow, no such events were recorded at Toolik Lake. The Lagrangian particle dispersion model FLEXPART was utilized to interpret the transport conditions and potential influence of oceanic air masses on depletion events observed at Toolik Lake. These analyses indicate that ODEs observed at Toolik Lake are correlated with depletion events observed at Barrow when the prevailing airflow is from the north and the air mass has spent substantial time over the Arctic Ocean or coast within the previous week. These observations suggest that coastal O_3 and GEM-depleted air masses are likely transported from the

Arctic Ocean up to ∼200 km inland and at least an altitude of 700 m above sea level. These observations underscore that O_3 and GEM depletion events impact not just the Arctic coastal zone but also extensive inland areas with possible implications for the cycling and bioavailability of mercury (Hg) to inland Arctic ecosystems.

4.2 Introduction

Abrupt and intermittent occurrences of low ground-level ambient ozone (O_3) mole fractions at or below instrument detection limits after polar sunrise have been observed since the 1980s in polar coastal locations including Barrow, AK (Oltmans, 1981), Alert, Canada (Bottenheim et al., 1986; Barrie et al., 1988), and Neumayer, Antarctica (Wessel et al., 1998). Episodes of depleted O_3 in the Arctic (typically termed O_3 depletion events, or ODEs) are mainly observed over the frozen ocean and near coastal sites after polar sunrise between March and May. These events were discovered to be closely linked to halogen chemistry, as ODEs were highly correlated with enhanced levels of filterable bromide (Barrie et al., 1988; Oltmans et al., 1989; Jobson et al., 1994). It is theorized that reactive bromine species sourced from sea salt bromide are responsible for the destruction of surface O_3 through a photochemically driven chain reaction, although the exact pathways involved in the conversion of inert halide salts in the Arctic Ocean to reactive halogens in the atmosphere are not fully understood (Perovich and Richtermenge, 1994; Foster et al., 2001; Simpson et al., 2007). The depleted air masses can remain in this state for several days due to limited vertical and horizontal mixing in the stable and stratified Arctic boundary layer (Anderson and Neff, 2008). While these air masses have been shown to be subject to transport to high and lower latitude coastal regions, transport inland away from coasts has been hypothesized but not shown clearly (Simpson et al., 2007; Gilman et al., 2010).

A little over a decade after the discovery of ODEs, the first continuous sampling of surface level gaseous elemental mercury (GEM, e.g. Hg^0) in the Arctic began at Alert, Canada in 1995 (Schroeder et al., 1998). It was discovered that episodic depletion of GEM was prevalent in the Arctic following polar sunrise, and that GEM concentrations during these events (termed Atmo-

spheric Mercury Depletion Events, or AMDEs) were correlated with surface level O_3 depletion. Observational and modeling data suggest that during AMDEs reactive bromine species act as the primary oxidant converting GEM into oxidized inorganic reactive gaseous mercury (RGM, e.g. HgO, HgBr, etc) or fine particulate-bound mercury (FPM) that can be readily deposited to the snowpack or ice surfaces (Lu et al., 2001; Lindberg et al., 2002; Berg et al., 2003; Sprovieri et al., 2005; Steffen et al., 2008; Stephens et al., 2012). AMDEs are an important pathway by which GEM, a long-lived form of mercury (Hg) that can undergo long-range transport, can be oxidized and then efficiently scavenged in the Arctic. Once deposited, Hg is subject to either re-volatilization back to the atmosphere or it remains in the ecosystem with the potential to bioaccumulate into the environment, marine mammals, and eventually humans (Macdonald and Bewers, 1996; Lalonde et al., 2002; Steffen et al., 2002; Ferrari et al., 2005). This potential for harmful environmental, animal and human health effects makes it critical to understand the trends and speciation of Hg throughout various Arctic ecosystems.

ODEs and AMDEs have been shown to originate over the frozen Arctic Ocean and subsequently be transported to coastal measurement sites (Bottenheim and Chan, 2006; Simpson et al., 2007; Gilman et al., 2010). There is limited understanding of if and how these events are transported further inland, away from coastal regions. To improve this understanding, conditions are compared between an inland and coastal environment by taking advantage of unique parallel data sets at two locations that reflect these environments. This study 1) shows detailed surface O_3 and GEM measurements throughout the Arctic springtime at an elevated site located several hundred kilometers inland from the Arctic Ocean coastline, 2) demonstrates that ODEs and AMDEs are observed at this location, 3) investigates the frequency and strength of the inland depletion events and 4) examines the transport pathways during and prior to their occurrence.

4.3 Methods

4.3.1 Site description

An assortment of instruments to measure O_3, GEM and meteorological parameters were deployed at the National Science Foundation Long Term Ecological Research (LTER) site Toolik Lake, Alaska, between September 2010 and September 2011 (GEM was only measured between January to May, 2011). Toolik Lake is located at 68.63°N, 149.59°W, at an elevation of 720 m a.s.l., and approximately 200 km from the Arctic Ocean coastline (Figure 4.1). This site sits at the northern border of the foothills of the Brooks Range, at the edge of the arctic coastal plain that constitutes the north slope of Alaska. During the measurement year, the first snowfall occurred on 25 September 2010, snow cover was 100% by 3 October 2010, and the site was snow-free by 25 May 2011. Observations from Toolik Lake were compared with data from the US National Oceanic and Atmospheric Administration (NOAA)-Global Monitoring Division (GMD) site at Barrow, AK (71.32°N, 156.6°W, 8 m a.s.l.). This measurement station is located on the coast of the Arctic Ocean, 400 km to the northwest of Toolik Lake.

4.3.2 Meteorological measurements

A suite of meteorological instruments were deployed on a 4 m tower, approximately 30 m from a laboratory which sat at the south end of Toolik Lake. Wind speed and temperature were measured at three heights above ground level at 0.5 m, 1.9 m and 4.1 m. Wind speed was measured using three cup anemometers (Model O10C, MetOne Instruments); temperature was measured using three RTD temperature probes (Model 41342, R.M. Young Company, Traverse City, MI) housed in aspirated radiation shields (Model 43502, R.M. Young Company, Traverse City, MI). Regular same-height inter-comparisons of the temperature and wind speed instruments were conducted in order to detect and correct for any instrumental offsets, tower interference or drifting. Turbulence values were calculated as described in Cohen et al. (2007) using data from two 3-D ultrasonic anemometers (Metek USA-1) at 1.4 m and 3.4 m on the same tower. Incoming and reflected

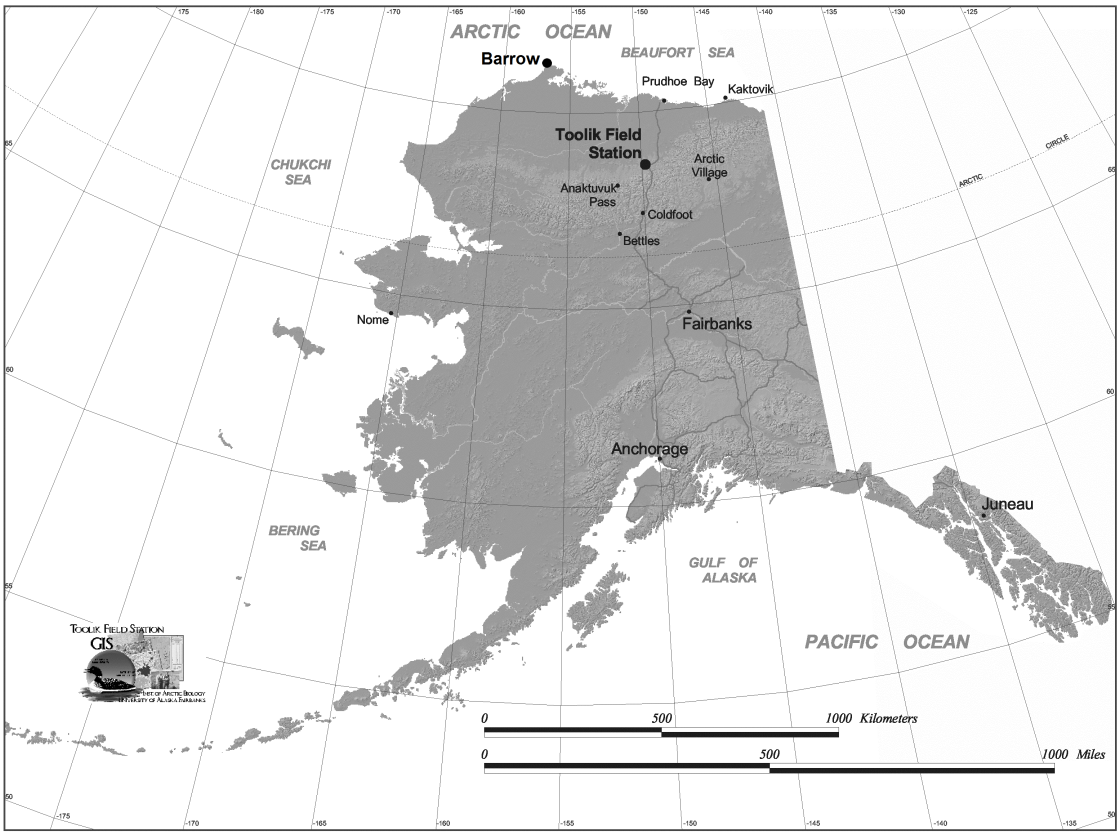

Figure 4.1: Toolik Field Station GIS map showing the locations of Toolik Lake and Barrow, Alaska (http://toolik.alaska.edu/gis).

solar radiation was measured using two LI200X pyranometers (Campbell Scientific Instruments) from a small tower located ∼15 m northeast. Wind direction was inferred from the 3-D ultrasonic anemometer data, as well as a wind vane (Model 030B, MetOne Instruments). These wind direction values were additionally compared with wind direction data provided by the Toolik Field Station Environmental Data Center for accuracy. A schematic of the primary measurement tower and instrumentation is shown in Figure 4.2.

4.3.3 O_3 measurement

Surface O_3 measurements were conducted at 4.1 m on the meteorological tower. This measurement was accomplished using a Model 49C UV photometric O3 analyzer (Thermo Environmental Instruments (TEI), Franklin, MA) with calibration traceable to the U.S. National Institute of Standards and Technology (NIST). These instruments have a standard detection limit of 1 ppbv, response time of 20 s, and precision of 1 ppbv. Air was sampled at 1.0 L min^{-1} through a 35 m Teflon sampling line (perfluoroalkoxy copolymer [PFA]) with 0.64 cm outer and 0.40 cm inner diameter. A PFA filter holder (Savillex Corp., Minnetonka, MN) was implemented to house a Teflon membrane inlet filter (5 m, Millipore, Billerica, MA, USA). The sampling frequency of the instrument was 10 s, readings were averaged to 1 min. The O_3 data reported here were also compared to surface O_3 measurements from two other instruments. First, another NIST traceable TEI Model 49 analyzer was used with inlets located approximately 10 m from the main meteorological tower; this snow-tower set-up (which is similar to the sampling manifold and valve system described in Seok et al. (2009)) allowed air collection at multiple heights, however for the ambient air observations detailed in this work only the inlet located 1.95 m above the ground was used. The TEI 49 sampled air through a similar 35 m sampling line, with the exception that a 25 mm Acrodisc hydrophobic polytetrauoroethylene (PTFE) syringe filter (Pall Life Sciences, Ann Arbor, Michigan, USA) was used instead of the filters described above. Second, the data were compared to O_3 measurements taken through an inlet at 3.4 m on the meteorological tower, using a fast response chemiluminescence ozone instrument (FRCI). For a detailed description and schematic of this instrument see

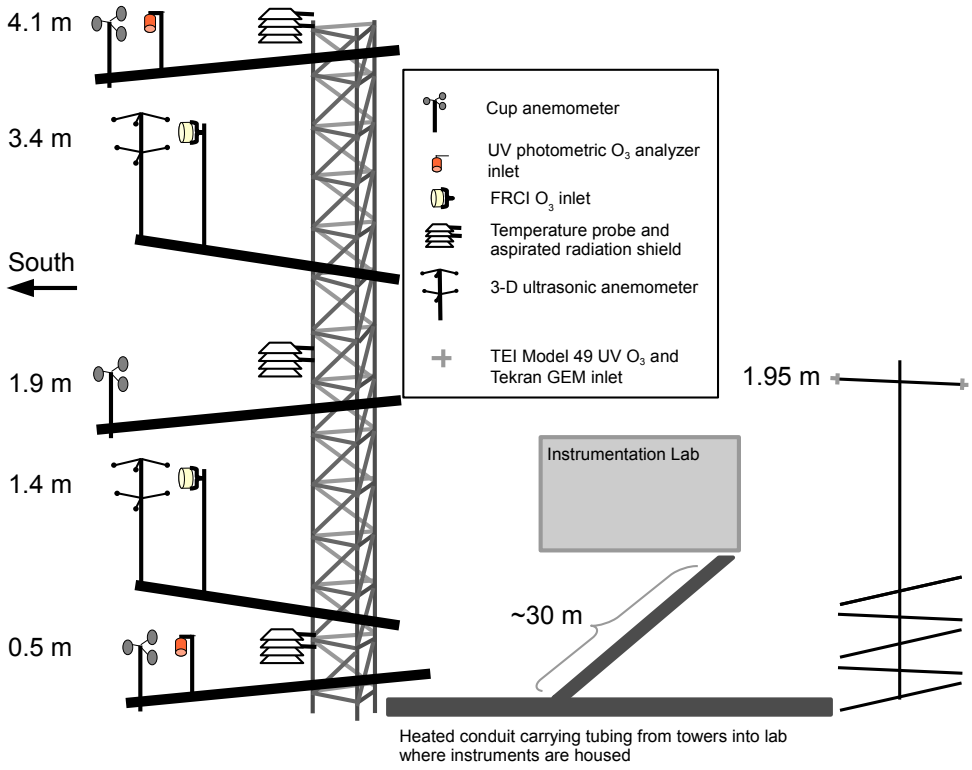

Figure 4.2: Schematic of the main sampling tower (shown at left) and snow sampling tower (at right) at Toolik Field Station. Data from the upper met tower inlet (UV photometric O_3 analyzer) at 4.1 m, the 3.4 m inlet for sampling with the FRCI, and the upper snow tower inlet at 1.95 m (for sampling with the Tekran) were utilized in the work presented here.

Bariteau et al. (2010). For this measurement, a 35 m sampling line with an inner diameter of 0.64 cm and outer diameter of 0.95 cm was used. For all described O_3 measurements, all PFA sampling lines and filters were conditioned before use by purging with air containing ∼300 ppbv O_3 at a flow rate of 3 L min^{-1} for 24 h. A regression analysis of the FRCI observations against the TEI 49C O_3 measurement used for the rest of the analysis (surface O_3 at 4.1 m on the main tower) was performed for the month of April 2011 (this relationship is shown as Figure A.1 in the Appendix). The slope of a linear regression between these observations was 1.01, and the coefficient of determination, R^2, was 0.99. These parameters both point to the excellent comparison between these two measurements, and give high confidence in the quality of surface O_3 data measured at this site.

Surface O_3 data from Barrow, AK were collected by the NOAA/ESRL Global Monitoring Division using a UV TEI Model 49C photometric O_3 analyzer. Details of these measurements are described in Oltmans et al. (2012).

4.3.4 GEM measurement

GEM was measured using a Tekran gas phase GEM analyzer (Model 2537A; Tekran Inc., Toronto, Canada). Samples were drawn through an approximately 1 m long piece of Teflon tubing connected through a Swagelok PFA tee to the snow tower system as described above for the TEI 49 O_3 instrument. Consequently, ambient air GEM measurements were also taken at a height of 1.95 m above the surface and ∼10 m from the main sampling tower. The GEM analyzer was operated at a flow rate of 1.0 L min^{-1} and with 5-min temporal resolution; however, due to the snow tower sampling cycle, ambient GEM measurements were performed only for 10 min every hour. Automatic internal calibrations were performed every 25 h. The manufacturers reported detection limit for 2.5 min samples measured with the Model 2537 analyzer is less than 0.10 ng m^{-3}; others have reported detection limits of 0.17 ng m^{-3} for 5 min samples (Aspmo et al., 2005).

4.3.5 FLEXPART

The Lagrangian Particle Dispersion Model (LPDM) FLEXPART (Stohl et al., 2005) was used to calculate 20-day retroplumes for the Toolik Lake observations. FLEXPART has been extensively used for Arctic atmospheric transport studies (Helmig et al., 2007d; Sjostedt et al., 2007; Gilman et al., 2010; Vay et al., 2011) and is frequently applied to the investigation of long-range atmospheric transport. The model was run using ECMWF (0.25° x 0.25° horizontal resolution, 92 vertical levels) global meteorological fields. Two tracers were used for the modeling, a passive tracer with no wet or dry removal, and an 'aerosol-like' tracer having limited wet and dry removal parameters. The use of these two tracers allows for an upper and lower limit of reasonable losses for aerosol species, despite the lack of chemical reactions in the modeling. For every 3-hourly meteorological input data time step (e.g. 00, 03, 06, ... 21 hours) 90,000 particles of each tracer were released, therefore in total the location of 180,000 particles are tracked internally, with no interaction occurring between the tracers. The particles were released at the Toolik Lake site at a height of 10 m above ground level. The FLEXPART model produces output (reported as seconds) that is proportional to the residence time of the particles in a given volume of air. To produce a footprint Potential Emissions Sensitivity (PES) map, the lowest model layer (less than 100 m above ground level) is used independently and provides a plot with units (s kg^{-1}). This provides information on where and when the air mass would be sensitive to surface emissions. The surface layer is important in this analysis because AMDEs have been shown to be limited to the lowest 1 km of the atmosphere (Banic et al., 2003; Steffen et al., 2008), and the primary halogen chemistry impacting Hg during these events is limited to less than 200 m above the snow surface (Tackett et al., 2007).

4.4 Results and discussion

4.4.1 Site comparison

The surface O_3 record for Toolik Lake shows some similar characteristics to other remote Arctic sites, where annual records typically show summer minima and late winter or early spring

maxima (Helmig et al., 2007c). A 1-year surface record at Toolik Lake is compared to the same year annual record at Barrow in Figure 4.3 panels (a) and (b) to illustrate the similarity in seasonal cycles at both locations. January, February, and particularly March had the highest mean and median monthly O_3 mixing ratios. The highest variability in surface O_3 is due to the influence of ODEs and observed during April and May. Conversely, during the summer months of June − August, the lowest monthly mean O_3 values were observed. During June − August, the lowest 5th percentile of observed O_3 values at Toolik Lake are of similar magnitude as during spring. However, these data are not associated with ODEs, but instead are due to a strong diurnal signal in the summertime O_3 record.

Throughout the winter months Barrow and Toolik Lake show similar low variability in hourly O_3 and similar monthly mean O_3 mixing ratios. The influence of springtime ODEs are observed at the beginning of March in the Barrow record (discussed in detail in the next section). It is interesting that surface O_3 at Barrow remains substantially lower than Toolik Lake levels throughout the remainder of the spring, even during the periods between ODEs. During March through May monthly median O_3 values at Barrow were on the order of 10−20 ppbv lower than the Toolik Lake monthly medians. In the summertime, the two locations again show similar monthly medians, although the diurnal variability at Toolik Lake is significantly greater.

4.4.2 ODE and AMDE observations

The majority of ODEs and AMDEs observed at Toolik Lake in 2011 occurred during the month of April. Surface O_3 and GEM concentrations are shown for that time period in Figure 4.4. Throughout most of the month, GEM observations reflect typical remote northern hemisphere background concentrations between 1.5 to 1.7 ng m^{-3} (Slemr et al., 2003; Temme et al., 2004; Steffen et al., 2008). Episodic depletion of GEM in the near surface atmosphere was observed throughout April; during several events GEM concentrations decreased rapidly to as low as 0.2 ng m^{-3}. As these values are above the instrumental detection limit, this result implies that measurable GEM was observed even during AMDEs. This is in contrast to data from Barrow, where GEM concentrations

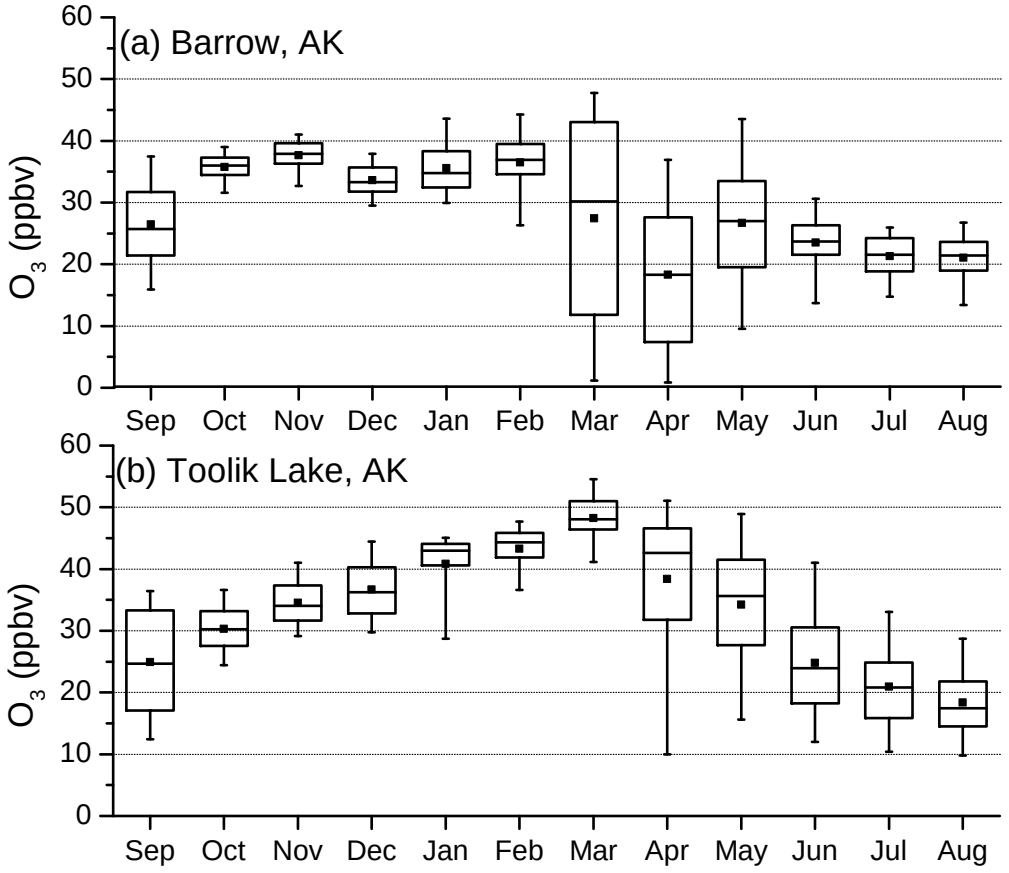

Figure 4.3: Whisker plots showing the seasonal surface O_3 behavior at (a) Barrow and (b) Toolik Lake. Black squares indicate the monthly means, lower and upper box borders correspond to the 25th and 75th percentile, and the horizontal line in each box corresponds to the monthly median. Lower and upper whiskers correspond to the 5th and 95th percentile. Sampling dates for both locations range from September 2010 to August 2011.

typically drop to less than 0.1 ng m^{-3} during AMDEs (Lu et al., 2001). The higher residual GEM values seen during AMDE at Toolik Lake are likely due to mixing of GEM−depleted air with air masses richer in GEM during transport from the coast (a further discussion of transport occurs later in the text). Reductions in GEM are correlated temporally with observed ODEs for this month. During the month of April, a linear regression analysis of GEM versus O_3 for periods when GEM was below 1.5 ng m^{-3} gave a correlation coefficient of 0.67. This correlation is moderate compared to what has been observed, for example, at Ny-Ȧlesund or the Dead Sea (Schroeder et al., 1998; Eneroth et al., 2007; Obrist et al., 2011). One hypothesis for the cause of the weaker correlation measured at Toolik Lake is that GEM oxidation is occurring near the coast, with subsequent mixing of GEM-depleted air with air masses that have different GEM to O_3 ratios during transport inland.

A striking feature in the April GEM record is the rapid increase of atmospheric GEM concentrations to above-ambient levels, up to a maximum of 2.6 ng m^{-3}, immediately following each observed AMDE. After this notable increase, levels eventually return to prior ambient concentrations before entering the next event. The length of these enhancement periods varied from 5 to 15 h, while depletion periods were typically longer, ranging from 5 to near 24 h. This phenomenon has been observed at other locations, including at Alert and Cornwallis Island, Nunavut, Canada, Hudson Bay, Canada, and Barrow (Kirk et al., 2006; Johnson et al., 2008). These enhancements following AMDEs are likely due to a portion of the deposited Hg being photoreduced back to GEM and subsequently re-volatilized back into the atmosphere (Lalonde et al., 2002; Steffen et al., 2002; Poulain et al., 2004; Brooks et al., 2006). Periods with enhanced GEM occurred only during daytime when incoming solar radiation was present. These GEM enhancements potentially point towards surface re-volatilization events that could be promoted by a pulse of RGM transported to and deposited at the site during the prior GEM depletion event. In contrast to ODEs, where O_3 is chemically destroyed in the surface layer, during an AMDE Hg is not chemically removed, but instead GEM is oxidized into RGM which can deposit rapidly to the snow surface. If RGM is indeed transported to the interior Arctic, then it will be important to determine the portion of deposited Hg that becomes bioavailable to the varied ecosystems. The bioavailability of Hg following AMDEs

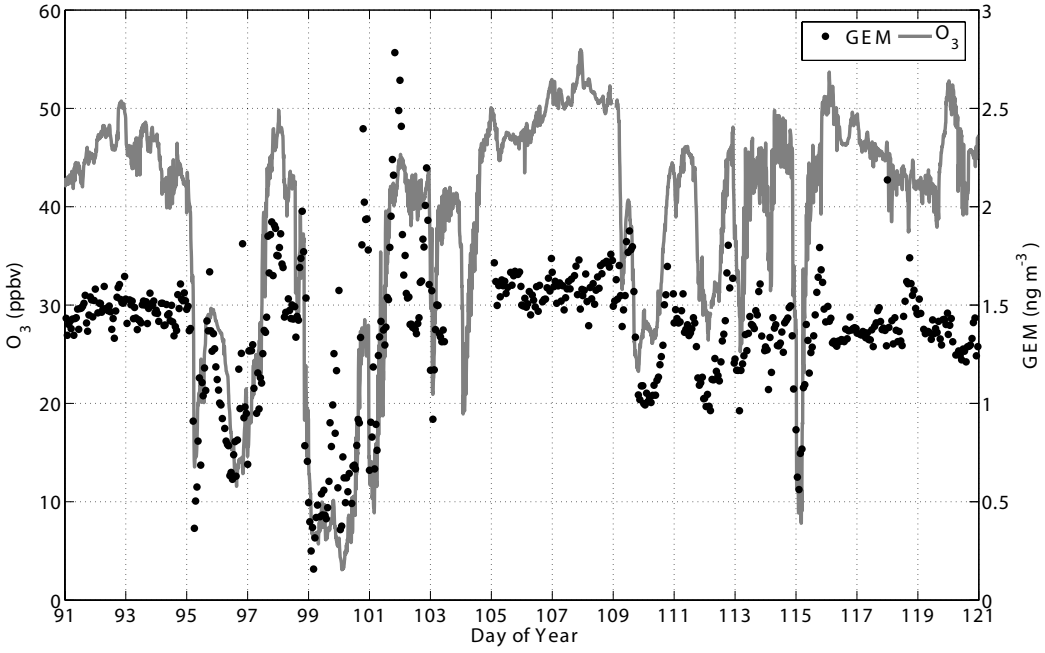

Figure 4.4: Surface O_3 (gray line) and GEM (black dots) at Toolik Lake during the month of April 2011. These records show a strong correlation during several observed depletion events.

is not well understood; results from several studies have found that a significant fraction of total deposited Hg resides in the ecosystem, while the remainder is photoreduced and re-emitted back to the atmosphere as GEM. Douglas et al. (2012) summarized 10 separate studies that measured total Hg concentrations in snow following AMDEs, finding that $\sim 10 - 25\%$ of Hg remains in the snow one week after deposition.

Ten minute mean surface O_3 observations at Toolik Lake throughout the springtime are shown in detail in Figure 4.5, in comparison with hourly mean surface O_3 measurements from Barrow. ODEs were observed throughout the springtime at both locations, although the influence of ODEs was not observed at Toolik Lake until a month later than Barrow. During March 2011, low O_3 conditions (defined here as values less than 15 ppbv) were present at Barrow 29% of the time, largely contrasting with Toolik Lake, where no low O_3 events were recorded during that month. In April 2011, low O_3 was present at Barrow 41% of the time, and at Toolik Lake low O_3 was recorded during 8.8% of the month. Additionally, during ODEs the minimum recorded O_3 value at Toolik Lake was 3.1 ppbv, while O_3 mixing ratios at Barrow frequently dropped to below 1 ppbv. Higher accuracy measurements during the Barrow OASIS experiment found that residual O_3 levels were $0.010-0.100$ ppbv during ODE (Helmig et al., 2012a). These events reduce monthly mean values, and increase the concentration variability of the data. Through March and April, monthly median O_3 values were 20 ppbv higher at Toolik Lake, and in May the Toolik Lake monthly median was $\sim$10 ppbv higher than for Barrow. These substantial differences indicate that ODEs at Barrow start earlier during the year, have a higher frequency, result in lower O_3 levels, and are also more sustained as compared with Toolik Lake. The weaker ODEs observed at Toolik Lake are expected to be due to mixing of depleted air masses with O_3 rich air during transport from the coast (see transport analysis in the following section).

Following the first ODEs at Barrow in March, O_3 mixing ratios at the surface increased back to levels similar to Toolik Lake (as shown in Figure 4.3, Barrow and Toolik showed similar wintertime O_3 mixing ratios). However, later on in the springtime it appears that surface O_3 at Barrow remains suppressed substantially below Toolik Lake levels. These sustained low levels of

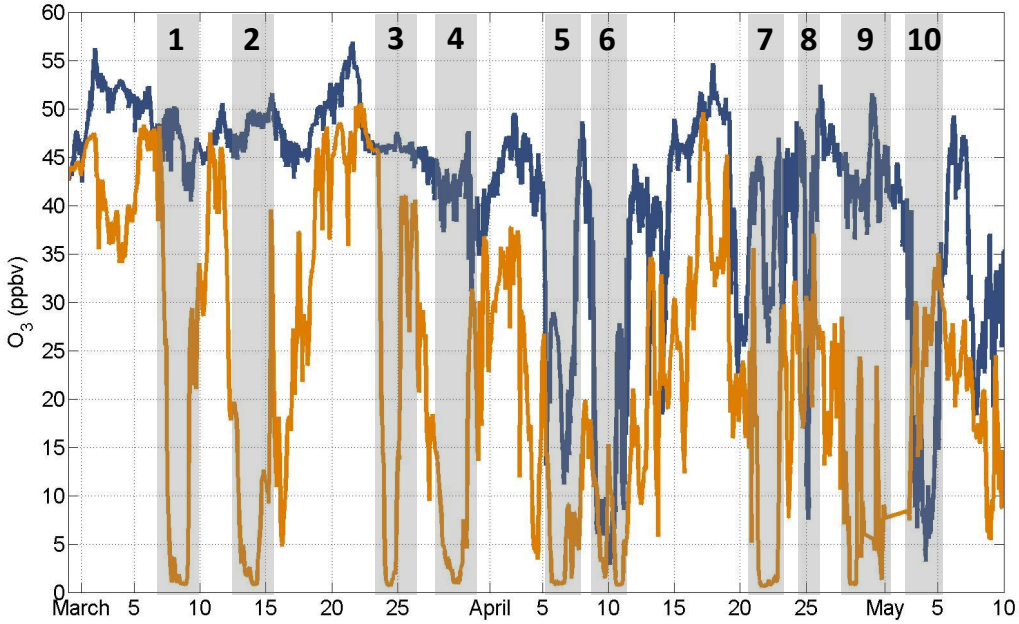

Figure 4.5: Surface O_3 at Toolik Lake and Barrow during March 1 May 10, 2011. Barrow data (orange) are 1 h averages, while the Toolik Lake data (dark blue) are averaged over 10 min. Significant ODEs observed at Barrow (when O_3 dropped below 5 ppbv) and Toolik Lake (when O_3 dropped to roughly $\leq$10 ppbv) are highlighted in grey and numbered in sequence for easy identification in the text.

O_3 at Barrow later in the spring are typical, yet 2011 actually showed fewer ODEs later in spring than during previous years. The monthly O_3 record from May 2011 has higher mean and 5th and 25th percentile values as compared with the 1999−2008 May Barrow record (Oltmans et al., 2012). Integrating over the full year between September 2010 and September 2011, ODEs at Barrow reduce the annual mean O_3 value by approximately 1.7 ppbv. At Toolik Lake the reduction in mean O_3 is smaller; integrating over the measurement year, the influence of ODEs caused a reduction in mean O_3 of ∼0.5 ppbv.

4.4.3 Meteorological and transport analysis

Located well north of the Arctic Circle, meteorological conditions at Toolik Lake are influenced by a strong seasonal cycle of incoming solar radiation (Figure 4.6 panel (a)), and also impacted by the nearby Brooks Range to the south. A wide range of temperatures was observed at the site, from a minimum of −50°C to a maximum of 25°C. Figure 4.6 panel (b) shows that winter and springtime temperatures displayed similar monthly averages and variability during December April, with a near 20 degree increase in the median monthly temperature in May, coincident with the maximum in mean and median insolation. During the September 2010 August 2011 campaign, Toolik Lake was characterized by moderate to low wind speeds. The mean wind speed was below 4 m s^{-1} for all months other than February, when a notable increase in amplitude and variability was observed (Figure 4.6 panel (c)). Low O_3 conditions were not observed at wind speeds above 4 m s^{-1}. During the month of April, Toolik Lake experienced colder mean temperatures, lower mean wind speeds, yet higher incoming solar radiation than during March. Simpson et al. (2007) has documented that these are ideal conditions for the occurrence of ODEs, and these environmental factors could in part explain why Toolik Lake experienced the highest frequency of ODEs and AMDEs in April 2011.

To determine whether local meteorology contributed to the observances of ODEs, the relationships between O_3 mixing ratios and wind direction, as well as between GEM concentrations and wind direction were investigated. This analysis is shown in Figure 4.7, where March − April

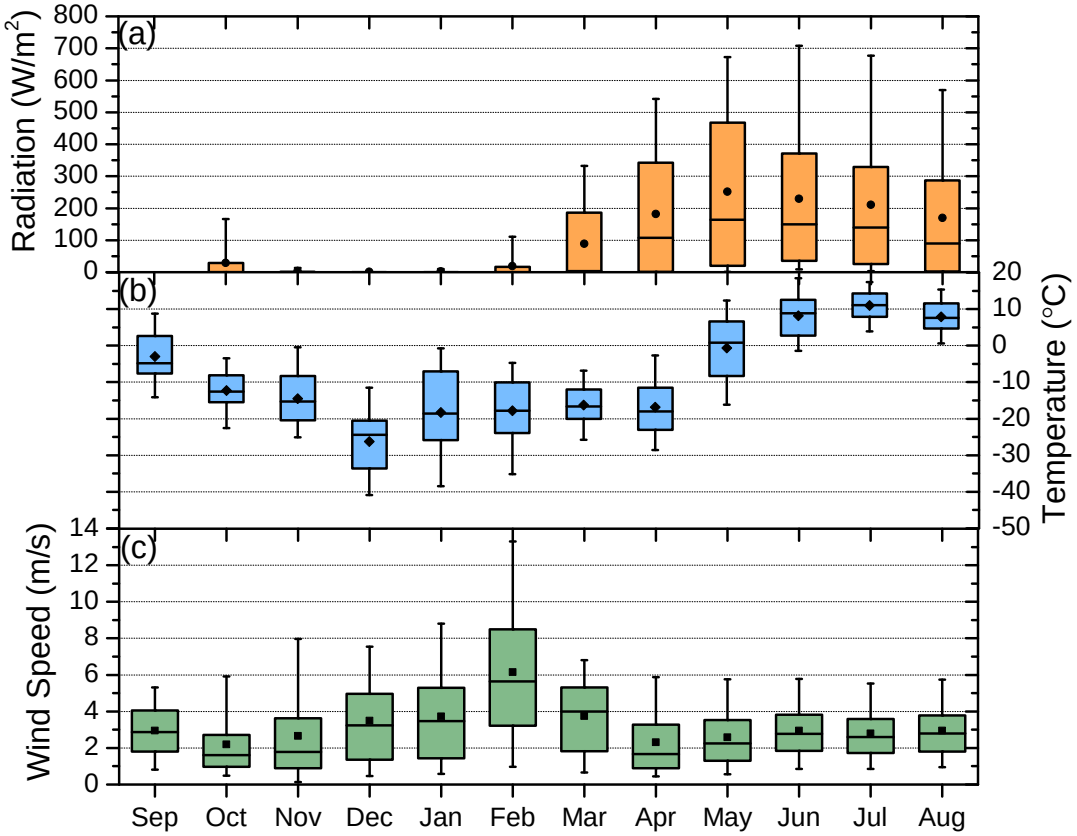

Figure 4.6: Whisker plots showing monthly (a) radiation, (b) temperature, and (c) wind speed for the measurement period at Toolik Lake. Box lines, whiskers, and symbols are the same as defined for Figure 4.3. Radiation sensors were not installed at the site until October, so no data are available during the month of September 2010.

surface O_3 mixing ratios and GEM (color contours) are plotted as a function of wind direction (measured from the 3-d ultrasonic anemometer located at 3.4 m above the surface). The data clearly show that springtime winds at Toolik Lake during this time were highly constrained to two narrow bands, from the WNW and SSE. It can also be seen that low O_3 and GEM values are not clearly correlated with any particular wind direction, indicating that wind direction measured near the surface cannot be used as a reliable indicator of when springtime ODEs occur at Toolik Lake. This is in stark contrast to Barrow, where measurements of ODEs and AMDEs are closely linked to the surface wind direction, due to the proximity to the source of depletion over the Arctic Ocean (Simpson et al., 2007).

Synoptic transport conditions were investigated for the events numbered 3, 4, 6, and 10 labeled in Figure 4.4. Surface data from Barrow (the only measurement site available on the Arctic Alaskan coastline for comparison) were included as an indicator of time periods when ODE/AMDE were observed both at the coast and at Toolik Lake. This set includes two events when an ODE was observed at Barrow but not at Toolik Lake (3 and 4) and two events when depletion was observed at both Toolik Lake and Barrow (6 and 10). This allowed an investigation of transport conditions at Toolik Lake during all times when a coastal ODE/AMDE was experienced. Examples of FLEXPART footprint PES maps for transport regimes at Toolik Lake during events 1, 2, 5, 7, 8, and 9 are shown in Figure A.1 panels (a) − (f) in the Appendix. The FLEXPART footprint PES maps show a color contour of the emission sensitivity, which is proportional to the residence time of particles in a unit area, a good estimate of the location of the transported air at a given time. For events 3 and 4, when an ODE was seen at Barrow but no depletion was observed at Toolik Lake, FLEXPART results indicate that the air masses sampled at Toolik Lake originated from the south and were transported mainly over land (Figure 4.8). In contrast, during events when O_3 depletion was observed at both Barrow and Toolik Lake, FLEXPART results indicate that the air masses sampled at Toolik Lake had passed over the Arctic Ocean, and were transported to Toolik Lake mainly from the north to northeast (Figure 4.9). Figure 4.9 (a)−(d) shows the difference in transport conditions before and after an ODE/AMDE was experienced at Toolik Lake. The

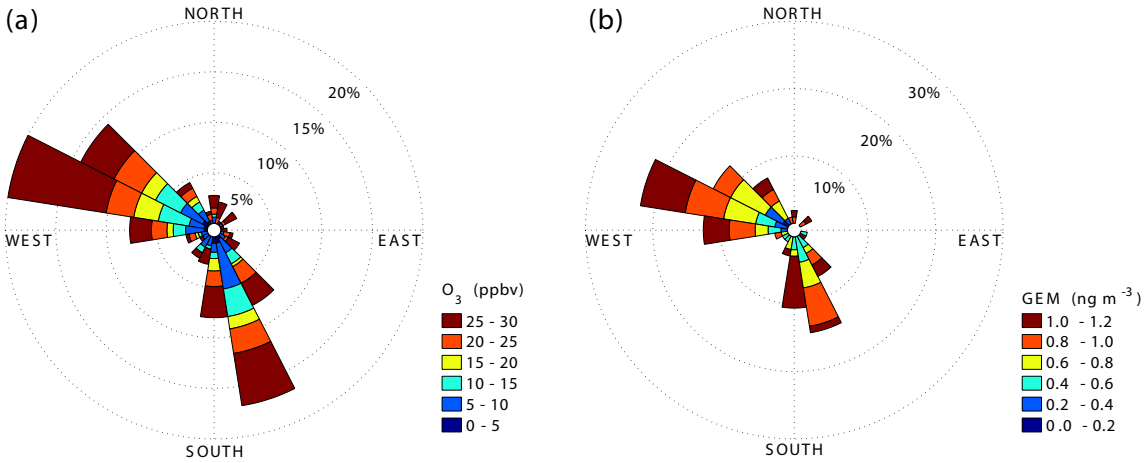

Figure 4.7: (a) Surface O_3 and (b) GEM plotted as a function of wind direction measured by an ultrasonic anemometer at Toolik Lake. Data span March 1 – April 30, 2011. Color contours correspond to (a) the O_3 concentrations in ppbv and (b) GEM concentrations in ng m^{-3}, and the length of each wedge indicates the frequency of each concentration range in that particular wind direction sector. Only data with O_3 values less than 30 ppbv and GEM less than 1.2 ng m^{-3} were included in these figures.

two maps in panels (a) and (c) show transport before events 6 and 10. The centroid location for the plume prior to events 6 and 10 (indicated by the circle markers and numbers on the figures) indicates transport coming from the west over north-western inland Alaska (panel a, event 6) or from the south-west (panel c, event 10). This is in direct contrast to panels (b) and (d), which show an Arctic Ocean source for the events 6 and 10 observed at Toolik Lake.

The air masses associated with the Toolik Lake ODEs and AMDEs spent a substantial period over the Arctic Ocean before arriving at Toolik Lake. Within the 10 day back trajectory for each ODE investigated, the air masses had spent at least $5-7$ of those days over the Arctic Ocean. FLEXPART indicates that once reaching land, the air masses then traveled the remaining $3-5$ days either along the coast and then moved inward to Toolik Lake (as exemplified during the May 4 event, when the air mass sat near the coast for $\sim$2 days before moving inland for 3 days until arrival over Toolik Lake), or moved directly inland to Toolik Lake (for example, during the April 8 event when the air mass spent 7 days moving over the Arctic Ocean before reaching the coast to the northeast of Toolik Lake and then traveled 3 days to reach the measurement site). Footprint sensitivity analysis by FLEXPART indicates that the ODEs observed at Toolik Lake have a common transport source region over the Arctic Ocean. Previous studies have shown that ODEs originate over the frozen surface of the Arctic Ocean and are subsequently transported to coastal stations (Bottenheim and Chan, 2006; Simpson et al., 2007; Gilman et al., 2010). This is likely to be the case at Toolik Lake, as opposed to O_3 depletion chemistry occurring in proximity to this measurement site. This is a significant finding, as detailed ODE and AMDE at a site located as far from the coast and at an elevation this high above sea level to my knowledge have not been previously observed. ODEs are typically associated with bromine monoxide (BrO) production, and satellite observations of BrO have been used to investigate the spatial extent of ODEs and AMDEs. For instance, Nghiem et al. (2012) showed using satellite measurements that topography constrains BrO distribution to north of the Brooks Range, further suggesting that these far-inland AMDE measurements could impact the entire Alaskan Arctic foothills and coastal tundra. Quantitatively, this means that deposition of Hg from the lower atmosphere to the snow surface could impact an

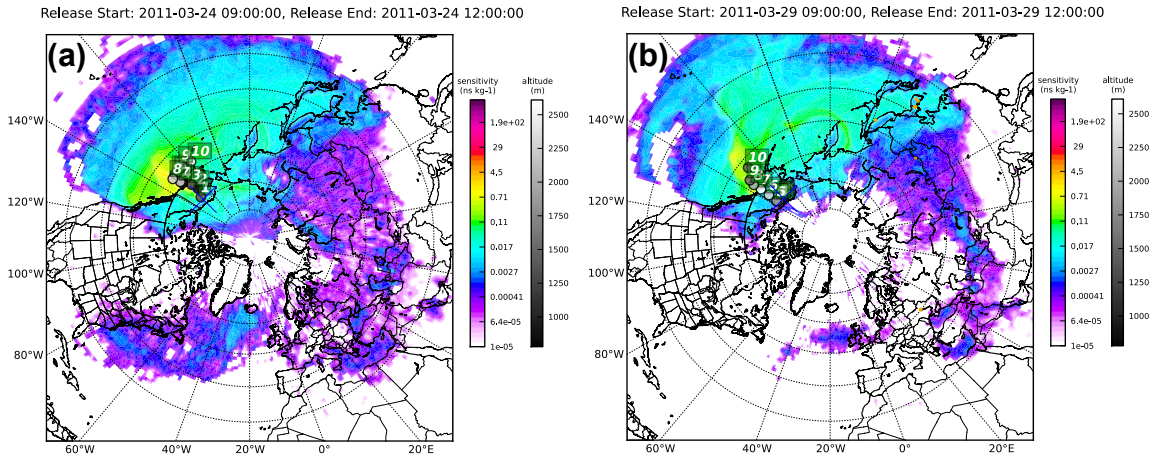

Figure 4.8: FLEXPART footprint sensitivity plots for events (a) 3 and (b) 4. These are cases when depletion was observed at Barrow but not at Toolik Lake. Color contours, using a logarithmic scale, show the emissions sensitivity averaged over the lowest 100 m of the atmosphere. This sensitivity is proportional to the residence time of particles in a unit area. The numbers and circle markers indicate the centroid location for the particle cloud on a given 24-hour increment back in time, giving a good indication of where the transported air was at a given time. The circle markers are color contoured using the gray altitude scale to indicate the mean altitude of the plume (location of highest particle density). For simplicity, only 10 days back in time are shown, but the particles were left in simulations for 20 days total. The PES represents the full complement of particles for the 20-day air parcel history.

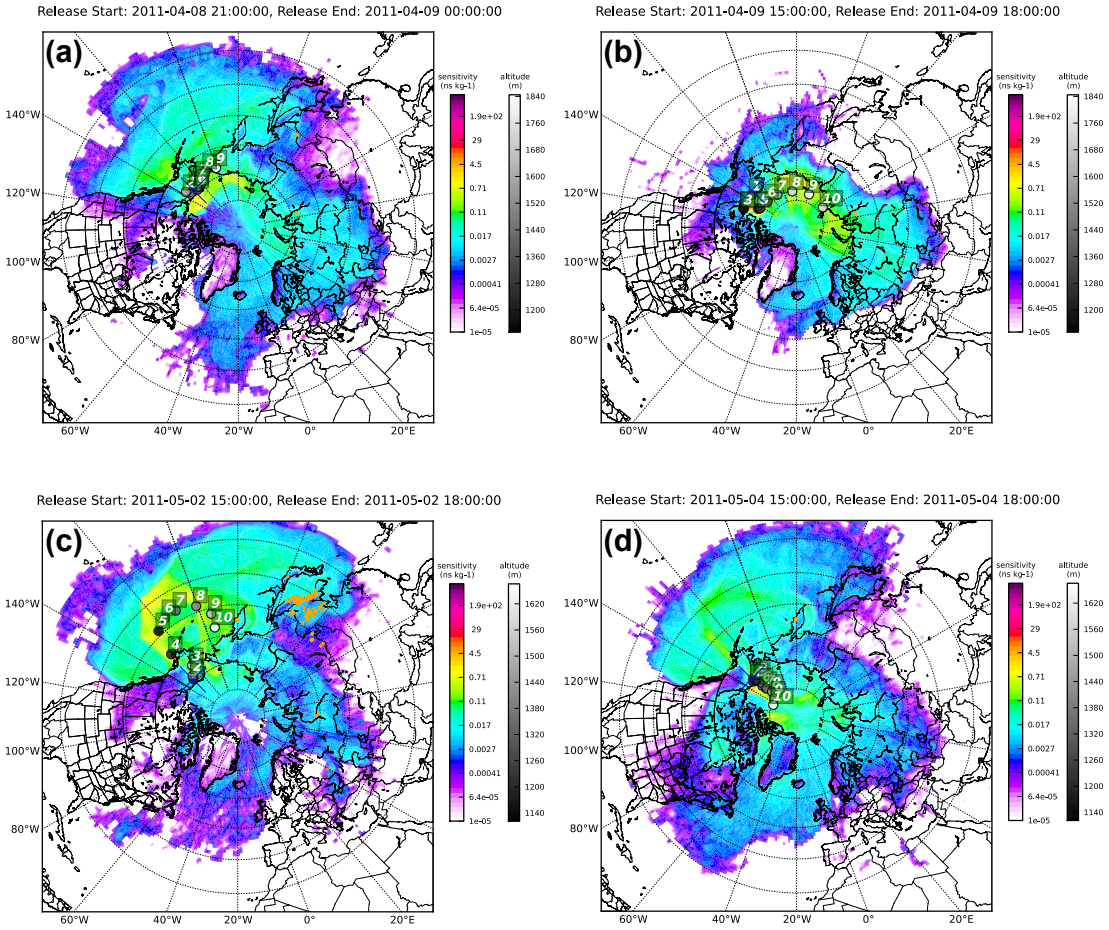

Figure 4.9: FLEXPART footprint sensitivity analysis plots for events 6 (a and b) and 10 (c and d). Color contours are as described for Figure 4.8. Graphs (a) and (c) indicate the transport patterns for conditions before the ODE was observed at Toolik Lake, while (b) and (d) indicate the air mass origin during the actual event.

area in the Alaskan Arctic up to approximately 230,000 km^2. Douglas and Sturm (2004) calculated an effective distance from the coast using meteorological conditions such as winds and storm tracks. They concluded that this variable is important for determining if a location is susceptible to Hg deposition to the snow associated with AMDEs. This study, as well as several others conducted in the Alaskan Arctic including Snyder-Conn et al. (1997) and Garbarino et al. (2002), have shown that Hg levels in snow on the northern slope of the Alaskan Arctic decrease with increasing distance from the coast, but are still elevated up to 50 km inland. The atmospheric measurements presented here indicate that areas even further inland could be impacted by Hg deposition to the snow surface.

4.5 Conclusions

Episodic depletion of surface O_3 and GEM were observed throughout the Arctic springtime at Toolik Lake, an inland site located over 200 km from the coast and 720 m above sea level. Rapid reduction in O_3 and GEM concentrations occurred simultaneously, with levels falling below 10 ppbv and 0.5 ng m^{-3}, respectively. The Toolik Lake data were compared to the annual surface O_3 record at Barrow for the measurement period of September 2010August 2011. Barrow and Toolik Lake showed similar O_3 behavior throughout the late fall and winter seasons. At Toolik Lake the influence of ODEs was observed one month later than at Barrow (April as opposed to March). Toolik Lake surface O_3 recovered to prior levels quickly after each ODE, unlike Barrow, where O_3 mixing ratios remained suppressed throughout the spring.

Analyses by the Lagrangian particle dispersion model FLEXPART indicate that air sampled during ODEs originated to the north, having spent significant time over the Arctic Ocean before reaching Toolik Lake. During periods when an ODE was present at the coast but no depletion was observed at Toolik Lake, the associated air flow was from the south. These observations provide the first direct evidence for ODEs being transported several hundred kilometers inland and to an elevation of over 700 m above sea level. These findings point towards a potential impact of observed ODEs and AMDEs on the chemistry of the boundary layer as well as towards a mechanism for the import and cycling of Hg within the lower North Slope and Arctic foothills ecosystem.

Chapter 5

Summertime surface O_3 behavior and deposition to tundra in the Alaskan Arctic

5.1 Abstract

Atmospheric turbulence quantities, boundary layer O_3 levels and deposition to the tundra surface were investigated at Toolik Lake, AK during the 2011 summer season. Beginning immediately after snowmelt, a diurnal cycle of O_3 developed with a mean amplitude of 13 ppbv, far larger than observed at other high Arctic locations. This diurnal cycle is attributed to a combination of surface deposition to the tundra and stable boundary layer conditions at night, and the entrainment of O_3 from higher in the atmosphere during increased daytime mixing. The mean O_3 deposition velocity during the month of June was 0.11 cm s^{-1}. A small diurnal signal was observed with a mean of 0.2 cm s^{-1} during the daytime and 0.08 cm s^{-1} at night. These values are slightly lower than previously reported summertime deposition velocities in the northern latitudes over tundra or fen, although measurements for comparison were limited.

5.2 Introduction

Levels of ozone (O_3) in the troposphere have more than doubled since pre-industrial times due largely to increased emissions of photochemical precursors (Lelieveld and Dentener, 2000; Fusco and Logan, 2003; Vingarzan, 2004; Lamarque et al., 2005; Oltmans et al., 2006). O_3 chemistry is of interest on account of its essential influence on the oxidation capacity of the atmosphere, the role of O_3 as a harmful pollutant, and the contribution of O_3 to greenhouse gas forcing. Due to important

environmental changes including accelerated warming, sea ice loss, and reductions in snow cover and permafrost extent (Lemke et al., 2007; Trenberth et al., 2007; Post et al., 2009; Cavalieri and Parkinson, 2012), the Arctic is a region of primary interest.

Quantifying the relative importance of sources and sinks of tropospheric O_3 has been a focus of several campaigns over the past few decades (Gregory et al., 1992; Mauzerall et al., 1996; Wang et al., 2003; Dibb et al., 2003; Stroud et al., 2004; Jacob et al., 2010). In the remote northern hemisphere the important source terms include transport (via intrusion of stratospheric air as well as long-range transport) and in situ photochemical production (Gregory et al., 1992; Dibb et al., 2003; Stroud et al., 2004). In situ photochemical loss and deposition at the surface are the primary loss mechanisms (Gregory et al., 1992). The seasonal cycle of tropospheric O_3 in the Arctic has been shown to display a distinct springtime maximum and summer minimum (Monks, 2000; Helmig et al., 2007c). Understanding the O_3 budget in the Arctic troposphere is necessary in order to incorporate production and loss processes in chemistry climate models, allowing for higher accuracy climate projections in the Arctic and lower latitudes.

Research presented here focuses on surface layer O_3 measurements on the North Slope of Alaska in the summertime. Tundra makes up a large portion of the land surface area in the high northern latitudes, and the very limited prior measurements of O_3 surface fluxes to tundra show values of approximately 0.2 cm s^{-1} with weak diurnal dependence when the surface is not snow covered (Jacob et al., 1992; Tuovinen et al., 1998; Wesely and Hicks, 2000). The length of the snow-free season in the Arctic has been observed to be increasing by up to $\sim$9 days $decade^{-1}$ (Chapin et al., 2005). Thus, it is important to accurately represent the surface O_3 deposition term to tundra during snow-free months. This is investigated by first characterizing the influence of changes in snow cover on the dynamics of surface layer O_3. Next, the hypothesis that boundary layer stability and surface deposition are primary controls on the large diurnal cycle observed in surface O_3 is examined. Lastly, eddy covariance is used to quantify the magnitude and diurnal cycle of surface O_3 deposition velocities at this Arctic tundra location.

5.3 Measurements

5.3.1 Site characterization

Measurements were conducted at the National Science Foundation Long-Term Ecological Research (LTER) site at Toolik Lake, Alaska (68.6 °N, 149.6 °W, 720 m a.s.l.). Toolik Lake is located in the foothills region of the Brooks Range on the North Slope of Alaska. This region is underlain by continuous permafrost ranging from approximately 250−300 m thick, with only the surface layer thawing each season (Osterkamp and Payne, 1981). Four main terrestrial ecosystem types are present in the Toolik Lake region: tussock tundra, heath, wet sedge tundra, and deciduous shrub stands (http://ecosystems.mbl.edu/ARC). Aside from Toolik Lake, many smaller lakes, streams, and rivers exist in the region. Measurements described here were made at a 4-m tower at the southern edge of Toolik Lake (south west of the main field camp facilities). The tower was in an area of mainly dry tundra, with moist tussock tundra comprising much of the extended region to the south and south west (Walker and Maier, 2008). Figure 5.1 is an aerial photo of Toolik Lake which shows the field station (located in the sector designated S1), as well as the location of the measurement tower indicated by a black cross (photo was obtained from http://toolik.alaska.edu/gis/).

5.3.2 Ambient measurements and surface turbulence

Atmospheric O_3 and surface turbulence measurements were conducted at a height of 4 m above the tundra surface during a full year spanning September 2010 − August 2011. In this analysis, I focus on the snow-free period including snow melt in May through August 31, 2011. To characterize summer conditions, a UV photometric O_3 analyzer with inlet at 4.1 m, 3-d sonic anemometer at 3.4 m, and an incoming solar radiation sensor were implemented. A detailed description of these instruments, the tower, sampling methods, and turbulence data processing is included in Van Dam et al. (2013). The O_3 flux measurements are described below. To avoid erroneous sampling of emissions from the field camp facilities, sampling periods from sector S1 in Figure 5.1 were removed from the data set. This effectively removed 10.9% of the data between May

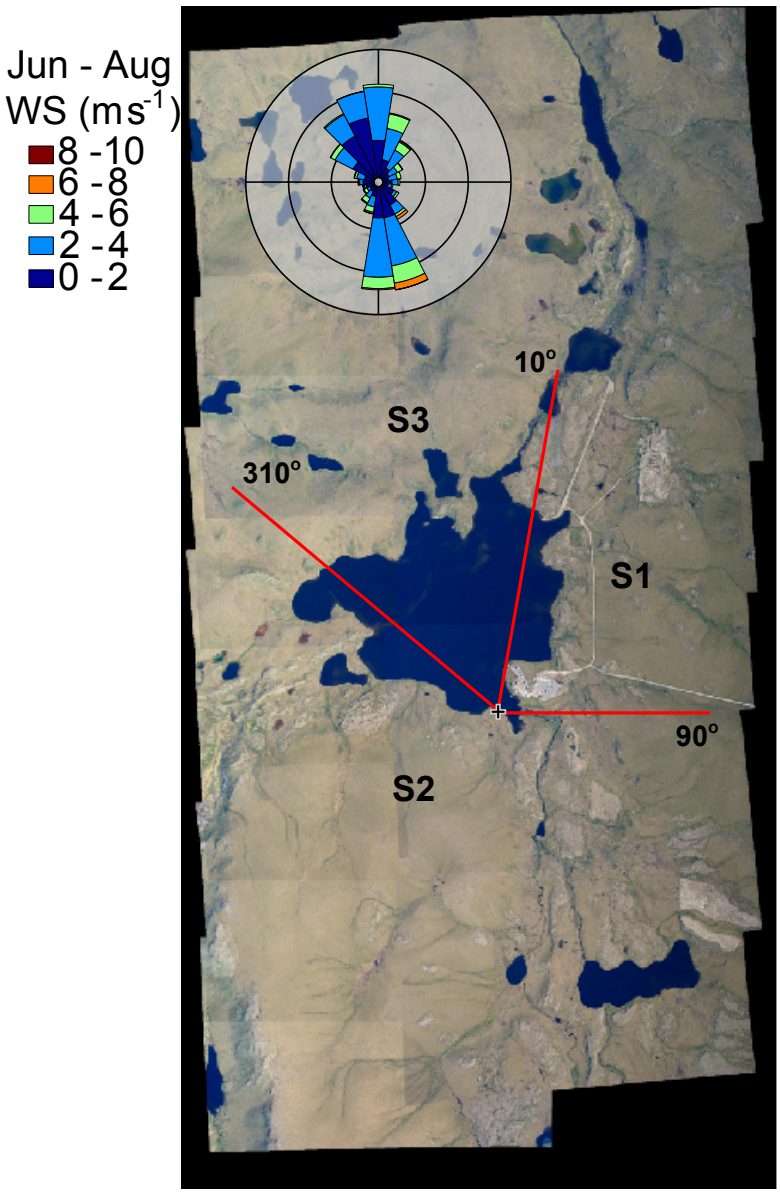

Figure 5.1: Aerial photo of Toolik Lake and surrounding area from Toolik Field Station Remote Sensing and GIS (http://toolik.alaska.edu/gis). Overlain on the photo is the location of the sampling site (black cross), and the red lines indicate sectors used for data filtering described in the text. The Toolik Field Station camp facilities can be seen at the south east side of the lake in S1. Data from this sector are filtered from the measurements due to the potential influence of camp pollution. Sector S2 contains a mainly tundra footprint, whereas sector 3 includes Toolik Lake. Data from the 3-d sonic anemometer were implemented to create the wind rose at top left in the figure, showing wind speeds as a function of the wind direction averaged over June through August 2011.

25 − August 31. A wind rose showing wind speeds as a function of the wind direction between June 1 − August 31 is shown in Figure 5.1 as well. During the summer low wind speeds are prevalent at Toolik Lake, with winds not exceeding 10 m s^{-1}. Winds were constrained to two narrow bands either from the south to SSE or the north. Ambient temperatures in June, July, and August range from nighttime lows of -5 °C early and late in the season to daytime highs up to 25 °C in mid-summer (Van Dam et al., 2013).

Surface O_3 data were also implemented from Barrow, AK (71.3°N, 156.6°W, 8 m a.s.l.), Tiksi, Russia (71.6°N, 128.9°E, 7 m a.s.l.), and Denali National Park, AK (63.73°N, 148.96°W, 661 m a.s.l.). The measurements from Barrow and Tiksi were collected by the NOAA/ESRL GMD using a UV TEI model 49i photometric O_3 analyzer. Surface O_3 measurements from Denali are a part of the EPA Clean Air Status and Trends Network (CASTNET) and were obtained through the Air Quality System (AQS). Surface O_3 at Denali was measured with a UV photometric O_3 analyzer.

5.3.3 O_3 fluxes

The eddy covariance method was used to calculate surface O_3 fluxes (F_{O3}). The primary components of this method include a 3-d sonic anemometer (referenced in the previous section) and a fast-response chemiluminescence O_3 instrument (FRCI). The FRCI is based in principle on the chemiluminescence reaction of O_3 with nitric oxide (NO). This instrument has previously been implemented for eddy covariance O_3 flux determination over the ocean on numerous ship cruises and at Barrow, AK, and is described in detail for these locations by Bariteau et al. (2010) and Helmig et al. (2012b,c). More detail on the sonic anemometer and FRCI as it was operated at Toolik Lake, including a comparison with a UV-photometric ozone analyzer, is included in Van Dam et al. (2013). At Toolik Lake, the FRCI was used with a 35 m sampling line with an inner diameter of 0.64 cm and outer diameter of 0.95 cm. A PFA filter holder (Savillex Corp., Minnetonka, MN) housed a Teflon membrane filter (5 m, Millipore, Billerica, MA) at the inlet, which was co-located with the 3-d sonic anemometer at 3.4 m above the tundra surface. The line and filter were conditioned by purging with approximately 300 ppbv of O_3 at a flow rate of 3 L min^{-1} for 24 h prior to use. The

flow rate in the purge line was controlled to 8 L min^{-1} using a mass flow controller, and the FRCI sample flow rate was controlled at 1.5 L min^{-1}. The instrument sensitivity was approximately 2360 counts s^{-1} $ppbv^{-1}$. The time delay between the turbulence measurements and the O_3 signal acquisition (delayed due to transport time of air between the inlet and the FRCI reaction chamber) was determined on a regular basis using a puff system (Bariteau et al., 2010). The average lag time during the summer period was 6 s. Fluxes were processed in 30-min increments, and are converted to deposition velocities ($v_d = -F_{O3}/[O_3]$) to remove the dependence on the O_3 mole fraction. Deposition velocities are reported in cm s^{-1}, with positive values indicating a downward flux to the surface (deposition).

Numerous quality control filters were applied to the O_3 flux data at Toolik Lake. As mentioned above, wind directions from the field camp sector ($10° - 90°$, S1 in Figure 5.1) were removed. Additionally, data were filtered for very low wind speeds (less than 0.5 m s^{-1}) due to the difficulty in determining the magnitude of the streamwise wind accurately. In determining O_3 fluxes the assumption of a constant flux layer is important. Periods when the Monin-Obukhov length ratio was greater than 0.2 were filtered, as this indicates conditions are too stable for a constant flux layer to exist (Sorbjan and Grachev, 2010). Another requirement for ozone flux calculations is the stationarity of mean O_3 measurements, therefore data were filtered for periods when the standard deviation of O_3 during the 30-min period exceeded 3 ppbv. In total, all of the filters described accounted for the removal of 32% of the data during June 2011 (the period focused on for deposition velocities in this study).

5.4 Results and Discussion

5.4.1 Year-round variation in O_3 at Toolik Lake

To provide some context for the summertime measurements, Figure 5.2 shows the annual cycle of ambient O_3 mole fractions (10-min averages). Plotted in orange in the background is the annual record of incoming solar radiation. Incoming solar radiation levels at Toolik Lake vary

from less than 50 W m^{-2} during the winter months to greater than 750 W m^{-2} during daytime in summer. Surface layer O_3 values show a generally increasing trend starting in the beginning of the measurement period in September and reaching a maximum in early spring in March. The influence of ODEs is observed beginning in April as investigated in detail by Van Dam et al. (2013). The summertime months of June, July, and August are characterized by the lowest mean values for the seasonal record. The general trend in this seasonal cycle, with early springtime maximum and summer minimum O_3 levels is characteristic of many documented Arctic locations (Oltmans et al., 1996; Monks, 2000; Helmig et al., 2007c). Strikingly for an Arctic site however, the summertime O_3 values show large variability, ranging from less than 10 ppbv (similar magnitude as observations during springtime ODEs) to greater than 35 ppbv. Upon closer inspection it can be seen that this variability is actually a marked diurnal cycle in O_3 mole fractions observed at Toolik Lake beginning in late May. This feature is considered in detail in the following sections.

5.4.2 Diurnal cycles in O_3 and surface turbulence

The initiation of the diurnal surface O_3 cycle is investigated in Figure 5.3, where a time series of O_3 mole fractions is plotted between May 8−31, 2011. Images from a webcam in operation on the top of the instrument building are shown at corresponding dates through this period to illustrate snow extent. Due to the variable topography at Toolik Lake, snow depth is not homogenous in the area surrounding the measurement site. The webcam was pointed towards a snow sampling manifold located approximately 10 m to the east of the tower where the surface O_3 measurements were conducted. These images show the site becoming snow free between May 20−22, whereas the field station did not report as 100% snow free until several days later (http://toolik.alaska.edu/edc). As shown in this figure, shortly after the time rapid snow melt began on May 20, a diurnal cycle in surface O_3 developed with nighttime minima occurring at 02:00−06:00 AKST and daytime maxima occurring between 14:00−19:00 AKST. An amplitude on the order of 10−15 ppbv was measured initially after snow melt. Starting on May 24, the amplitude increased to a daily value of 20 ppbv. The amplitude of the diurnal cycle increased further at the end of the month, reaching values

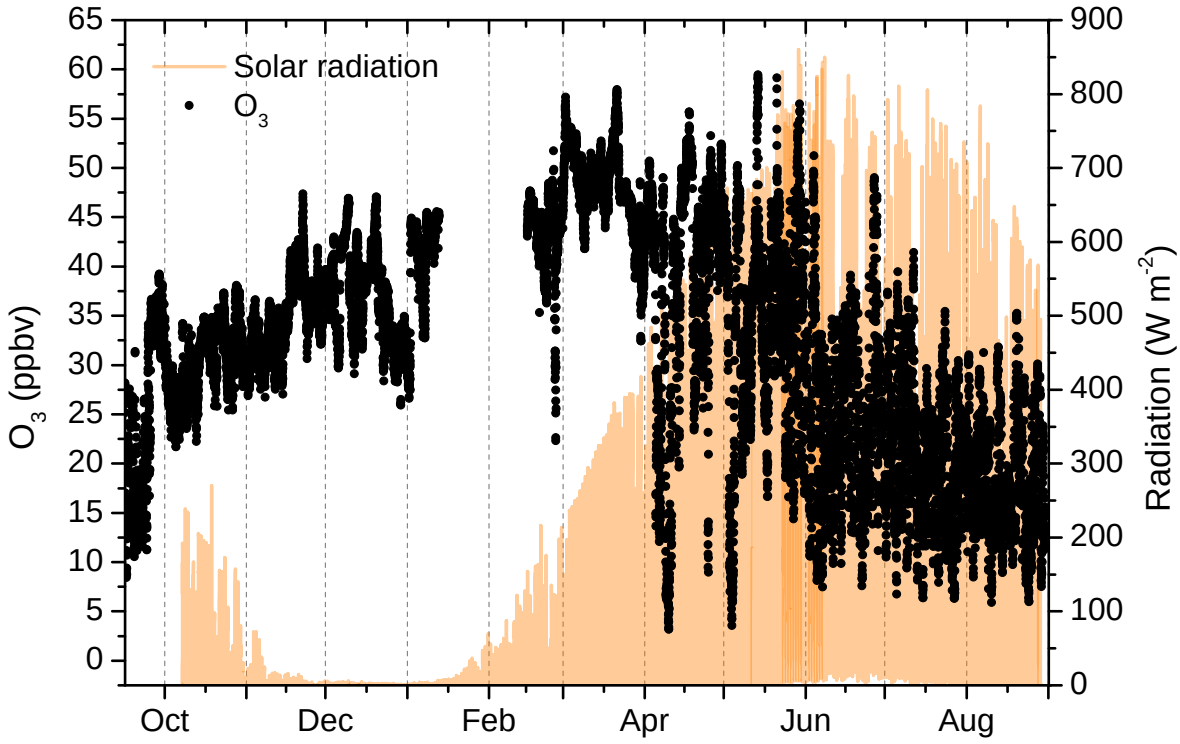

Figure 5.2: Annual cycle of O_3 measured at 4.1 m above the surface (black dots, left axis) and incoming solar radiation (orange line, right axis) at Toolik Lake. The measurement period spans September 2010 through August 2011, although the solar radiation sensor was not installed until the beginning of October 2010.

of greater than 30 ppbv difference between nighttime and daytime O_3 values. Figure 5.4 shows the daily amplitude of the O_3 cycle from June to August. Black dots show the daily amplitude calculated as the maximum O_3 mole fraction minus the minimum mole fraction for each 24-hr period. The red line gives a 5-pt running mean of the data set. The amplitude of the diurnal cycle in O_3 indicates a generally decreasing trend between June 1 − August 31. A linear regression analysis of the data indicates that the amplitude of the diurnal O_3 cycle diminished in magnitude by just over 0.1 ppbv day^{-1} on average; this amounts to approximately 10 ppbv over the three-month summer period.

To illustrate the unique conditions at Toolik Lake, Figure 5.5 shows a comparison with two other Arctic locations with available surface O_3 records that were snow-free in July 2011 (Barrow and Tiksi). A fourth site located in interior Alaska south of the Arctic Circle was included as an additional comparison (Denali). Figure 5.5 shows the median diurnal cycle in surface O_3 from each of these four sites in July 2011, calculated by computing the median O_3 value for each hour over the entire month. The median hourly values of incoming solar radiation as measured at Toolik Lake during July 2011 are plotted for reference, although solar radiation conditions were different at each of these sites due to their varying locations. With a 12 ppbv difference between the daily maximum and minimum averaged over July, Toolik Lake showed the largest median diurnal cycle amplitude. Toolik Lake also had the lowest daily value of 13.5 ppbv (the median value measured at 03:00 AKST). Denali also exhibited a pronounced diurnal cycle, with median amplitude of 9 ppbv. However, the maxima and minima hourly medians at Denali are shifted by 7−9 hours relative to the other sites, indicating that the controls on the surface O_3 level at Denali are very different as compared to the sites located in the Arctic. This is not unexpected, as Denali is a subarctic site with highly different topography, vegetation types, and proximity to anthropogenic sources. Tiksi and Barrow show very small changes in O_3 levels throughout the day. The diurnal cycle amplitude at Barrow has been investigated previously, and it was found that the average diurnal cycle during the month of June was approximately 1−1.2 ppbv (Oltmans, 1981; Helmig et al., 2007c). The magnitude of the diurnal cycle at Tiksi during June 2011 was on the order of 4.5 ppbv.

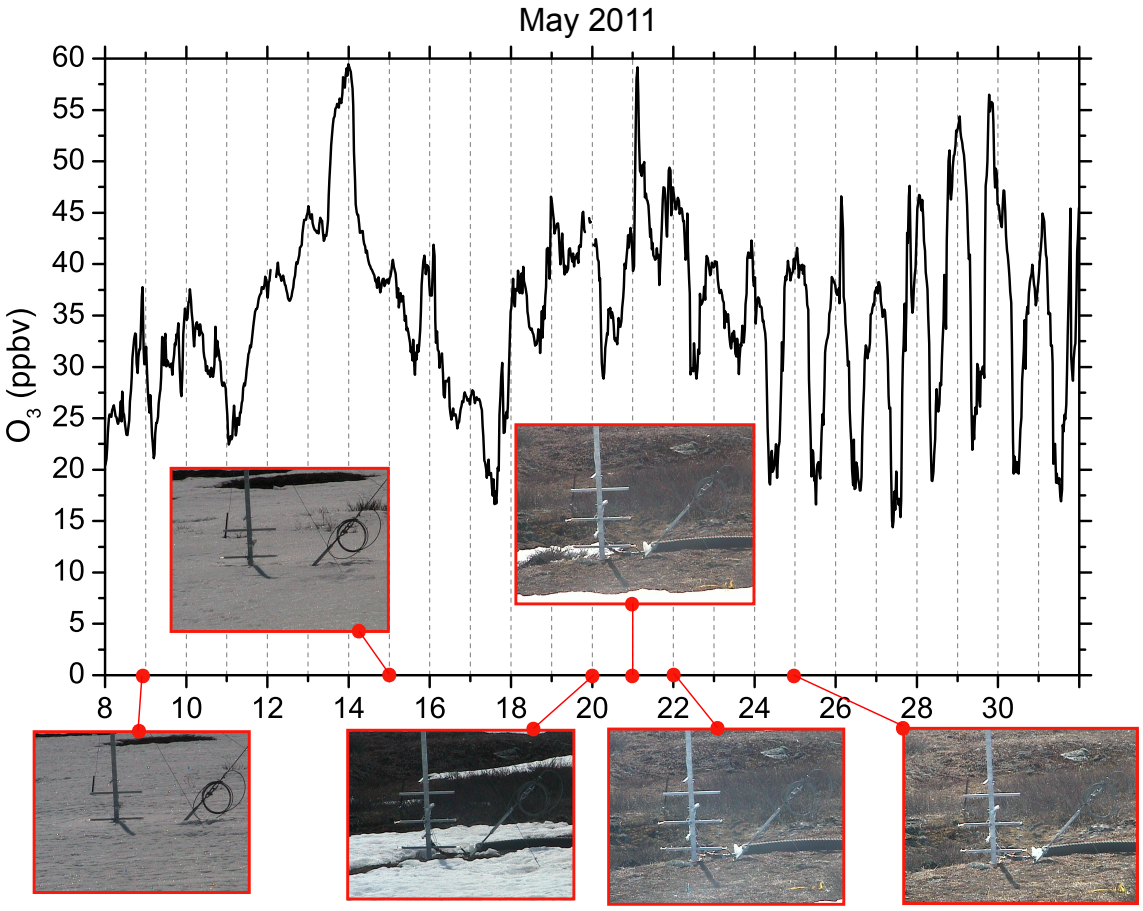

Figure 5.3: O_3 measured at 4.1 m is shown for the period May 8−31, 2011. Overlain on this plot are images from a webcam mounted on the instrument building and monitoring snow extent near a snow sampling tower. The red lines and dots indicate the day the photo was taken along the time axis of the figure. All photos were taken at ∼12:00 AKST. Small topographical variations significantly influence snow depth and extent around Toolik Lake, but the site was essentially snow free ∼May 22.

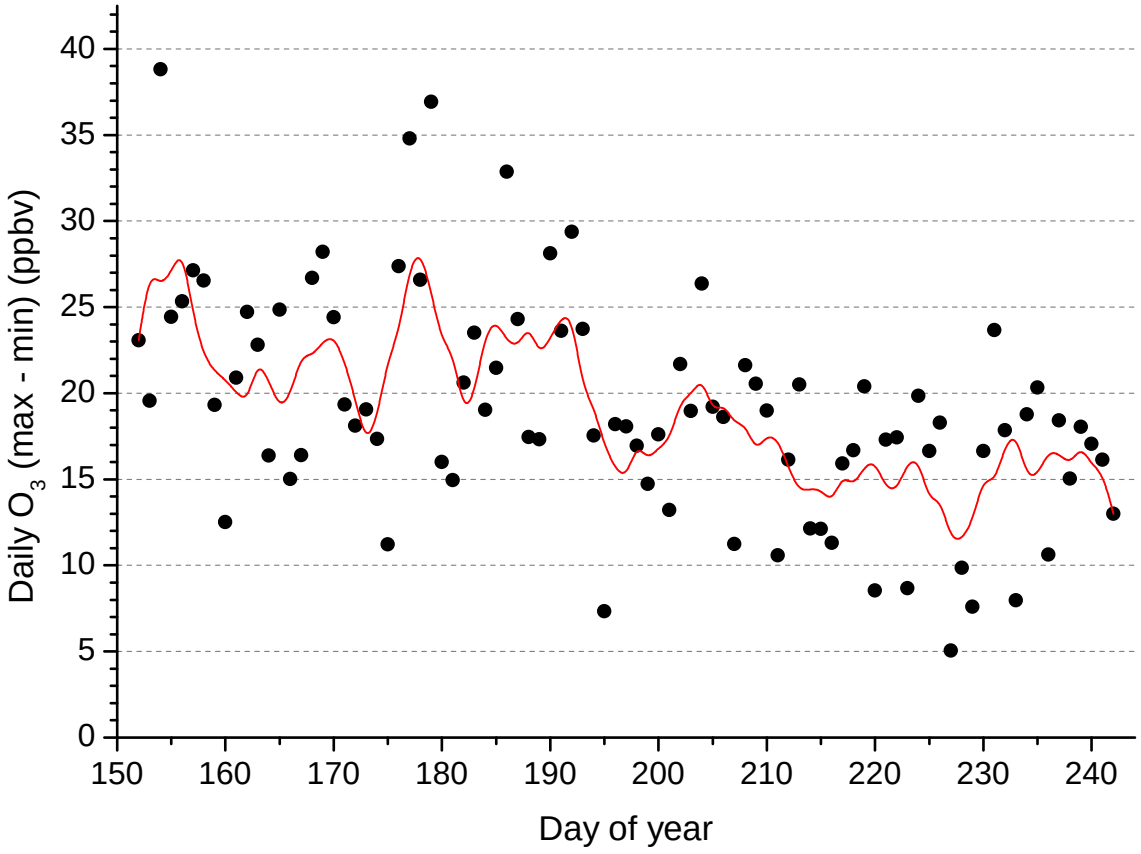

Figure 5.4: Change in the amplitude of the diurnal cycle of surface O_3 from June 1 – August 31, 2011. The amplitude was calculated by subtracting the minimum recorded value from the maximum recorded value for each 24-hr period. Black dots show the calculated amplitude, while the red line shows a 5-pt running mean of the data.

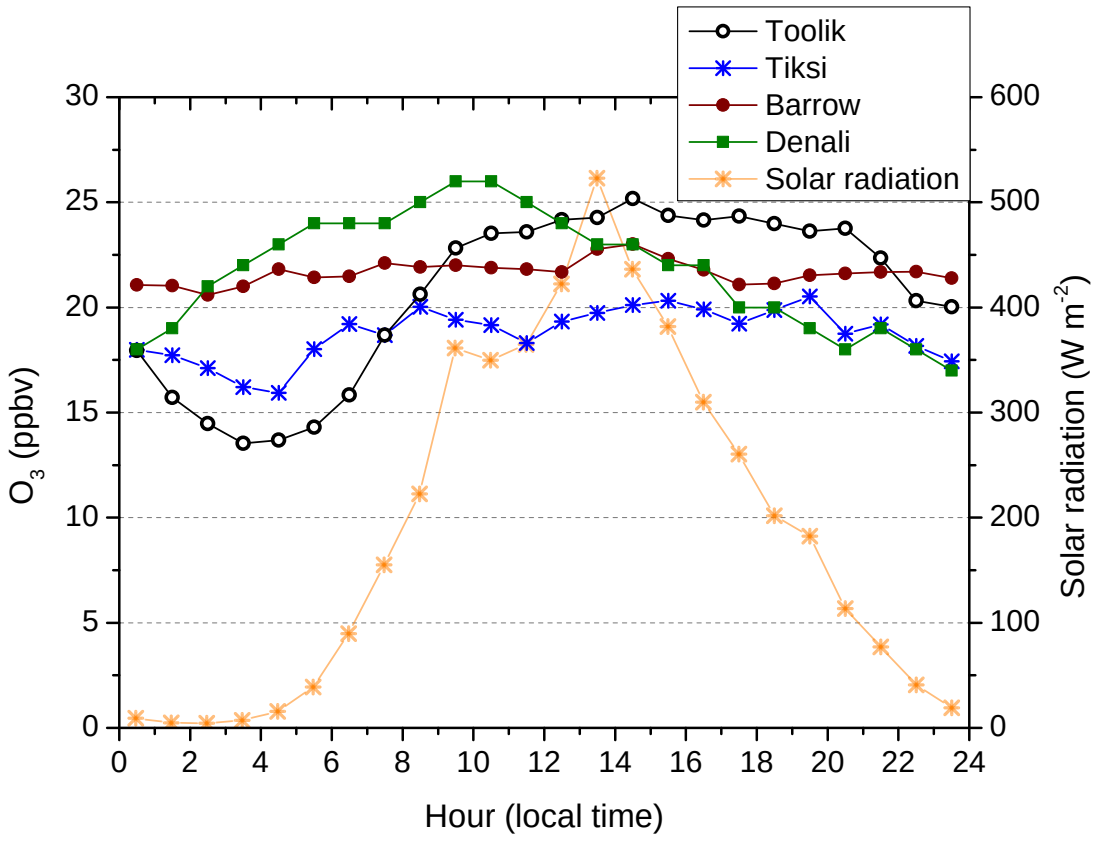

Figure 5.5: Comparison of the summertime (June-August) mean surface O_3 diurnal cycle between three Arctic locations: Toolik Lake (open black circles), Tiksi (blue stars), and Barrow (dark red dots). A subarctic site in interior Alaska (Denali, green squares) is included for additional comparison. Average diurnal cycles are calculated by taking the median June-August O_3 value for each hour of the day. The average summer incoming solar radiation (orange stars) data from Toolik Lake are shown as well.

The only evidence of a diurnal O_3 cycle of similar magnitude over tundra that I have found is described in Jacob et al. (1992). While that study was a part of the Arctic Boundary Layer Expedition (ABLE 3A), the actual surface O_3 mole fractions and deposition velocities were measured near Bethel in southwest Alaska (61.08°N, 162.04°W) in 1988. That measurement location was similar to Toolik Lake in that it was comprised of flat terrain ranging from dry upland to wet meadow tundra, with several small lakes in the tower footprint. Jacob et al. (1992) measured an average range of surface O_3 values between approximately 17 ppbv and 25 ppbv. Other northern latitude sites besides those discussed here have shown diurnal cycle amplitudes of a smaller value (Tuovinen et al., 1998). NO_x ($NO + NO_2$) was also measured at the ABLE 3A flux tower. Levels of NO_x in the Arctic are typically very low, for example Honrath and Jaffe (1992) measured NO less than 10 pptv during most periods at Barrow, AK, and Bakwin et al. (1992) measured NO_x levels less than 20 pptv during the ABLE 3A experiment.

It has been shown previously that significant O_3 reductions at night in rural areas can be observed as a result of the combination of surface deposition and stable conditions (Colbeck, 1988; Johansson and Janson, 1993; Wesely and Hicks, 2000). I investigate here the hypothesis that changes in surface stability conditions and deposition to the tundra are the primary contributors to the large diurnal cycle observed in surface O_3 at Toolik Lake during the summer. The Monin-Obukhov length ratio, zL^{-1}, is implemented to evaluate stability conditions, where z is the measurement height, and L is the Monin-Obukhov length defined as:

$$L = \frac{-u_*^3 T_0}{kgH_s} \tag{5.1}$$

In this equation, T_0 is the temperature, u_* is the friction velocity, k is the von Karman constant, g is gravitational acceleration, and H_s is the sensible heat flux.

Figure 5.6 is a histogram of 30-min averaged zL^{-1}. The histogram shows the distribution of zL^{-1} measured June through August at Toolik Lake. Of the entire summer period, stable conditions were measured approximately 23.1% of the time. Unstable conditions were measured 50% of the period, and no value for zL^{-1} was recorded for 26.9% due to either instrumental issue

or one of the quality control filters described above. Figure 5.7 shows this same data set, plotted as median hourly values over the June through August period. Values of the stability parameter were negative, indicating instability, during sunlit hours. Conditions transitioned to near neutral and stable during the nighttime hours, approximately 21:00−06:00 AM. This is indicative of a stable and stratified boundary layer during nighttime when O_3 levels were seen to decrease significantly.

To investigate the relationship between O_3 levels and atmospheric stability in more detail, Figure 5.8 shows time series data for two 6-day periods in (a) June and (b) August. In these figures, individual data points are color-coded for a range of stability conditions. The dark and light blue colors indicate varying degrees of weakly stable to stable conditions, and the red hued colors indicate periods where conditions are neutral to unstable. The amplitude of the diurnal O_3 cycle was approximately 20 ppbv in the June period, and slightly less at approximately 15 ppbv during the August period. The color-coding clearly shows that atmospheric conditions were generally stable during the nighttime periods when low O_3 values were observed. To quantify this relationship, O_3 data were divided into stable and unstable conditions determined by zL^{-1}. Figure 5.9 shows box charts for these separated data. O_3 data for unstable conditions have higher mean and median value than for stable conditions. The 5th and 95th percentiles (whiskers) are also higher than for stable conditions. There was a statistically significant difference in the mean O_3 mole fractions during stable conditions (positive zL^{-1}) and unstable conditions (negative zL^{-1}), with $t(3157) = 12.2, p < 0.001$. Relationships between O_3 mole fractions and surface friction or the sensible heat flux were not readily apparent. The above is convincing evidence that the nighttime occurrence of a stably stratified atmosphere is an important control on O_3 values at this location. Surface deposition to the tundra is investigated below.

5.4.3 Surface O_3 deposition velocities

O_3 deposition velocities were calculated for the month of June 2011. Implementing the quality control filters described in the measurements section left 477.5 h of O_3 v_d measurements remaining for analysis (of a total of 720 h in June). The distribution of the 30 min data is shown

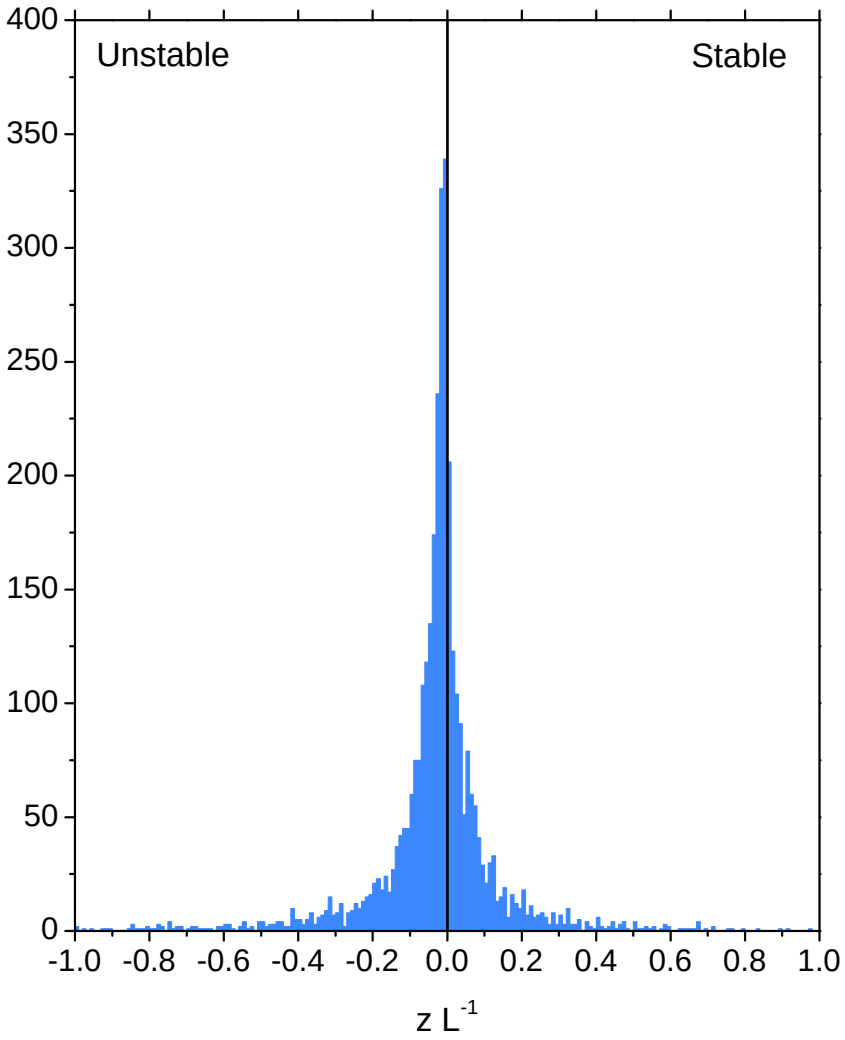

Figure 5.6: Histogram of zL^{-1} for June-August. Negative values indicate unstable conditions, and positive values suggest stable conditions.

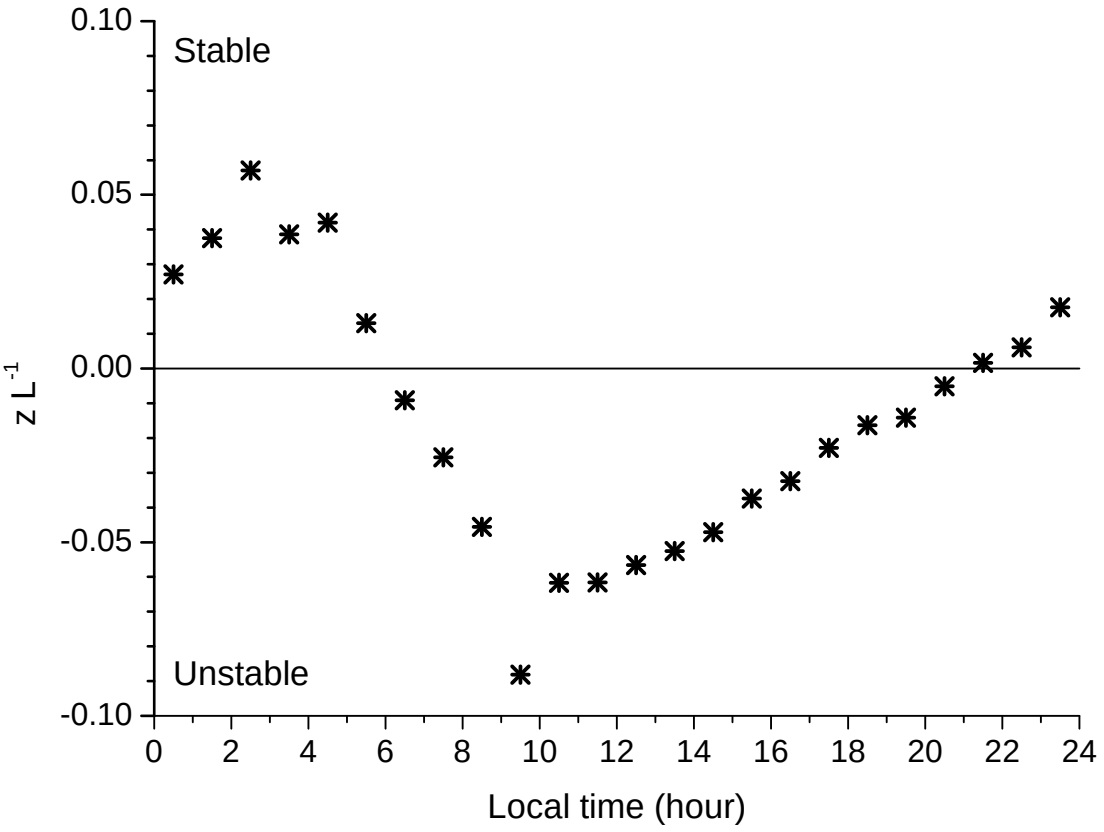

Figure 5.7: Average summertime diurnal cycle of zL^{-1} at Toolik Lake, calculated by taking the median value of the June-August data for each hour of the day. Conditions were generally stable between 22:00 - 06:00 AKST, and generally unstable during the daytime hours of 07:00 - 20:00 AKST.

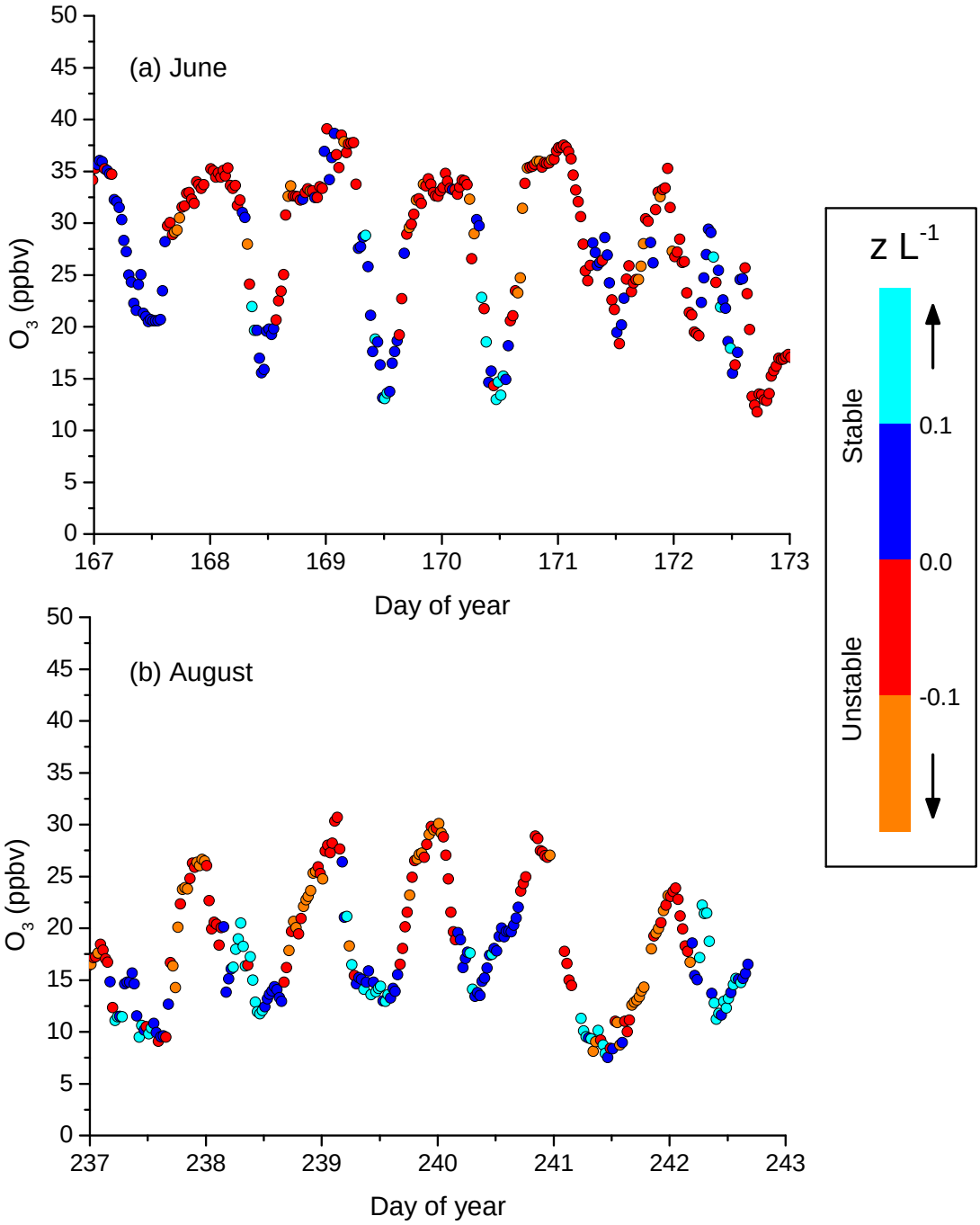

Figure 5.8: Time series of surface O_3 data for (a) June and (b) August. The time series data are color-coded by the value of zL^{-1} in order to assess typical stability conditions during periods when surface O_3 was low or high.

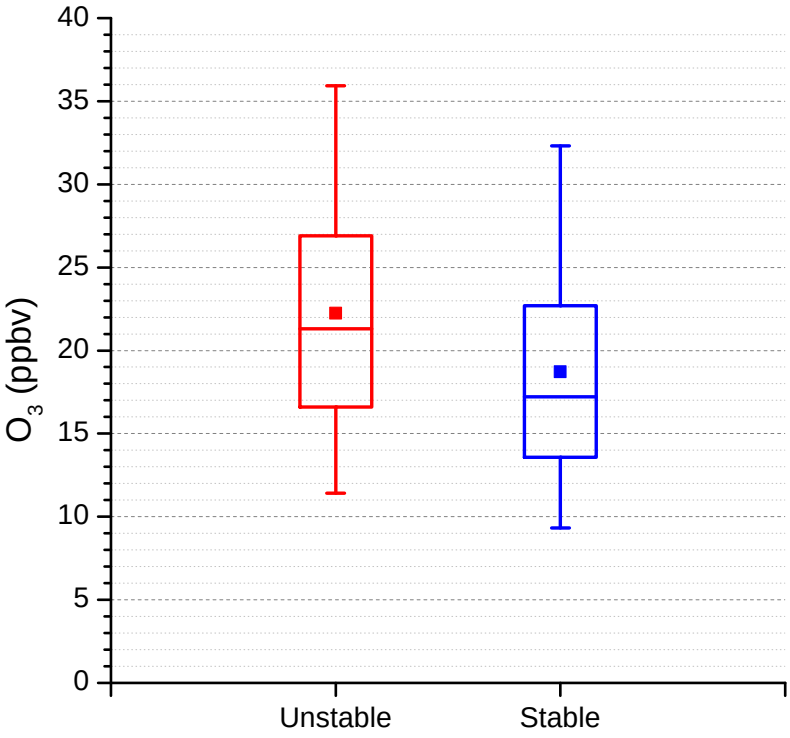

Figure 5.9: Box and whisker charts of O_3 during unstable (red) and stable (blue) conditions defined by the value of zL^{-1}. Filled squares indicate the mean, the central line in the box indicates the median, and the upper/lower box limit indicate 25th and 75th percentiles. Whiskers show the 5th and 95th percentile of the data. The mean O_3 during unstable conditions was 22 ppbv and median 21 ppbv, while the mean O_3 during stable conditions was ∼19 ppbv, with median 17 ppbv.

as a histogram in Figure 5.10 (a), and also displayed using a box chart in panel (b). The box chart shows that the central 50% of the data was spread between 0.01 and 0.2 cm s^{-1}. The mean O_3 v_d value for June 2011 was 0.11 cm s^{-1}. There was a statistically significant difference between the daytime and nighttime deposition velocity, with $t(929) = 3.4, p < 0.001$. Hourly means from the month of June are shown in Figure 5.11 to illustrate the average diurnal cycle in v_d. Based on hourly averages, the diurnal cycle had amplitude of approximately 0.10 cm s^{-1}. The mean daytime value was 0.14 cm s^{-1} and the mean nighttime value was 0.08 cm s^{-1}.

Ozone deposition velocities to water surfaces, including fresh water and ocean, are known to be very small compared to land (Galbally and Roy, 1980; Wesely et al., 1981; Wesely and Hicks, 2000; Bariteau et al., 2010; Helmig et al., 2012c). Toolik Lake is a relatively large body of water near the measurement site, so it is important to investigate the possible influence of the lake on calculated deposition velocities. In the deposition velocity measurements detailed above, all wind directions aside from sector S1 (shown in Figure 5.1) were included in the calculations. A comparison of calculated O_3 deposition velocities and observed wind direction did not clearly show a direct relationship. Thus, the measurement periods were further broken apart into sector S2 (comprised of largely dry or moist tussock tundra dotted with small lakes) and sector S3 (containing most of Toolik Lake). The mean v_d from S2 was 0.12 cm s^{-1}, and the mean v_d from S3 was 0.09 cm s^{-1}. A t-test determined that the difference in the means of the S2 and S3 data sets were only statistically significant at the 0.15 level ($t(980) = 1.55, p = 0.12$). This result indicates that calculated deposition velocities with a lake footprint are likely lower than that for tundra alone, although the higher significance level suggests that there is $\sim$ 15% chance that the conclusion of different means is in error. The difference in calculated deposition velocities to the tundra and to the lake warrants further research, likely involving a thorough analysis of the tower footprint and associated data filtering.

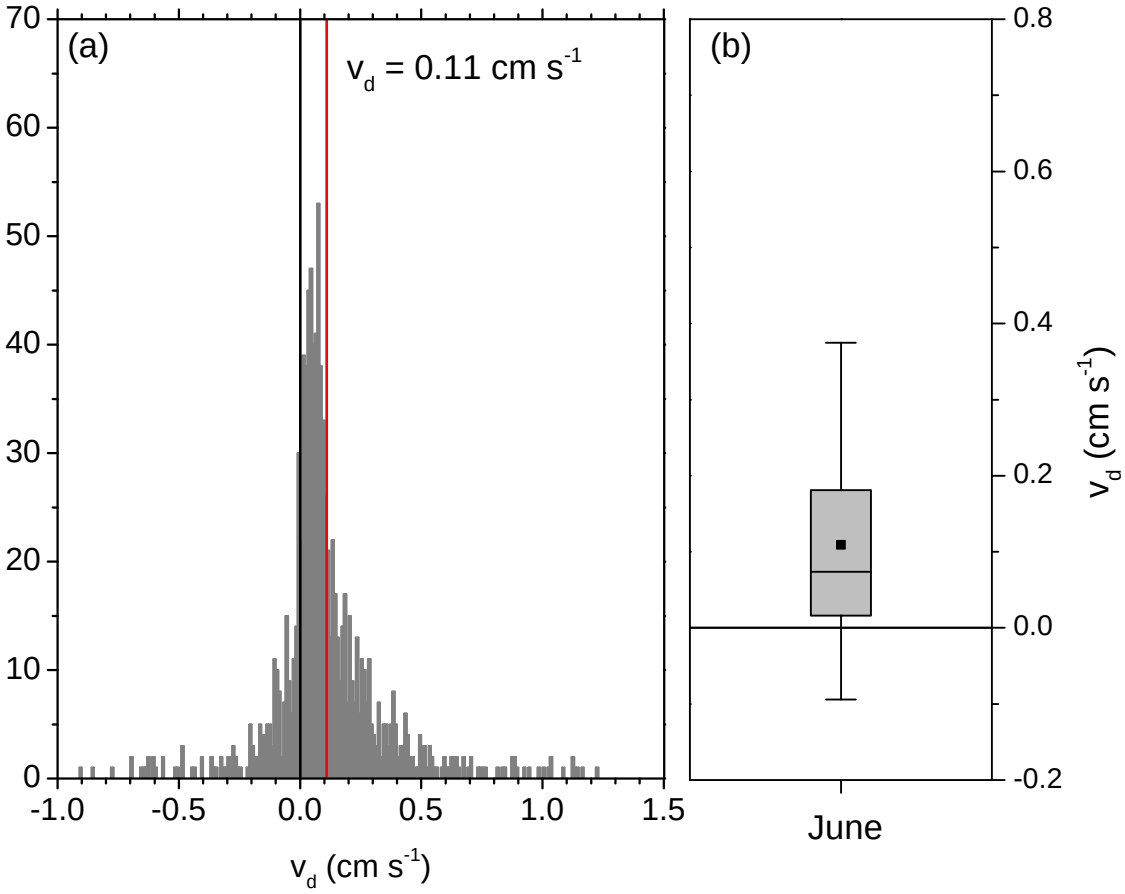

Figure 5.10: (a) Histogram and (b) box chart of v_d during June 2011. The mean value of v_d during this period was 0.11 cm s^{-1}, as indicated by the red line in the histogram. In (b) the black square is the mean value, the center box line indicates the median, and upper and lower box bounds are the 25th and 75th percentile. The whiskers show the 10th and 90th percentile value. The range of the 10th to 90th percentile of the v_d values in June span $\sim$ -0.1 to 0.4 cm s^{-1}.

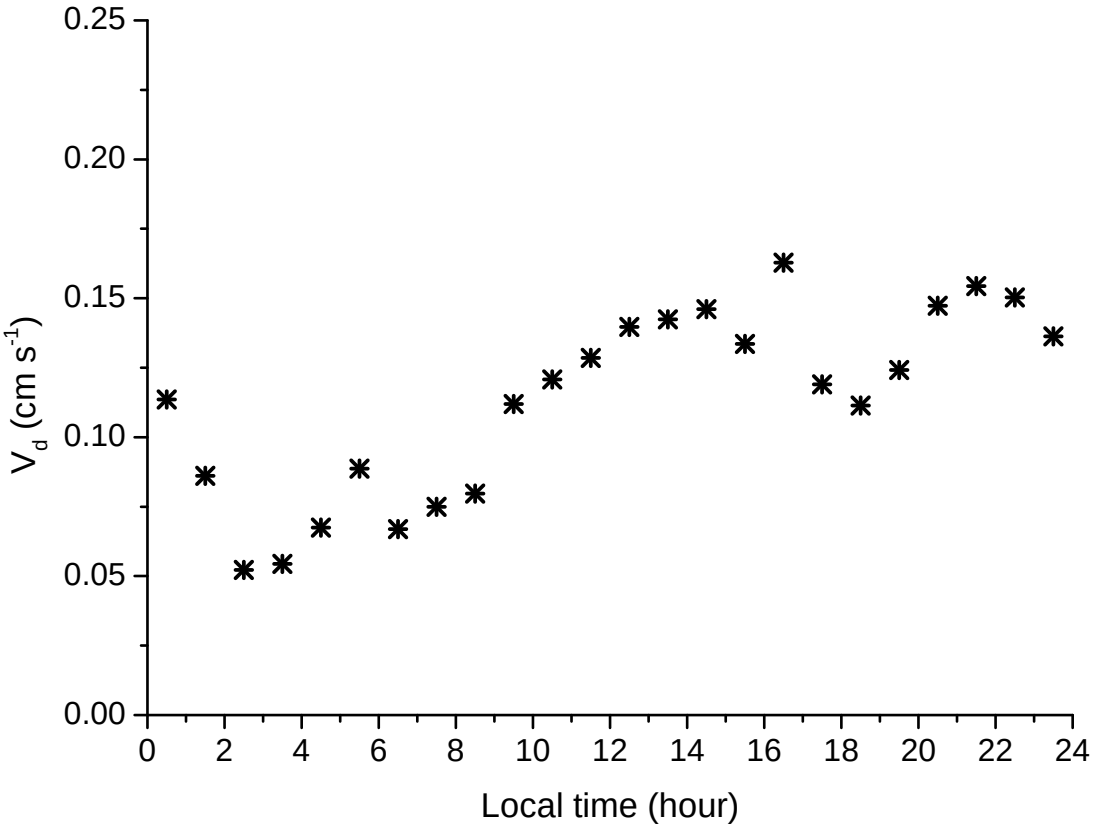

Figure 5.11: Average diurnal cycle of v_d, calculated as the median hourly value for the month of June. O_3 v_d varied from an hourly minimum of 0.05 cm s^{-1} between 02:00-03:00 AKST, to a maximum hourly value between 20:00-22:00 AKST (also at 16:00 AKST).

5.4.4 Discussion

There are limited published studies showing O_3 deposition to the snow-free Arctic, particularly over tundra. The Jacob et al. (1992) study in southwest AK between July and August 1988 resulted in mean hourly O_3 v_d ranging from 0.24 cm s^{-1} during the day and 0.12 cm s^{-1} at night. At a similar latitude to Toolik Lake in northern Finland over a flark fen (comprised of open water pools, bare peat, and ridges of drier ground) a weak diurnal cycle in O_3 v_d was also measured, spanning 0.15−0.2 cm s^{-1} between night and day (Tuovinen et al., 1998). Over a fen in northern Quebec a mean value of 0.17 cm s^{-1} was observed during daytime. The mean value of the Toolik Lake measurements is lower than O_3 v_d values previously reported over tundra or in the snow-free Arctic or subarctic. The amplitude of the diurnal cycle in deposition velocities during June at Toolik Lake is similar to that measured over fen, and smaller than measured over tundra in southwest Alaska. Past modeling work has shown that incorporating a diurnal O_3 deposition velocity cycle scheme into a chemistry general circulation model (as opposed to using a constant deposition velocity) can change the summertime O_3 dry deposition term in the northern hemisphere by up to 10% (Ganzeveld and Lelieveld, 1995).

Studies by Jacob et al. (1992) and Mauzerall et al. (1996) implemented data from the ABLE 3A and 3B campaigns to quantify the important source and sink terms in the tropospheric ozone budget in high northern latitudes. These studies found the 24-hour mean photochemical ozone loss rate in the 0-6 km layer to be 8 x 10^{10} molecules cm^{-2} s^{-1} for northern latitudes above 60°, and on the order of 23 x 10^{10} molecules cm^{-2} s^{-1} for latitudes above 45°N. To estimate a regional deposition flux above 60°N, they implemented surface types by Matthews (1985) and published summertime average O_3 deposition velocities for each surface type. For tundra, which comprised 17.5% of the total area, they implemented the average deposition velocity measured by Jacob et al. (1992) in south west Alaska. Using these values they calculated an average deposition flux of 8.2 x 10^{10} molecules cm^{-2} s^{-1} for latitudes greater than 60°N. As a comparison, I considered the mean O_3 deposition velocity measured at Toolik Lake of 0.11 cm s^{-1} to be a potential lower

limit for deposition over tundra, and implemented this in a regional estimate of the depositional loss term. To be consistent for comparison with the Jacob et al. (1992) and Mauzerall et al. (1996) studies, I implemented an average O_3 mole fraction of 30 ppbv. Modifying the mean tundra deposition velocity led to a decreased summertime deposition flux estimate of 6.7 x 10^{10} molecules cm^{-2} s^{-1}, an ~20% reduction in the deposition flux term. This exercise is useful as a simplified sensitivity estimate which provides evidence that precisely representing O_3 deposition velocities to different Arctic surface types is important in accurately quantifying the tropospheric ozone surface deposition loss term. To get an improved estimate of O_3 loss by surface deposition, more recent land surface types and extent for the Arctic, and characteristic deposition velocities would need to be implemented. Understanding the relative importance of photochemical versus depositional O_3 loss has implications for our understanding of the tropospheric O_3 budget and its sensitivity to further anthropogenic perturbations.

5.5 Conclusions

Summertime surface turbulence parameters, boundary layer O_3, and surface O_3 fluxes were measured north of the Brooks Range in Alaska over tundra. Stability conditions ranged from stable at night to well mixed during the daytime. A diurnal O_3 signal with amplitude between 5 and 35 ppbv was observed throughout the summer months of June, July, and August, immediately following snowmelt in the spring. The surface stability regime was a key contributor to the large diurnal cycle observed in O_3.

Summertime O_3 deposition velocities to tundra were calculated for the month of June using the eddy covariance method. The average value was 0.11 cm s^{-1}. A weak diurnal signal was observed in the deposition velocity, with a daytime mean of 0.2 cm s^{-1} and nighttime mean of 0.08 cm s^{-1}. Uptake of O_3 to the tundra, stably stratified nighttime conditions limiting mixing, and enhanced mixing with higher O_3 air from aloft during the daytime (Bakwin et al., 1992) are attributed as the primary controls leading to large differences between O_3 levels during day and night.

Measured O_3 deposition velocities to Arctic snow reported in the literature during the spring, summer, and fall are significantly lower than that reported to Arctic tundra. For instance, Helmig et al. (2009a) found a mean daily O_3 deposition velocity to Summit, Greenland snow in the summer of 0.02 cm s^{-1}. The summer observations of O_3 deposition to the tundra imply that the current trend of a lengthening snow-free season would lead to a larger surface O_3 sink in the tropospheric O_3 budget.

Chapter 6

Conclusions

My thesis has focused on understanding the complex relationship between chemical and physical processes in the snowpack and the chemistry of the overlying atmosphere. I implemented a two-year data record from Summit, Greenland, and one year of observations from Toolik Lake, AK to investigate these relationships. The primary results from my work are detailed in the following paragraphs.

In Chapter 2 I displayed and examined two years of interstitial air observations of O_3, NO, and NO_2 at Summit, a location with snowpack over an ice sheet. With this detailed record, I showed that interstitial air levels of O_3 are depleted throughout the year, and the magnitude of this depletion increases during the sunlit months. The maximum snowpack depletion occurred following the peak in incoming solar radiation. NO showed enhancements during spring, summer, and autumn, with levels reaching over 200 pptv. NO enhancements were primarily constrained to a layer between the surface and 60 cm depth, with maxima occurring at the time of maximum solar radiation. In contrast to NO and O_3, NO_2 showed diurnal maxima shifted by approximately 6-12 hours later in the day. This interesting result cannot be explained by any mechanisms currently proposed in the literature. To end the chapter, I proposed several theories including a physical process causing a 'lag' in the NO_2 enhancement, and a different chemical mechanism such as the reaction between nitrite and O_3, which could potentially explain the observed O_3 depletion within snow.

In Chapter 3 I implemented surface layer turbulence parameters and observations from a min-

isodar located at Summit to investigate the development of the stable boundary layer at a location subject to diurnal cycles in surface heat exchange. I determined that in this environment surface friction is the primary scaling parameter for the depth of the stable to weakly stable boundary layer. Analyzing boundary layer depth results alongside surface layer mole fractions of O_3 and NO indicated that boundary layer dynamics at Summit do not play as crucial a role in determining O_3 and NO at Summit, when compared with a location such as South Pole.

Given the expectation that snow chemistry is not driven by the same controls at all locations, a seasonally snow-covered location at the edge of the Arctic coastal plain north of the Brooks Range is the primary subject of Chapters 4 and 5. In Chapter 4 I show that springtime O_3 and GEM depletion events are observed at this interior location, located several hundred kilometers from the coast and over 700 m above sea level. FLEXPART simulations for Toolik Lake were implemented to illustrate that the air masses associated with observed ODEs and AMDEs have a common source region over the Arctic Ocean.

The behavior of surface O_3 during the period of snow melt and during the snow-free season in the Arctic was investigated in Chapter 5. In this chapter it is shown that atmospheric stability and deposition to the tundra play a significant role in the development of a large diurnal cycle in ambient O_3 immediately following snowmelt in the spring. The diurnal cycle persists throughout summer, although at a reduced amplitude later in the season. In this chapter I also determined the magnitude of the O_3 deposition velocity in June using eddy covariance methods. While O_3 deposition velocities to polar snow are typically on the order of <0.01 to ~ 0.05 cm s^{-1} in the summer (Helmig et al., 2009a), I found deposition velocities on the order of $0.1 - 0.2$ cm s^{-1} over tundra at Toolik Lake. O_3 deposition velocity displayed a small diurnal cycle on the order of 0.1 cm s^{-1} change between day and night. With demonstrated feedback loops in the Alaskan Arctic involving decreasing snow cover, increased temperatures, and changing vegetation type (Chapin et al., 2005), this result indicates that surface deposition could become an increasingly important sink in the Arctic tropospheric O_3 budget.

These results demonstrate that the influence of the snowpack on the overlying atmosphere

is complex, significant, and varies by location. In the context of a dynamically shifting Arctic, characterizing the influence of snow cover (or lack there-of during a lengthening snow-free season in some regions) on surface layer O_3 and NO_x chemistry is essential for accurately representing the budgets of these important constituents. Advanced modeling incorporating the observations and analyses presented here will be necessary to extrapolate these results (1) on a local scale to elucidate acting chemical and physical mechanisms, and (2) on a regional or global scale to understand the tropospheric effects from emissions and uptake at the snow surface, and how these influences may develop in a rapidly changing Arctic environment.

Bibliography

M. R. Albert and R. L. Hawley. Seasonal differences in surface energy exchange and accumulation at Summit, Greenland, volume 31 of Annals of Glaciology, pages 387–390. 2000. ISBN 0260-30550-946417-26-1. doi: 10.3189/172756400781820129. URL <Go to ISI>://WOS:000166916600062.

M. R. Albert and E. F. Shultz. Snow and firn properties and air-snow transport processes at summit, greenland. Atmospheric Environment, 36(15-16):2789–2797, 2002.

M. R. Albert, A. M. Grannas, J. Bottenheim, P. B. Shepson, and F. E. Perron. Processes and properties of snow-air transfer in the high arctic with application to interstitial ozone at alert, canada. Atmospheric Environment, 36(15-16):2779–2787, 2002.

P. S. Anderson and W. D. Neff. Boundary layer physics over snow and ice. Atmospheric Chemistry and Physics, 8(13):3563–3582, 2008. Anderson, P. S. Neff, W. D.

K. Aspmo, P. A. Gauchard, A. Steffen, C. Temme, T. Berg, E. Bahlmann, C. Banic, A. Dommergue, R. Ebinghaus, C. Ferrari, N. Pirrone, F. Sprovieri, and G. Wibetoe. Measurements of atmospheric mercury species during an international study of mercury depletion events at ny-alesund, svalbard, spring 2003. how reproducible are our present methods? Atmospheric Environment, 39(39):7607–7619, 2005.

R. Atkinson, D. L. Baulch, R. A. Cox, J. N. Crowley, R. F. Hampson, R. G. Hynes, M. E. Jenkin, M. J. Rossi, and J. Troe. Evaluated kinetic and photochemical data for atmospheric chemistry: Volume i - gas phase reactions of o-x, hox, nox and sox species. Atmospheric Chemistry and Physics, 4:1461–1738, 2004.

P. S. Bakwin, S. C. Wofsy, S. M. Fan, and D. R. Fitzjarrald. Measurements of nox and noy concentrations and fluxes over arctic tundra. Journal of Geophysical Research-Atmospheres, 97 (D15):16545–16557, 1992.

C. M. Banic, S. T. Beauchamp, R. J. Tordon, W. H. Schroeder, A. Steffen, K. A. Anlauf, and H. K. T. Wong. Vertical distribution of gaseous elemental mercury in canada. Journal of Geophysical Research-Atmospheres, 108(D9), 2003.

L. Bariteau, D. Helmig, C. W. Fairall, J. E. Hare, J. Hueber, and E. K. Lang. Determination of oceanic ozone deposition by ship-borne eddy covariance flux measurements. Atmospheric Measurement Techniques, 3(2):441–455, 2010.

L. A. Barrie. Arctic air-pollution - an overview of current knowledge. Atmospheric Environment, 20(4):643–663, 1986.

L. A. Barrie, J. W. Bottenheim, R. C. Schnell, P. J. Crutzen, and R. A. Rasmussen. Ozone destruction and photochemical reactions at polar sunrise in the lower arctic atmosphere. Nature, 334(6178):138–141, 1988.

H. J. Beine, R. E. Honrath, F. Domine, W. R. Simpson, and J. D. Fuentes. Nox during background and ozone depletion periods at alert: Fluxes above the snow surface. Journal of Geophysical Research-Atmospheres, 107(D21), 2002.

T. Berg, S. Sekkesaeter, E. Steinnes, A. K. Valdal, and G. Wibetoe. Springtime depletion of mercury in the european arctic as observed at svalbard. Science of the Total Environment, 304 (1-3):43–51, 2003.

J. Bock and H. W. Jacobi. Development of a mechanism for nitrate photochemistry in snow. Journal of Physical Chemistry A, 114(4):1790–1796, 2010.

F. Bocquet, D. Helmig, and S. J. Oltmans. Ozone in interstitial air of the mid-latitude, seasonal snowpack at niwot ridge, colorado. Arctic Antarctic and Alpine Research, 39(3):375–387, 2007.

F. Bocquet, D. Helmig, B. A. Van Dam, and C. W. Fairall. Evaluation of the flux gradient technique for measurement of ozone surface fluxes over snowpack at summit, greenland. Atmospheric Measurement Techniques, 4(10):2305–2321, 2011.

J. W. Bottenheim and E. Chan. A trajectory study into the origin of spring time arctic boundary layer ozone depletion. Journal of Geophysical Research-Atmospheres, 111(D19), 2006.

J. W. Bottenheim, A. G. Gallant, and K. A. Brice. Measurements of noy species and o3at 82-degrees-n latitude. Geophysical Research Letters, 13(2):113–116, 1986.

C. S. Boxe and A. Saiz-Lopez. Multiphase modeling of nitrate photochemistry in the quasi-liquid layer (qll): implications for no(x) release from the arctic and coastal antarctic snowpack. Atmospheric Chemistry and Physics, 8(16):4855–4864, 2008.

P. Boylan, D. Helmig, R. Staebler, A. Turnipseed, C. Fairall, and W. Neff. Boundary layer dynamics during the ocean-atmosphere-sea-ice-snow (oasis) 2009 experiment at barrow, ak. Boundary Layer Meteorology, in preparation, 2013.

S. B. Brooks, A. Saiz-Lopez, H. Skov, S. E. Lindberg, J. M. C. Plane, and M. E. Goodsite. The mass balance of mercury in the springtime arctic environment. Geophysical Research Letters, 33 (13):4, 2006.

D.J. Cavalieri and C.L. Parkinson. Arctic sea ice variability and trends. The Cryosphere, 6:881–889, 2012.

F. S. Chapin, M. Sturm, M. C. Serreze, J. P. McFadden, J. R. Key, A. H. Lloyd, A. D. McGuire, T. S. Rupp, A. H. Lynch, J. P. Schimel, J. Beringer, W. L. Chapman, H. E. Epstein, E. S. Euskirchen, L. D. Hinzman, G. Jia, C. L. Ping, K. D. Tape, C. D. C. Thompson, D. A. Walker, and J. M. Welker. Role of land-surface changes in arctic summer warming. Science, 310(5748): 657–660, 2005.

L. Chu and C. Anastasio. Temperature and wavelength dependence of nitrite photolysis in frozen and aqueous solutions. Environmental Science and Technology, 41(10):3626–3632, 2007.

L. Cohen, D. Helmig, W. D. Neff, A. A. Grachev, and C. W. Fairall. Boundary-layer dynamics and its influence on atmospheric chemistry at summit, greenland. Atmospheric Environment, 41 (24):5044–5060, 2007.

I. Colbeck. The occurrence of nocturnal ozone maxima at a rural site in northwest england. Environmental Technology Letters, 9(1):75–80, 1988. Times Cited: 0 COLBECK, I.

J. H. Crawford, D. D. Davis, G. Chen, M. Buhr, S. Oltmans, R. Weller, L. Mauldin, F. Eisele, R. Shetter, B. Lefer, R. Arimoto, and A. Hogan. Evidence for photochemical production of ozone at the south pole surface. Geophysical Research Letters, 28(19):3641–3644, 2001.

N. J. Cullen and K. Steffen. Unstable near-surface boundary conditions in summer on top of the greenland ice sheet. Geophysical Research Letters, 28(23):4491–4493, 2001.

D. Davis, J. B. Nowak, G. Chen, M. Buhr, R. Arimoto, A. Hogan, F. Eisele, L. Mauldin, D. Tanner, R. Shetter, B. Lefer, and P. McMurry. Unexpected high levels of no observed at south pole. Geophysical Research Letters, 28(19):3625–3628, 2001.

D. Davis, G. Chen, M. Buhr, J. Crawford, D. Lenschow, B. Lefer, R. Shetter, F. Eisele, L. Mauldin, and A. Hogan. South pole nox chemistry: an assessment of factors controlling variability and absolute levels. Atmospheric Environment, 38(32):5375–5388, 2004.

D. Davis, J. Seelig, G. Huey, J. Crawford, G. Chen, Y. Wang, M. Buhr, D. Helmig, W. Neff, D. Blake, R. Arimoto, and F. Eisele. A reassessment of antarctic plateau reactive nitrogen based on antci 2003 airborne and ground based measurements. Atmospheric Environment, 42(12): 2831–2848, 2008.

J. E. Dibb, R. W. Talbot, J. W. Munger, D. J. Jacob, and S. M. Fan. Air-snow exchange of hno(3) and no(y) at summit, greenland. Journal of Geophysical Research-Atmospheres, 103 (D3):3475–3486, 1998.

J. E. Dibb, M. Arsenault, M. C. Peterson, and R. E. Honrath. Fast nitrogen oxide photochemistry in summit, greenland snow. Atmospheric Environment, 36(15-16):2501–2511, 2002.

J. E. Dibb, R. W. Talbot, E. Scheuer, G. Seid, L. Debell, B. Lefer, and B. Ridley. Stratospheric influence on the northern north american free troposphere during topse: Be-7 as a stratospheric tracer. Journal of Geophysical Research-Atmospheres, 108(D4), 2003.

J. E. Dibb, L. D. Ziemba, J. Luxford, and P. Beckman. Bromide and other ions in the snow, firn air, and atmospheric boundary layer at summit during gshox. Atmospheric Chemistry and Physics, 10(20):9931–9942, 2010.

F. Domine and P. B. Shepson. Air-snow interactions and atmospheric chemistry. Science, 297 (5586):1506–1510, 2002.

F. Domine, M. Albert, T. Huthwelker, H. W. Jacobi, A. A. Kokhanovsky, M. Lehning, G. Picard, and W. R. Simpson. Snow physics as relevant to snow photochemistry. Atmospheric Chemistry and Physics, 8(2):171–208, 2008.

T. A. Douglas and M. Sturm. Arctic haze, mercury and the chemical composition of snow across northwestern alaska. Atmospheric Environment, 38(6):805–820, 2004.

Thomas A. Douglas, Lisa L. Loseto, Robie W. Macdonald, Peter Outridge, Aurlien Dommergue, Alexandre Poulain, Marc Amyot, Tamar Barkay, Torunn Berg, John Chtelat, Philippe Constant, Marlene Evans, Christophe Ferrari, Nikolaus Gantner, Matthew S. Johnson, Jane Kirk, Niels Kroer, Catherine Larose, David Lean, Torkel Gissel Nielsen, Laurier Poissant, Sigurd Rognerud, Henrik Skov, Sren Srensen, Feiuye Wang, Simon Wilson, and Christian M. Zdanowicz. The fate of mercury in arctic terrestrial and aquatic ecosystems, a review. Environmental Chemistry, 9 (4):321–355, 2012.

Y. Dubowski, A. J. Colussi, and M. R. Hoffmann. Nitrogen dioxide release in the 302 nm band photolysis of spray-frozen aqueous nitrate solutions. atmospheric implications. Journal of Physical Chemistry A, 105(20):4928–4932, 2001.

K. Eneroth, K. Holmen, T. Berg, N. Schmidbauer, and S. Solberg. Springtime depletion of tropospheric ozone, gaseous elemental mercury and non-methane hydrocarbons in the european arctic, and its relation to atmospheric transport. Atmospheric Environment, 41(38):8511–8526, 2007.

C. P. Ferrari, P. A. Gauchard, K. Aspmo, A. Dommergue, O. Magand, E. Bahlmann, S. Nagorski, C. Temme, R. Ebinghaus, A. Steffen, C. Banic, T. Berg, F. Planchon, C. Barbante, P. Cescon, and C. F. Boutron. Snow-to-air exchanges of mercury in an arctic seasonal snow pack in ny-alesund, svalbard. Atmospheric Environment, 39(39):7633–7645, 2005.

B. J. Finlayson-Pitts, L. M. Wingen, A. L. Sumner, D. Syomin, and K. A. Ramazan. The heterogeneous hydrolysis of no2 in laboratory systems and in outdoor and indoor atmospheres: An integrated mechanism. Physical Chemistry Chemical Physics, 5(2):223–242, 2003.

Barbara J. Finlayson-Pitts and James N. Pitts. Chemistry of the Upper and Lower Atmosphere: Theory, Experiments, and Applications, volume 1. Academic Press, 2000.

K. L. Foster, R. A. Plastridge, J. W. Bottenheim, P. B. Shepson, B. J. Finlayson-Pitts, and C. W. Spicer. The role of br-2 and brcl in surface ozone destruction at polar sunrise. Science, 291 (5503):471–474, 2001.

M. M. Frey, N. Brough, J. L. France, P. S. Anderson, O. Traulle, M. D. King, A. E. Jones, E. W. Wolff, and J. Savarino. The diurnal variability of atmospheric nitrogen oxides (no and no_2) above the antarctic plateau driven by atmospheric stability and snow emissions. Atmospheric Chemistry and Physics, 13(6):3045–3062, 2013. doi: 10.5194/acp-13-3045-2013. URL `http://www.atmos-chem-phys.net/13/3045/2013/`.

K. Fuhrer, M. Hutterli, and J. McConnell. Overview of recent field experiments for the study of the air-snow transfer of H2O2 and HCHO, pages 307–318. Springer-Verlag, 1996.

A. C. Fusco and J. A. Logan. Analysis of 1970-1995 trends in tropospheric ozone at northern hemisphere midlatitudes with the geos-chem model. Journal of Geophysical Research-Atmospheres, 108(D15), 2003. Times Cited: 48 Fusco, AC Logan, JA.

I. E. Galbally and C. R. Roy. Destruction of ozone at the earths surface. Quarterly Journal of the Royal Meteorological Society, 106(449):599–620, 1980.

E. S. Galbavy, C. Anastasio, B. Lefer, and S. Hall. Light penetration in the snowpack at summit, greenland: Part 2 nitrate photolysis. Atmospheric Environment, 41(24):5091–5100, 2007a.

E. S. Galbavy, C. Anastasio, B. L. Lefer, and S. R. Hall. Light penetration in the snowpack at summit, greenland: Part i nitrite and hydrogen peroxide photolysis. Atmospheric Environment, 41(24):5077–5090, 2007b.

L. Ganzeveld and J. Lelieveld. Dry deposition parameterization in a chemistry general-circulation model and its influence on the distribution of reactive trace gases. Journal of Geophysical Research-Atmospheres, 100(D10):20999–21012, 1995.

J. R. Garbarino, E. Snyder-Conn, T. J. Leiker, and G. L. Hoffman. Contaminants in arctic snow collected over northwest alaskan sea ice. Water Air and Soil Pollution, 139(1-4):183–214, 2002.

J. B. Gilman, J. F. Burkhart, B. M. Lerner, E. J. Williams, W. C. Kuster, P. D. Goldan, P. C. Murphy, C. Warneke, C. Fowler, S. A. Montzka, B. R. Miller, L. Miller, S. J. Oltmans, T. B. Ryerson, O. R. Cooper, A. Stohl, and J. A. de Gouw. Ozone variability and halogen oxidation within the arctic and sub-arctic springtime boundary layer. Atmospheric Chemistry and Physics, 10(21):10223–10236, 2010.

A. M. Grannas, A. E. Jones, J. Dibb, M. Ammann, C. Anastasio, H. J. Beine, M. Bergin, J. Bottenheim, C. S. Boxe, G. Carver, G. Chen, J. H. Crawford, F. Domine, M. M. Frey, M. I. Guzman, D. E. Heard, D. Helmig, M. R. Hoffmann, R. E. Honrath, L. G. Huey, M. Hutterli, H. W. Jacobi, P. Klan, B. Lefer, J. McConnell, J. Plane, R. Sander, J. Savarino, P. B. Shepson, W. R. Simpson, J. R. Sodeau, R. von Glasow, R. Weller, E. W. Wolff, and T. Zhu. An overview of snow photochemistry: evidence, mechanisms and impacts. Atmospheric Chemistry and Physics, 7(16):4329–4373, 2007.

G. L. Gregory, B. E. Anderson, L. S. Warren, E. V. Browell, D. R. Bagwell, and C. H. Hudgins. Tropospheric ozone and aerosol observations - the alaskan arctic. Journal of Geophysical Research-Atmospheres, 97(D15):16451–16471, 1992.

D. Helmig, F. Bocquet, L. Cohen, and S. J. Oltmans. Ozone uptake to the polar snowpack at summit, greenland. Atmospheric Environment, 41(24):5061–5076, 2007a.

D. Helmig, L. Ganzeveld, T. Butler, and S. J. Oltmans. The role of ozone atmosphere-snow gas exchange on polar, boundary-layer tropospheric ozone - a review and sensitivity analysis. Atmospheric Chemistry and Physics, 7, 2007b.

D. Helmig, S. J. Oltmans, D. Carlson, J. F. Lamarque, A. Jones, C. Labuschagne, K. Anlauf, and K. Hayden. A review of surface ozone in the polar regions. Atmospheric Environment, 41(24): 5138–5161, 2007c.

D. Helmig, S. J. Oltmans, T. O. Morse, and J. E. Dibb. What is causing high ozone at summit, greenland? Atmospheric Environment, 41(24):5031–5043, 2007d.

D. Helmig, B. Johnson, S. J. Oltmans, W. Neff, F. Eisele, and D. D. Davis. Elevated ozone in the boundary layer at south pole. Atmospheric Environment, 42(12):2788–2803, 2008a.

D. Helmig, B. J. Johnson, M. Warshawsky, T. Morse, W. D. Neff, F. Eisele, and D. D. Davis. Nitric oxide in the boundary-layer at south pole during the antarctic tropospheric chemistry investigation (antci). Atmospheric Environment, 42(12):2817–2830, 2008b.

D. Helmig, L. D. Cohen, F. Bocquet, S. Oltmans, A. Grachev, and W. Neff. Spring and summertime diurnal surface ozone fluxes over the polar snow at summit, greenland. Geophysical Research Letters, 36, 2009a.

D. Helmig, B. Seok, M. W. Williams, J. Hueber, and R. Sanford. Fluxes and chemistry of nitrogen oxides in the niwot ridge, colorado, snowpack. Biogeochemistry, 95(1):115–130, 2009b.

D. Helmig, P. Boylan, B. Johnson, S. Oltmans, C. Fairall, R. Staebler, A. Weinheimer, J. Orlando, D. J. Knapp, D. D. Montzka, F. Flocke, U. Friess, H. Sihler, and P. B. Shepson. Ozone dynamics and snow-atmosphere exchanges during ozone depletion events at barrow, alaska. Journal of Geophysical Research-Atmospheres, 117, 2012a.

D. Helmig, P. Boylan, B. Johnson, S. Oltmans, C. Fairall, R. Staebler, A. Weinheimer, J. Orlando, D. J. Knapp, D. D. Montzka, F. Flocke, U. Friess, H. Sihler, and P. B. Shepson. Ozone dynamics and snow-atmosphere exchanges during ozone depletion events at barrow, alaska. Journal of Geophysical Research-Atmospheres, 117, 2012b.

D. Helmig, E. K. Lang, L. Bariteau, P. Boylan, C. W. Fairall, L. Ganzeveld, J. E. Hare, J. Hueber, and M. Pallandt. Atmosphere-ocean ozone fluxes during the texaqs 2006, stratus 2006, gomecc 2007, gasex 2008, and amma 2008 cruises. Journal of Geophysical Research-Atmospheres, 117: 15, 2012c.

R. E. Honrath and D. A. Jaffe. The seasonal cycle of nitrogen-oxides in the arctic troposphere at barrow, alaska. Journal of Geophysical Research-Atmospheres, 97(D18):20615–20630, 1992.

R. E. Honrath, M. C. Peterson, S. Guo, J. E. Dibb, P. B. Shepson, and B. Campbell. Evidence of nox production within or upon ice particles in the greenland snowpack. Geophysical Research Letters, 26(6):695–698, 1999.

R. E. Honrath, S. Guo, M. C. Peterson, M. P. Dziobak, J. E. Dibb, and M. A. Arsenault. Photochemical production of gas phase nox from ice crystal no3. Journal of Geophysical Research-Atmospheres, 105(D19):24183–24190, 2000.

R. E. Honrath, Y. Lu, M. C. Peterson, J. E. Dibb, M. A. Arsenault, N. J. Cullen, and K. Steffen. Vertical fluxes of nox, hono, and hno3 above the snowpack at summit, greenland. Atmospheric Environment, 36(15-16):2629–2640, 2002.

D. J. Jacob, S. C. Wofsy, P. S. Bakwin, S. M. Fan, R. C. Harriss, R. W. Talbot, J. D. Bradshaw, S. T. Sandholm, H. B. Singh, E. V. Browell, G. L. Gregory, G. W. Sachse, M. C. Shipham, D. R. Blake, and D. R. Fitzjarrald. Summertime photochemistry of the troposphere at high northern latitudes. Journal of Geophysical Research-Atmospheres, 97(D15):16421–16431, 1992.

D. J. Jacob, J. H. Crawford, H. Maring, A. D. Clarke, J. E. Dibb, L. K. Emmons, R. A. Ferrare, C. A. Hostetler, P. B. Russell, H. B. Singh, A. M. Thompson, G. E. Shaw, E. McCauley, J. R. Pederson, and J. A. Fisher. The arctic research of the composition of the troposphere from aircraft and satellites (arctas) mission: design, execution, and first results. Atmospheric Chemistry and Physics, 10(11):5191–5212, 2010.

H. W. Jacobi and B. Hilker. A mechanism for the photochemical transformation of nitrate in snow. Journal of Photochemistry and Photobiology a-Chemistry, 185(2-3):371–382, 2007.

H. W. Jacobi, R. C. Bales, R. E. Honrath, M. C. Peterson, J. E. Dibb, A. L. Swanson, and M. R. Albert. Reactive trace gases measured in the interstitial air of surface snow at summit, greenland. Atmospheric Environment, 38(12):1687–1697, 2004.

B. T. Jobson, H. Niki, Y. Yokouchi, J. Bottenheim, F. Hopper, and R. Leaitch. Measurements of c-2-c-6 hydrocarbons during the polar sunrise 1992 experiment - evidence for cl atom and br atom chemistry. Journal of Geophysical Research-Atmospheres, 99(D12):25355–25368, 1994.

C. Johansson and R. W. Janson. Diurnal cycle of o-3 and monoterpenes in a coniferous forest - importance of atmospheric stability, surface exchange, and chemistry. Journal of Geophysical Research-Atmospheres, 98(D3):5121–5133, 1993.

K. P. Johnson, J. D. Blum, G. J. Keeler, and T. A. Douglas. Investigation of the deposition and emission of mercury in arctic snow during an atmospheric mercury depletion event. Journal of Geophysical Research-Atmospheres, 113(D17):11, 2008.

J. L. Kirk, V. L. S. Louis, and M. J. Sharp. Rapid reduction and reemission of mercury deposited into snowpacks during atmospheric mercury depletion events at churchill, manitoba, canada. Environmental Science and Technology, 40(24):7590–7596, 2006.

D. Kley and M. McFarland. Chemiluminescence detector for no and no2. Atmos. Tech., 12:62–69, 1980.

K. Kreher, J. G. Keys, P. V. Johnston, U. Platt, and X. Liu. Ground-based measurements of oclo and hcl in austral spring 1993 at arrival heights, antarctica. Geophysical Research Letters, 23 (12):1545–1548, 1996.

J. D. Lalonde, A. J. Poulain, and M. Amyot. The role of mercury redox reactions in snow on snow-to-air mercury transfer. Environmental Science and Technology, 36(2):174–178, 2002.

J. F. Lamarque, P. Hess, L. Emmons, L. Buja, W. Washington, and C. Granier. Tropospheric ozone evolution between 1890 and 1990. Journal of Geophysical Research-Atmospheres, 110(D8), 2005. 0148-0227.

J. Lelieveld and F. J. Dentener. What controls tropospheric ozone? Journal of Geophysical Research-Atmospheres, 105(D3):3531–3551, 2000.

P. Lemke, J. Ren, R.B. Alley, and et al. Climate Change 2007: The Physical Science Basis. Contribution of Working Group I to the Fourth Assessment Report of the Intergovernmental Panel on Climate Change. Cambridge University Press, Cambridge, UK and New York, NY, USA, 2007.

J. Liao, L. G. Huey, D. J. Tanner, N. Brough, S. Brooks, J. E. Dibb, J. Stutz, J. L. Thomas, B. Lefer, C. Haman, and K. Gorham. Observations of hydroxyl and peroxy radicals and the impact of bro at summit, greenland in 2007 and 2008. Atmospheric Chemistry and Physics, 11 (16):8577–8591, 2011.

S. E. Lindberg, S. Brooks, C. J. Lin, K. J. Scott, M. S. Landis, R. K. Stevens, M. Goodsite, and A. Richter. Dynamic oxidation of gaseous mercury in the arctic troposphere at polar sunrise. Environmental Science and Technology, 36(6):1245–1256, 2002.

M. Lippmann. Health-effects of tropospheric ozone. Environmental Science and Technology, 25 (12):1954–1962, 1991.

X. H. Liu and E. Ohtaki. An independent method to determine the height of the mixed layer. Boundary-Layer Meteorology, 85(3):497–504, 1997.

J. Y. Lu, W. H. Schroeder, L. A. Barrie, A. Steffen, H. E. Welch, K. Martin, L. Lockhart, R. V. Hunt, G. Boila, and A. Richter. Magnification of atmospheric mercury deposition to polar regions in springtime: the link to tropospheric ozone depletion chemistry. Geophysical Research Letters, 28(17):3219–3222, 2001.

R. W. Macdonald and J. M. Bewers. Contaminants in the arctic marine environment: Priorities for protection. Ices Journal of Marine Science, 53(3):537–563, 1996.

W. J. Massman. A review of the molecular diffusivities of h2o, co2, ch4, co, o-3, so2, nh3, n2o, no, and no2 in air, o2, and n2 near stp. Atmospheric Environment, 32(6):1111–1127, 1998.

E. Matthews. Atlas of archived vegetation, land-use and seasonal albedo data sets, 1985.

D. L. Mauzerall, D. J. Jacob, S. M. Fan, J. D. Bradshaw, G. L. Gregory, G. W. Sachse, and D. R. Blake. Origin of tropospheric ozone at remote high northern latitudes in summer. Journal of Geophysical Research-Atmospheres, 101(D2):4175–4188, 1996.

P. S. Monks. A review of the observations and origins of the spring ozone maximum. Atmospheric Environment, 34(21):3545–3561, 2000.

W. Neff. An observational and numerical study of the atmospheric boundary layer overlying the east antarctic ice sheet. Ph.D Thesis, University of Colorado, Boulder, page 272pp, 1980.

W. Neff, D. Helmig, A. Grachev, and D. Davis. A study of boundary layer behavior associated with high no concentrations at the south pole using a minisodar, tethered balloons and sonic anemometer. Atmospheric Environment, 42(12):2762–2779, 2008.

S. V. Nghiem, I. G. Rigor, A. Richter, J. P. Burrows, P. B. Shepson, J. Bottenheim, D. G. Barber, A. Steffen, J. Latonas, F. Y. Wang, G. Stern, P. Clemente-Colon, S. Martin, D. K. Hall, L. Kaleschke, P. Tackett, G. Neumann, and M. G. Asplin. Field and satellite observations of the formation and distribution of arctic atmospheric bromine above a rejuvenated sea ice cover. Journal of Geophysical Research-Atmospheres, 117, 2012.

D. Obrist, E. Tas, M. Peleg, V. Matveev, X. Fain, D. Asaf, and M. Luria. Bromine-induced oxidation of mercury in the mid-latitude atmosphere. Nature Geoscience, 4(1):22–26, 2011.

S. J. Oltmans. Surface ozone measurements in clean-air. Journal of Geophysical Research-Oceans and Atmospheres, 86(NC2):1174–1180, 1981. OLTMANS, SJ.

S. J. Oltmans, R. C. Schnell, P. J. Sheridan, R. E. Peterson, S. M. Li, J. W. Winchester, P. P. Tans, W. T. Sturges, J. D. Kahl, and L. A. Barrie. Seasonal surface ozone and filterable bromine relationship in the high arctic. Atmospheric Environment, 23(11):2431–2441, 1989.

S. J. Oltmans, D. J. Hofmann, J. A. Lathrop, J. M. Harris, W. D. Komhyr, and D. Kuniyuki. Tropospheric ozone during mauna loa observatory photochemistry experiment 2 compared to long-term measurements from surface and ozonesonde observations. Journal of Geophysical Research-Atmospheres, 101(D9):14569–14580, 1996.

S. J. Oltmans, A. S. Lefohn, J. M. Harris, I. Galbally, H. E. Scheel, G. Bodeker, E. Brunke, H. Claude, D. Tarasick, B. J. Johnson, P. Simmonds, D. Shadwick, K. Anlauf, K. Hayden, F. Schmidlin, T. Fujimoto, K. Akagi, C. Meyer, S. Nichol, J. Davies, A. Redondas, and E. Cuevas. Long-term changes in tropospheric ozone. Atmospheric Environment, 40(17):3156–3173, 2006.

S. J. Oltmans, B. J. Johnson, and J. M. Harris. Springtime boundary layer ozone depletion at barrow, alaska: Meteorological influence, year-to-year variation, and long-term change. Journal of Geophysical Research-Atmospheres, 117:18, 2012.

S. P. Oncley, M. Buhr, D. H. Lenschow, D. Davis, and S. R. Semmer. Observations of summertime no fluxes and boundary-layer height at the south pole during iscat 2000 using scalar similarity. Atmospheric Environment, 38(32):5389–5398, 2004.

T. E. Osterkamp and M. W. Payne. Estimates of permafrost thickness from well logs in northern alaska. Cold Regions Science and Technology, 5(1):13–27, 1981.

F.W. Parmentier, T.R. Christensen, L.L. Sorensen, S. Rysgaard, A.D. McGuire, P.A. Miller, and D.A. Walker. The impact of lower sea-ice extent on arctic greenhouse-gas exchange. Nature Climate Change, 3(3), 2013.

D. K. Perovich and J. A. Richtermenge. Surface characteristics of lead ice. Journal of Geophysical Research-Oceans, 99(C8):16341–16350, 1994.

M. C. Peterson and R. E. Honrath. Observations of rapid photochemical destruction of ozone in snowpack interstitial air. Geophysical Research Letters, 28(3):511–514, 2001.

U. Platt and G. Honninger. The role of halogen species in the troposphere. Chemosphere, 52(2): 325–338, 2003.

R. Rhines P. Thompson R. Pollard. The deepening of the wind-mixed layer. Geophysical Fluid Dynamics, 3:381–404, 1973.

E. Post, M. C. Forchhammer, M. S. Bret-Harte, T. V. Callaghan, T. R. Christensen, B. Elberling, A. D. Fox, O. Gilg, D. S. Hik, T. T. Hoye, R. A. Ims, E. Jeppesen, D. R. Klein, J. Madsen, A. D. McGuire, S. Rysgaard, D. E. Schindler, I. Stirling, M. P. Tamstorf, N. J. C. Tyler, R. van der Wal, J. Welker, P. A. Wookey, N. M. Schmidt, and P. Aastrup. Ecological dynamics across the arctic associated with recent climate change. Science, 325(5946):1355–1358, 2009.

A. J. Poulain, J. D. Lalonde, M. Amyot, J. A. Shead, F. Raofie, and P. A. Ariya. Redox transformations of mercury in an arctic snowpack at springtime. Atmospheric Environment, 38(39): 6763–6774, 2004.

K. A. Pratt, K. D. Custard, P. B. Shepson, T. A. Douglas, D. Pohler, S. General, J. Zielcke, W. R. Simpson, U. Platt, D. J. Tanner, L. G. Huey, M. Carlsen, and B. H. Stirm. Photochemical production of molecular bromine in arctic surface snowpacks. Nature Geosciences, 6(5):351–356, 2013. ISSN 1752-0894. doi: 10.1071/en10074. URL http://dx.doi.org/10.1038/ngeo1779.

B. A. Ridley and F. E. Grahek. A small, low flow, high sensitivity reaction vessel for no chemiluminescence detectors. Journal of Atmospheric and Oceanic Technology, 7(2):307–311, 1990.

W. H. Schroeder, K. G. Anlauf, L. A. Barrie, J. Y. Lu, A. Steffen, D. R. Schneeberger, and T. Berg. Arctic springtime depletion of mercury. Nature, 394(6691):331–332, 1998.

J. H. Pandis S. N. Seinfeld. Atmospheric Chemistry and Physics: From Air Pollution to Climate Change. John Wiley and Sons, Inc., New Jersey, 2006.

B. Seok, D. Helmig, M. W. Williams, D. Liptzin, K. Chowanski, and J. Hueber. An automated system for continuous measurements of trace gas fluxes through snow: an evaluation of the gas diffusion method at a subalpine forest site, niwot ridge, colorado. Biogeochemistry, 95(1):95–113, 2009.

B. Seok, L. Ganzeveld, D. Helmig, R. Honrath, B. Van Dam, J. Hueber, C. Toro, and L. Kramer. Evaluation of snowpack ozone and nitrogen oxide exchange at summit, greenland, in a single-column chemistry-climate model, 2010.

M. C. Serreze, J. E. Walsh, F. S. Chapin, T. Osterkamp, M. Dyurgerov, V. Romanovsky, W. C. Oechel, J. Morison, T. Zhang, and R. G. Barry. Observational evidence of recent change in the northern high-latitude environment. Climatic Change, 46(1-2):159–207, 2000.

W. R. Simpson, R. von Glasow, K. Riedel, P. Anderson, P. Ariya, J. Bottenheim, J. Burrows, L. J. Carpenter, U. Friess, M. E. Goodsite, D. Heard, M. Hutterli, H. W. Jacobi, L. Kaleschke, B. Neff, J. Plane, U. Platt, A. Richter, H. Roscoe, R. Sander, P. Shepson, J. Sodeau, A. Steffen, T. Wagner, and E. Wolff. Halogens and their role in polar boundary-layer ozone depletion. Atmospheric Chemistry and Physics, 7(16):4375–4418, 2007.

S. J. Sjostedt, L. G. Huey, D. J. Tanner, J. Peischl, G. Chen, J. E. Dibb, B. Lefer, M. A. Hutterli, A. J. Beyersdorf, N. J. Blake, D. R. Blake, D. Sueper, T. Ryerson, J. Burkhart, and A. Stohl. Observations of hydroxyl and the sum of peroxy radicals at summit, greenland during summer 2003. Atmospheric Environment, 41(24):5122–5137, 2007.

F. Slemr, E. G. Brunke, R. Ebinghaus, C. Temme, J. Munthe, I. Wangberg, W. Schroeder, A. Steffen, and T. Berg. Worldwide trend of atmospheric mercury since 1977. Geophysical Research Letters, 30(10):4, 2003.

E. Snyder-Conn, J. R. Garbarino, G. L. Hoffman, and A. Oelkers. Soluble trace elements and total mercury in arctic alaskan snow. Arctic, 50(3):201–215, 1997.

Z. Sorbjan and A. A. Grachev. An evaluation of the flux-gradient relationship in the stable boundary layer. Boundary-Layer Meteorology, 135(3):385–405, 2010.

F. Sprovieri, N. Pirrone, M. S. Landis, and R. K. Stevens. Atmospheric mercury behavior at different altitudes at ny alesund during spring 2003. Atmospheric Environment, 39(39):7646–7656, 2005.

A. Steffen, W. Schroeder, J. Bottenheim, J. Narayan, and J. D. Fuentes. Atmospheric mercury concentrations: measurements and profiles near snow and ice surfaces in the canadian arctic during alert 2000. Atmospheric Environment, 36(15-16):2653–2661, 2002.

A. Steffen, T. Douglas, M. Amyot, P. Ariya, K. Aspmo, T. Berg, J. Bottenheim, S. Brooks, F. Cobbett, A. Dastoor, A. Dommergue, R. Ebinghaus, C. Ferrari, K. Gardfeldt, M. E. Goodsite, D. Lean, A. J. Poulain, C. Scherz, H. Skov, J. Sommar, and C. Temme. A synthesis of atmospheric mercury depletion event chemistry in the atmosphere and snow. Atmospheric Chemistry and Physics, 8(6):1445–1482, 2008.

C. R. Stephens, P. B. Shepson, A. Steffen, J. W. Bottenheim, J. Liao, L. G. Huey, E. Apel, A. Weinheimer, S. R. Hall, C. Cantrell, B. C. Sive, D. J. Knapp, D. D. Montzka, and R. S. Hornbrook. The relative importance of chlorine and bromine radicals in the oxidation of atmospheric mercury at barrow, alaska. Journal of Geophysical Research-Atmospheres, 117:16, 2012.

A. Stohl, C. Forster, A. Frank, P. Seibert, and G. Wotawa. Technical note: The lagrangian particle dispersion model flexpart version 6.2. Atmospheric Chemistry and Physics, 5:2461–2474, 2005.

C. Stroud, S. Madronich, E. Atlas, C. Cantrell, A. Fried, B. Wert, B. Ridley, F. Eisele, L. Mauldin, R. Shetter, B. Lefer, F. Flocke, A. Weinheimer, M. Coffey, B. Heikes, R. Talbot, and D. Blake. Photochemistry in the arctic free troposphere: Ozone budget and its dependence on nitrogen oxides and the production rate of free radicals. Journal of Atmospheric Chemistry, 47(2):107–138, 2004.

J. Stutz, J. L. Thomas, S. C. Hurlock, M. Schneider, R. von Glasow, M. Piot, K. Gorham, J. F. Burkhart, L. Ziemba, J. E. Dibb, and B. L. Lefer. Longpath doas observations of surface bro at summit, greenland. Atmospheric Chemistry and Physics, 11(18):9899–9910, 2011.

A. L. Sumner and P. B. Shepson. Snowpack production of formaldehyde and its effect on the arctic troposphere. Nature, 398(6724):230–233, 1999.

P. J. Tackett, A. E. Cavender, A. D. Keil, P. B. Shepson, J. W. Bottenheim, S. Morin, J. Deary, A. Steffen, and C. Doerge. A study of the vertical scale of halogen chemistry in the arctic troposphere during polar sunrise at barrow, alaska. Journal of Geophysical Research-Atmospheres, 112(D7), 2007.

N. Takenaka, A. Ueda, and Y. Maeda. Acceleration of the rate of nitrite oxidation by freezing in aqueous-solution. Nature, 358(6389):736–738, 1992.

C. Temme, R. Ebinghaus, J. W. Einax, A. Steffen, and W. H. Schroeder. Time series analysis of long-term data sets of atmospheric mercury concentrations. Analytical and Bioanalytical Chemistry, 380(3):493–501, 2004.

J. L. Thomas, J. Stutz, B. Lefer, L. G. Huey, K. Toyota, J. E. Dibb, and R. von Glasow. Modeling chemistry in and above snow at summit, greenland - part 1: Model description and results. Atmospheric Chemistry and Physics, 11(10):4899–4914, 2011.

J. L. Thomas, J. E. Dibb, L. G. Huey, J. Liao, D. Tanner, B. Lefer, R. von Glasow, and J. Stutz. Modeling chemistry in and above snow at summit, greenland - part 2: Impact of snowpack chemistry on the oxidation capacity of the boundary layer. Atmospheric Chemistry and Physics, 12(14):6537–6554, 2012.

E. Y. Tkachenko and S. G. Kozachkov. Possible contribution of triboelectricity to snow-air interactions. Environmental Chemistry, 9(2):109–115, 2012. ISSN 1448-2517. doi: 10.1071/en10074. URL <Go to ISI>://WOS:000303509300003.

K.E. Trenberth, P.D. Jones, P. Ambenje, R. Bojariu, D. Easterling, A. Klein Tank, D. Parker, F. Rahimzadeh, J.A. Renwick, M. Rusticucci, B. Soden, and P. Zhai. Observations: Surface and Atmospheric Climate Change. Cambridge University Press, Cambridge, United Kingdom and New York, NY, USA, 2007.

J. P. Tuovinen, M. Aurela, and T. Laurila. Resistances to ozone deposition to a flark fen in the northern aapa mire zone. Journal of Geophysical Research-Atmospheres, 103(D14):16953–16966, 1998.

Brie Van Dam, Detlev Helmig, John F. Burkhart, Daniel Obrist, and Samuel J. Oltmans. Springtime boundary layer o3 and gem depletion at toolik lake, alaska. Journal of Geophysical Research: Atmospheres, pages n/a–n/a, 2013. ISSN 2169-8996. doi: 10.1002/jgrd.50213. URL http://dx.doi.org/10.1002/jgrd.50213.

S. A. Vay, Y. Choi, K. P. Vadrevu, D. R. Blake, S. C. Tyler, A. Wisthaler, A. Hecobian, Y. Kondo, G. S. Diskin, G. W. Sachse, J. H. Woo, A. J. Weinheimer, J. F. Burkhart, A. Stohl, and P. O. Wennberg. Patterns of co2 and radiocarbon across high northern latitudes during international polar year 2008. Journal of Geophysical Research-Atmospheres, 116:22, 2011.

D. Vickers and L. Mahrt. Evaluating formulations of stable boundary layer height. Journal of Applied Meteorology, 43(11):1736–1749, 2004.

R. Vingarzan. A review of surface ozone background levels and trends. Atmospheric Environment, 38(21):3431–3442, 2004. Vingarzan, R.

R. von Glasow. Atmospheric chemistry - sun, sea and ozone destruction. Nature, 453(7199): 1195–1196, 2008.

D.A. Walker and H.A. Maier. Vegetation in the vicinity of the toolik field station, alaska, 2008.

Y. H. Wang, B. Ridley, A. Fried, C. Cantrell, D. Davis, G. Chen, J. Snow, B. Heikes, R. Talbot, J. Dibb, F. Flocke, A. Weinheimer, N. Blake, D. Blake, R. Shetter, B. Lefer, E. Atlas, M. Coffey, J. Walega, and B. Wert. Springtime photochemistry at northern mid and high latitudes. Journal of Geophysical Research-Atmospheres, 108(D4), 2003.

P. Warneck and C. Wurzinger. Product quantum yields for the 305-nm photodecomposition of no3- in aqueous-solution. Journal of Physical Chemistry, 92(22):6278–6283, 1988.

P. Wennberg. Atmospheric chemistry - bromine explosion. Nature, 397(6717):299–+, 1999.

M. L. Wesely and B. B. Hicks. A review of the current status of knowledge on dry deposition. Atmospheric Environment, 34(12-14):2261–2282, 2000.

M. L. Wesely, D. R. Cook, and R. M. Williams. Field measuremetn of small ozone fluxes to snow, wet bare soil, and lake water. Boundary-Layer Meteorology, 20(4):459–471, 1981.

S. Wessel, S. Aoki, P. Winkler, R. Weller, A. Herber, H. Gernandt, and O. Schrems. Tropospheric ozone depletion in polar regions - a comparison of observations in the arctic and antarctic. Tellus Series B-Chemical and Physical Meteorology, 50(1):34–50, 1998.

S. Zilitinkevich and A. Baklanov. Calculation of the height of the stable boundary layer in practical applications. Boundary-Layer Meteorology, 105(3):389–409, 2002.

S. Zilitinkevich, A. Baklanov, J. Rost, A. S. Smedman, V. Lykosov, and P. Calanca. Diagnostic and prognostic equations for the depth of the stably stratified ekman boundary layer. Quarterly Journal of the Royal Meteorological Society, 128(579):25–46, 2002.

Appendix A

Supplemental Figures

A.1 Supplemental figures from Chapter 4

Figure A.1: Relationship between the FRCI with inlet at 3.4 m above the surface, and the UV photometric analyzer with inlet at 4.1 m above surface. This comparison uses surface O_3 data from both instruments for the month of April.

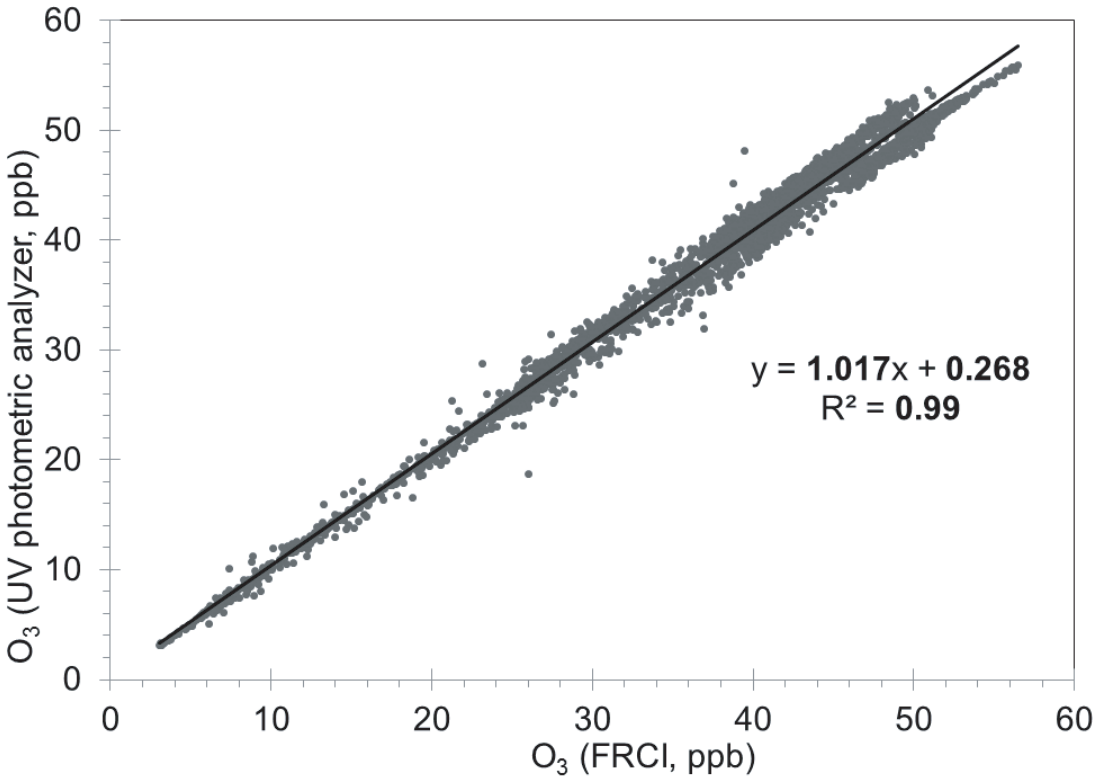

Figure A.2: Graphs (a) – (f) show examples of FLEXPART footprint sensitivity plots for events 1, 2, 5, 7, 8, and 9, respectively.

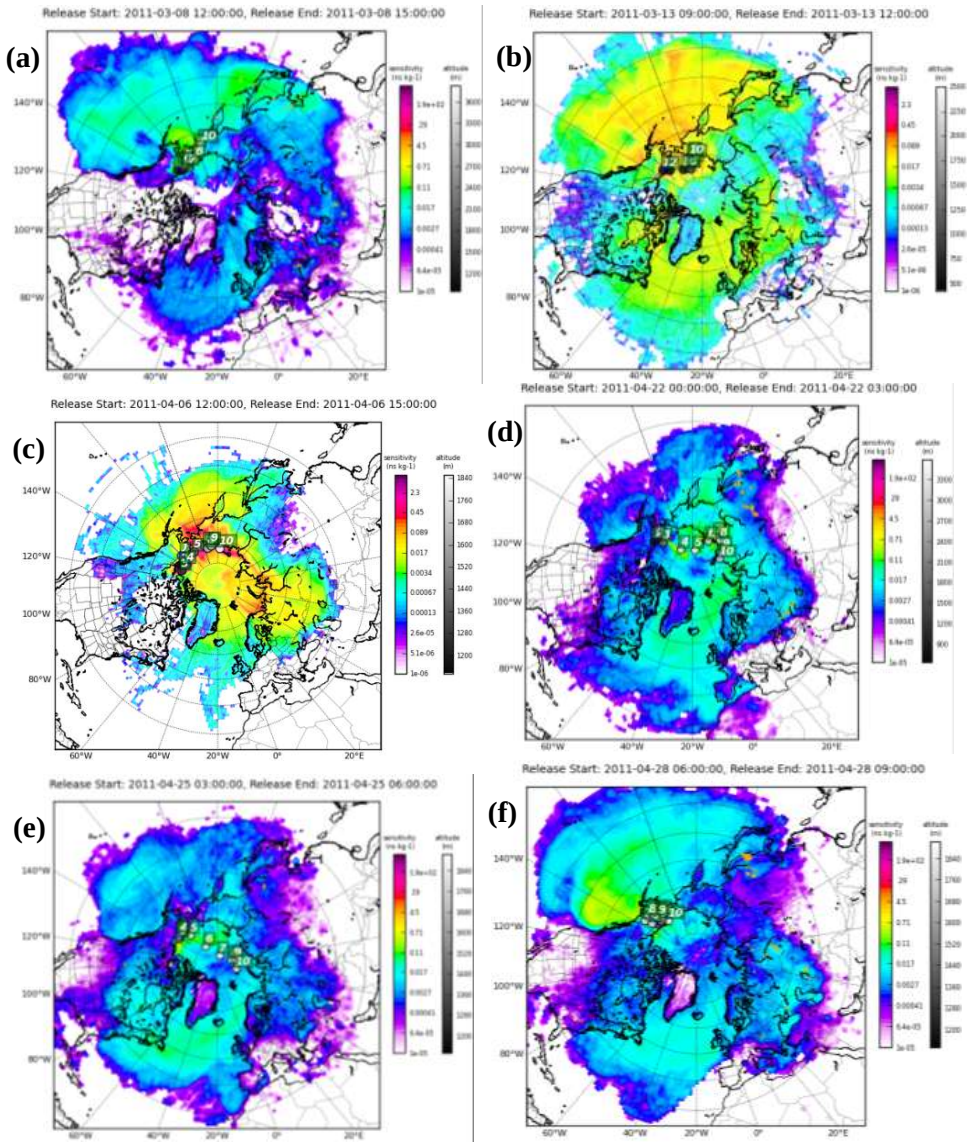

Appendix B

Additional manuscript contributions

B.1 Comments on 'Possible contribution of triboelectricity to snow-air interactions'

B. Van Dam, and D. Helmig. Comments on 'Possible contribution of triboelectricity to snow-air interactions'. Environmental Chemistry, 9(2):116-118, 2012.

This work comments on the Tkachenko and Kozachkov (2012) manuscript, which proposed that the triboelectrification of dry polar snow could be an important influence on the chemistry of the snowpack. This would occur primarily during windy periods when the electrification of snow would initiate various free radical processes that could result in ozone production in snow. In our article, we tested this hypothesis using snowpack ozone data from Summit, Greenland. Following the Tkachenko and Kozachkov (2012) hypothesis, during the winter time when there could be no photochemical destruction of ozone within the snowpack, it would be expected that emissions of ozone from snow would be observed during windy, dark conditions due to the proposed production mechanism. Snowpack ozone data from Summit do not show this behavior in winter. Thus, while the Tkachenko and Kozachkov (2012) paper presents interesting hypotheses worth investigating and discussing further, our data do not currently support this mechanism.

B.2 Evaluation of the flux gradient technique for measurement of ozone surface fluxes over snowpack at Summit, Greenland

F. Bocquet, D. Helmig, B. Van Dam, and C.W. Fairall. Evaluation of the flux gradient technique for measurement of ozone surface fluxes over snowpack at Summit, Greenland. Atmos. Meas. Tech., 4:2305-2321, 2011.

Abstract: A multi-step procedure for investigating ozone surface fluxes over polar snow by the tower gradient method was developed and evaluated. These measurements were then used to obtain five months (April − August 2004) of turbulent ozone flux data at the Summit research camp located at the center of the Greenland ice shield. Turbulent fluxes were determined by the gradient method incorporating tower measurements of (a) ozone gradients measured by commercial ultraviolet absorption analyzers, (b) ambient temperature gradients using aspirated thermocouple sensors, and (c) wind speed gradients determined by cup anemometers. All gradient instruments were regularly intercompared by bringing sensors or inlets to the same measurement height. The developed protocol resulted in an uncertainty on the order of 0.1 ppbv for 30-min averaged ozone gradients that were used for the ozone flux calculations. This protocol facilitated a lower sensitivity threshold for the ozone flux determination of $\sim 8 \times 10^{-3} \mu g m^{-2} s^{-1}$, respectively $\sim$0.01 cm s^{-1} for the ozone deposition velocity for typical environmental conditions encountered at Summit. Uncertainty in the 30-min ozone exchange measurements (evaluated by the Monte Carlo statistical approach) was on the order of 10^{-2} cm s^{-1}. This uncertainty typically accounted to $\sim$20-100% of the ozone exchange velocities that were determined. These measurements are among the most sensitive ozone deposition determinations reported to date. This flux experiment allowed for measurements of the relatively low ozone uptake rates encountered for polar snow, and thereby the study of their environmental and spring-versus-summer dependencies.